CONFORMAL ANTENNAS AND ARRAYS WITH LAYERS CONSISTING OF COPPER AND GRAPHENE-BASED CONDUCTORS FOR REDUNDANCY PROPERTIES

A Dissertation
Submitted to the Graduate Faculty
of the
North Dakota State University
of Agriculture and Applied Science

By

Sayeed Zebaul Haque Sajal

In Partial Fulfillment of the Requirements
for the Degree of
DOCTOR OF PHILOSOPHY

Major Department:
Electrical and Computer Engineering

April 2017

Fargo, North Dakota

NORTH DAKOTA STATE UNIVERSITY

Graduate School

Title

CONFORMAL ANTENNAS AND ARRAYS WITH LAYERS CONSISTING OF COPPER AND GRAPHENE-BASED CONDUCTORS FOR REDUNDANCY PROPERTIES

By

Sayeed Zebaul Haque Sajal

The supervisory committee certifies that this dissertation complies with North Dakota State University's regulations and meets the accepted standards for the degree of

DOCTOR OF PHILOSOPHY

SUPERVISORY COMMITTEE:

Dr. Benjamin D. Braaten
Chair

Dr. David A. Rogers

Dr. Ivan T. Lima

Dr. Debasis Dawn

Dr. Mijia Yang

Approved:

11 April 2017
Date

Dr. Scott C. Smith
Department Chair

ABSTRACT

Graphene is a new promising material with unique electrical, mechanical, optical and thermal characteristics. The use of graphene in the design of an antenna and other electromagnetic passive devices would be beneficial for miniaturization, efficient dynamic tuning, monolithic integration with graphene RF nano-electronics, and even transparency, mechanical flexibility, and reliability. However, there are some challenges to fabricate and design an antenna with pure graphene embedded in the layout. Here, an advanced study on the electrical and mechanical properties of graphene-based conductive material (not pure graphene), and how this material can be utilized in developing a first-ever graphene-based conformal antenna array for wireless communication systems has been done. More specifically, the important factors for antenna design, such as electrical and mechanical properties, will be studied here to ensure an effective and efficient design. Next, a graphene-based antenna array on a planar surface will be designed to validate the electrical and mechanical properties, and finally the trade-off of the graphene-based antenna array on a conformal surface is investigated. To mitigate the challenges of designing a graphene-based conformal antenna array, proper care is needed to achieve the optimal performance of the antenna array system. These new mechanisms of the graphene-based conformal antenna arrays will bring new possibilities in conformal antenna usage and wearable antenna applications for the first time.

ACKNOWLEDGEMENTS

Firstly I would like to thank my Almighty Allah for His endless blessings on me.

Secondly I would like to express my sincere thanks to my adviser, Dr. Benjamin D. Braaten for providing immense guidance, strong support, inspiration and supervision throughout my studies and research at North Dakota Sate University.

I am really grateful to Dr. Ivan T. Lima, Dr. David A. Rogers, Dr. Debasis Dawn and Dr. Mijia Yang who gave me inspiration and guidance to achieve my goal.

Finally, I would like to express a special gratitude to my family for their support and inspiration.

DEDICATION

To my family.

TABLE OF CONTENTS

LIST OF FIGURES

LIST OF SYMBOLS

α_c . . . . . Attenuation constant

ϵ . . . . . Electrical permittivity

ϵ_o . . . . . Free space permittivity

ϵ_r . . . . . Relative permittivity

Φ_0 . . . . . Progressive phase shift

λ_0 . . . . . Free-space wavelength

μ . . . . . Magnetic permeability

μ_0 . . . . . Permeability of free-space

μ_r . . . . . Relative permeability

Ω . . . . . Ohm

π . . . . . Constant PI

R_S . . . . . Sheet resistance

σ . . . . . Conductivity

$tan\delta$ . . . . . Loss tangent

Z_0 . . . . . Characteristic impedance

1. INTRODUCTION

1.1. Background

Recently Graphene has attracted tremendous interest in different research areas because of its unique electrical and mechanical properties [1]. These unique properties of graphene have led to a plethora of applications such as the development of high-speed devices based on field effect transistors and frequency multipliers [2]. However, the use of graphene in antennas has been less investigated, though there is some interesting work on graphene-based antennas in higher frequency band [3]. The capability of using conformal antennas opens up many applications such as placement on: (1) vibrating surfaces, (2) the skin of an aircraft, (3) a high speed moving vehicle and (4) wearable units (i.e., spacesuit) where a unique antenna is required [23, 4, 5]. In wireless communications, conformal antenna arrays are gaining popularity due to their superior performance and the ability to be implemented on complex geometries. Introducing a new graphene-based conformal antenna array will be extremely beneficial as advantages of both graphene and conformal antenna arrays can be utilized in the design. For the purpose of this research, the commercially available flexible graphene-based conductive material shown in Figure 1.1 was used to develop a redundancy mechanism for antenna and antenna array applications both on flat and conformal surfaces.

The following sections define and briefly discusses the properties of antenna arrays and conformal antennas. The discussion on these properties has laid the foundation for this research. Previous work on graphene, antenna arrays and conformal antennas are also presented to understand the background resources to conduct this research.

1.1.1. Graphene material, antenna arrays and conformal antennas

1.1.1.1. Pure Graphene Material

Graphene, the world's first two-dimensional material, is 1 million times thinner than a strand of hair, but 200 times stronger than steel [6]. The two physicists who discovered it in 2004, Andre Geim and Konstantin Novoselov [1], each earned a Nobel Prize and knighthoods from the Queen of England. Graphene is a single layer of carbon atoms arranged in a hexagon. It looks like a honeycomb under a microscope, as shown in Figure 1.2. This unique structure is the secret to

its incredible strength and is of interest for this research [6]. Because of its unique two-dimensional structure, the graphene material exhibits exceptionally high crystal and electrical qualities. Overall, one-atom-thick fabric of carbon is uniquely combined so that it has many capabilities such as extreme mechanical strength, exceptionally high electronic and thermal conductivities, impermeability to gases, as well as many other attractive properties, all of which make it highly attractive for numerous practical applications.

Figure 1.1. Commercially available flexible graphene-based conductive material.

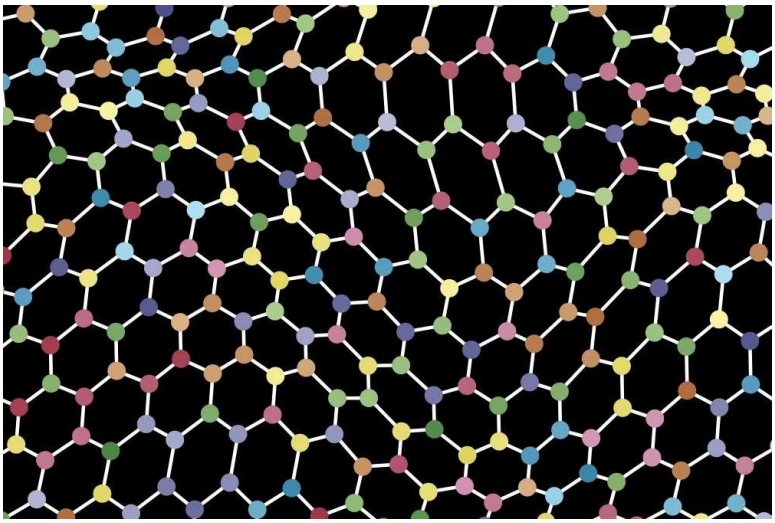

Figure 1.2. Graphene: a single layer of carbon atoms arranged in a hexagon.

1.1.1.2. Antenna Arrays

An antenna array is a set of individual antennas, used for transmitting and/or receiving radio waves, whose individual currents maintain a specified amplitude and phase relationship. The invention of the Yagi-Uda antenna array in 1926 opened up a new arena in array technology research followed by the mechanically steered and phased arrays around the World War II era. The world observed a paradigm shift in the design of antenna arrays by the invention of electronic phase shifters. The two most commonly used techniques in designing low profile printed antenna arrays are series-fed and parallel-fed. These feed techniques are shown in Figure 1.3 [7].

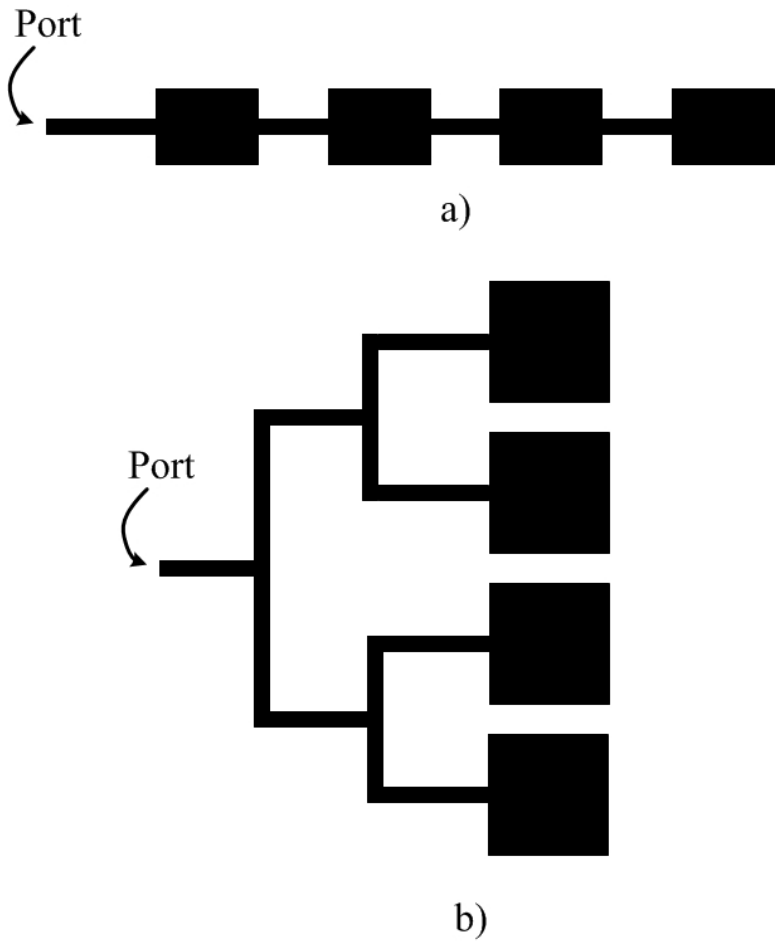

Figure 1.3. a) Microstrip series-fed antenna array. b) Microstrip parallel-fed antenna array.

In order to obtain directive characteristics in a radiation pattern, the antenna elements are arranged in a certain geometrical and electrical configuration. One such configuration is shown in

Figure 1.4 where the N antenna elements are arranged along the z-axis.

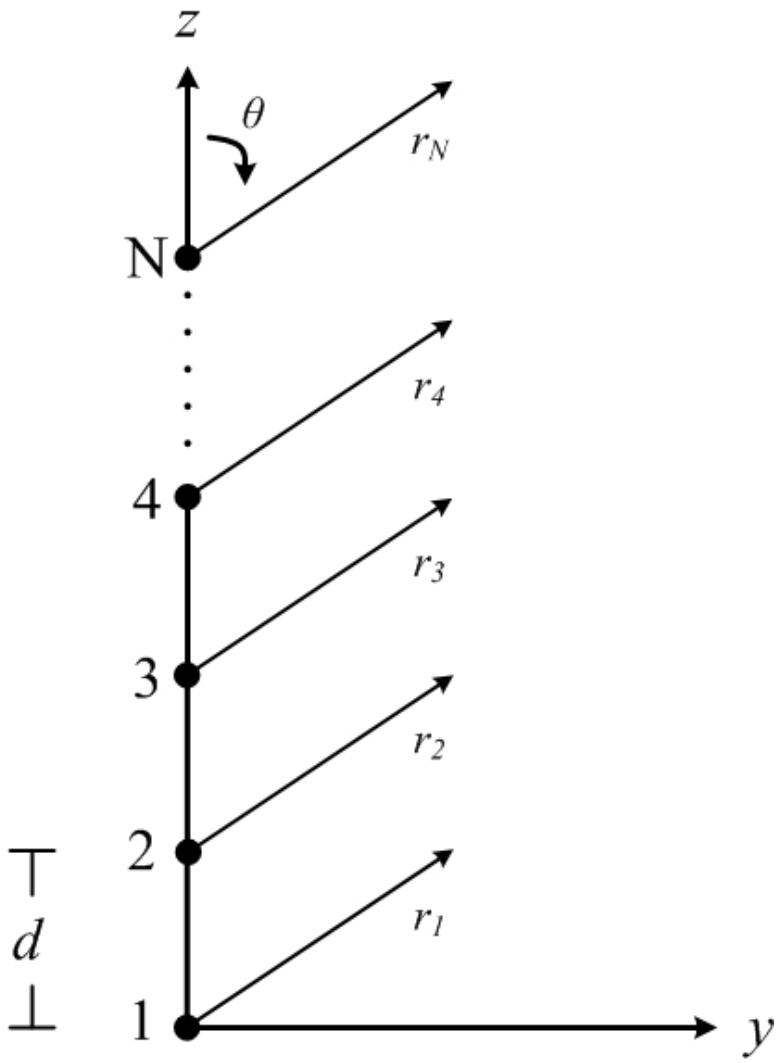

Figure 1.4. Far-field geometry of N-element linear array.

Let us assume that all elements have the same amplitudes and a progressive phase shift of Φ_o. The array factor expression for this uniform linear array is given by [7]:

$$AF = \sum_{n=1}^{N} e^{j(n-1)\psi} \tag{1.1}$$

and ψ is given by,

$$\psi = kd\ cos\theta + \Phi_o \tag{1.2}$$

where θ is the angle from broadside, d is the inter-element spacing and Φ_o represents the progressive phase shift. The normalized closed form array factor for a N-element linear array is given by:

$$AF = \frac{1}{N} \times (\frac{sin\frac{N\psi}{2}}{sin\frac{\psi}{2}}). \tag{1.3}$$

When the value of ψ is zero or $\pm 2n\pi$, the array generates a broadside radiation pattern. Here, the scan angle of a uniform linear array is given by [7]:

$$ScanAngle = sin^{-1}(-\frac{\Phi_o}{kd}). \tag{1.4}$$

For series-fed antenna arrays, the spacing between array elements is uniform but excitation amplitude distribution is not uniform. In this case, the normalized array factor for an even number of array elements becomes [7]:

$$AF_{even} = \sum_{n=1}^{M} a_n\ cos(\frac{(2n-1)}{2}\ kd\ cos\ \theta). \tag{1.5}$$

And for odd numbers of array elements the normalized array factor is given by [7]:

$$AF_{odd} = \sum_{n=1}^{M+1} a_n\ cos((n-1)\ kd\ cos\ \theta) \tag{1.6}$$

where a_n is the amplitude coefficient of the antenna array. An example of a microstrip patch antenna array is shown in Figure 1.5 [7].

1.1.1.3. Conformal antennas

An antenna placed on a conformal or curved surface is called a conformal antenna. Modern wireless communication systems are being required to operate in even more complicated environments. This is because these systems are being applied to problems that (I) involve surfaces that change shape with time, (II) include wearable networks and/or (III) are subjected extreme environmental temperature/pressure changes [8]. Because of the wireless nature of these systems, the

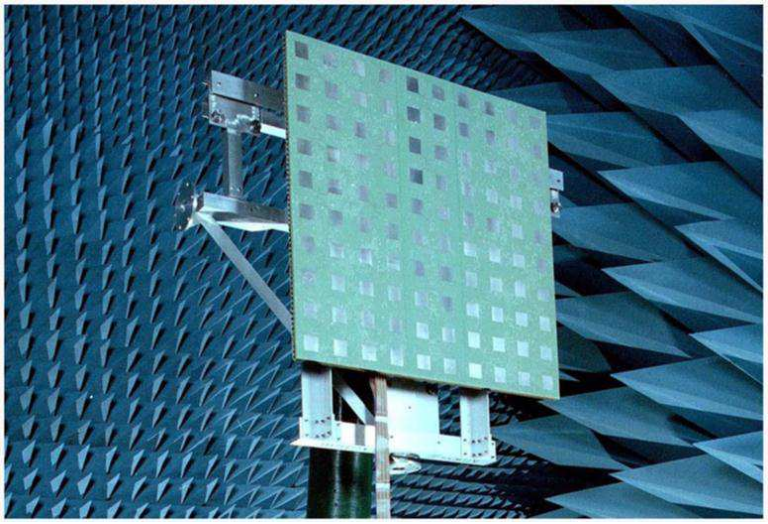

Figure 1.5. A microstrip patch antenna array.

antenna is a major part of the design, and conformal antennas have the potential to overcome some of the aforementioned difficulties. An example of a graphene-based conformal antenna is shown in Figure 1.6.

1.1.2. Previous works on graphene-based antennas

The applications of the unique properties of graphene have become quite popular. There are many of possible applications of graphene antennas but we have much more works to do to develop them. An initial investigation of pure graphene patch antennas at microwave frequencies was reported in [9] and later discussed in [10]. Moreover, the status and prospect of graphene was discussed by its inventor A. K. Geim [11]. Advanced mechanical properties of graphene paper was also explored in [12]. The use of graphene-based materials, having structural strength and high electrical conductivity, has hence been increasing to fill this developmental gap. As pure graphene is a carbon monolayer and we need sophisticated tools to work with pure graphene, we used 97% carbon content graphene-based conductor (GBC) in this research. GBC is flexible, commercially available, and provides good electrical conductivity [13]; therefore, it is considered in this research to be a good candidate for conformal antenna applications. Furthermore, the use of GBC as an alternative to copper for antenna designs on a conformal surface was initially explored in [14].

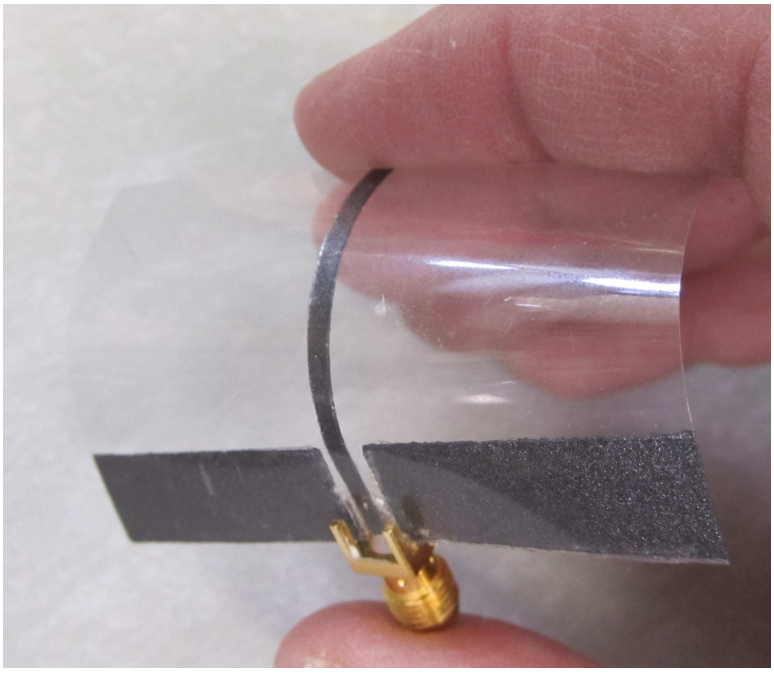

Figure 1.6. An example of graphene-based conformal antenna

1.1.3. Previous works on antenna arrays

High directivity is achieved through the use of antenna arrays. In the early days linear arrays were formed using cascaded microstrip half-wave resonators. Many different types of microstrip arrays, developed in the 1950s, 1960s, and early 1970s, can be classified as the first generation of antenna arrays. Four different independent solutions for lightweight and inexpensive arrays have been referred to in previous works on antenna arrays: the monolithic microstrip array developed by Munson [15, 16], the etched broadside and endfire arrays purposed by Fubini [17, 18], narrow line radiators proposed by James and Wilson [19], and multi-layer arrays proposed by Collings [20, 21, 22]. These arrays, having different bandwidths and radiation characteristics, provided a solid foundation for further work in antenna array technology.

1.1.4. Previous works on conformal antennas

There are many applications where unique antenna placement is required. Examples include: the integration of an antenna on a vehicle or aircraft [23, 24, 25, 26, 27], circular arrays for wider coverage than planar antennas [28, 29, 30], textile antennas for systems being integrated into a wearable wireless network [31, 32, 33, 34] or unique composites for embedding the antenna into a

structure for load-bearing purposes [35]. These conformal antennas that have been developed have provided us with a solid foundation to understand the diverse applications of conformal antennas. But copper conductors, widely used for such applications, commonly crack or break under iterative bending events. Therefore it is essential that new designs and techniques be developed that eliminate the problem of cracking conductors.

1.2. Current Work on Conformal Antenna Arrays and the Use of Graphene-based Conductors

A broadband conformal phased array antenna on a spherical surface [36], conformal array with high gain and low SLL [37], an autonomous self-adapting conformal array for cylindrical surfaces [38] and Bezier curves used to design self-adapting conformal phased-array antennas [39] were presented in the respective cited works. Different techniques are utilized to design the conformal array on different surfaces. Some work has been done for teraherz applications using graphene and graphene stack [40, 41, 42, 43]. This research on the graphene-based conformal array was based on all of the aforementioned work bringing together arrays, redundancy stratified conductors, and graphene-based conductors for the first time.

2. RESEARCH TASKS

Chapter 1 has illustrated that the study of graphene, antenna arrays, and conformal antennas involves many areas of research. The information presented in this dissertation, while summary of all the work conducted in the past four decades, also attests to a much larger scope for the significant research to be conducted.

2.1. Properties of Interest and Research Questions

The conformal antenna array is gaining interest because of its diverse applications. From the previous discussion, we know that graphene has unique properties. We have recounted the previous work on graphene, antenna arrays and conformal antennas. We noted that copper is currently the most common and widely used material in these antenna applications.

In this chapter, the concepts of graphene, antenna arrays and conformal antenans are presented. To introduce this research, we have to consider the 97% carbon content graphene-based conductive materials to design the conformal antenna array with redundancy properties. Many flexible substrates can be used to achieve the desired performance. Therefore, in this work, the research combined the benefits of 97% carbon content graphene-based conductive materials and the conformal antenna array. Thus this research focused on the following two questions.

- How can the electro-mechanical properties of the 97% carbon content graphene-based material be beneficial in applied electro-magnetism?
- How can the unique properties of graphene-based materials be used to improve the performance of conformal antennas? Or, what's the trade-off of using graphene-based conducive materials in conformal antenna applications?

2.2. Methodological Approach and Technical Objectives

This research is divided into three phases. The block diagram and the phases of the 97% carbon content graphene-based conformal antenna array system are shown in Figure 2.1

- Phase I: This phase deals with the study of the electrical and mechanical properties of the graphene-based conductive material, as well as with the fabrication challenges of the antenna with graphene-based conductive material embedded into the design.

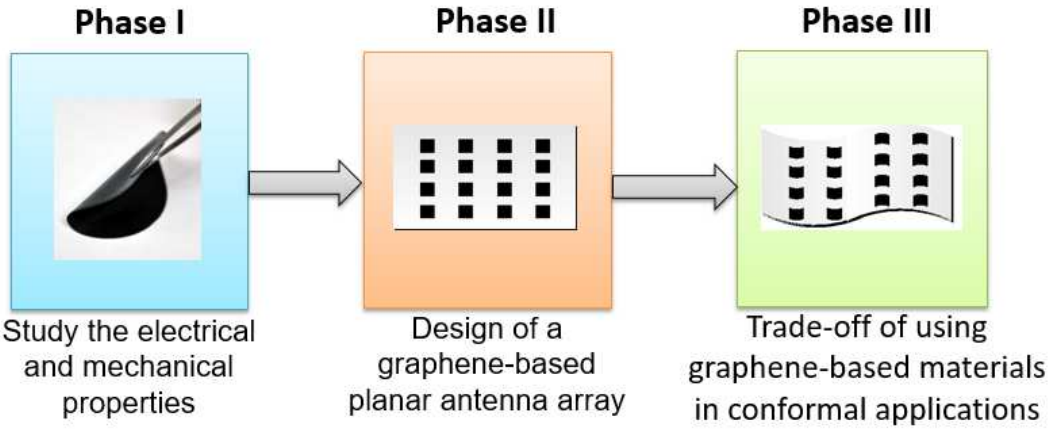

Figure 2.1. Block diagram and the phases of the proposed graphene-based conformal antenna array system.

- Phase II: In this phase, a graphene-based planar antenna array was designed and used to validate the electrical and mechanical properties on a flat surface.
- Phase III: Finally, in this phase, we discuss a mechanism for designing a conformal antenna array and trade-off of using graphene-based conductive materials for this purpose.

In summary, the development of a new graphene-based conformal antenna array the utilizes all the advantages of graphene-based materials and conformal antennas, opens up a completely new area of research.

3. DEVELOPMENT OF NEW MANUFACTURING TECHNIQUES WITH 97% CARBON CONTENT GRAPHENE-BASED CONDUCTIVE MATERIALS FOR ANTENNA APPLICATIONS

For this work, the potential of using 97% carbon content graphene-based conductors that are commercially available at Graphene Laboratories Inc. (part number: GRAPH-SHEET- 8×8-10) [44] and much thicker than a single layer for printed antenna purposes was explored.

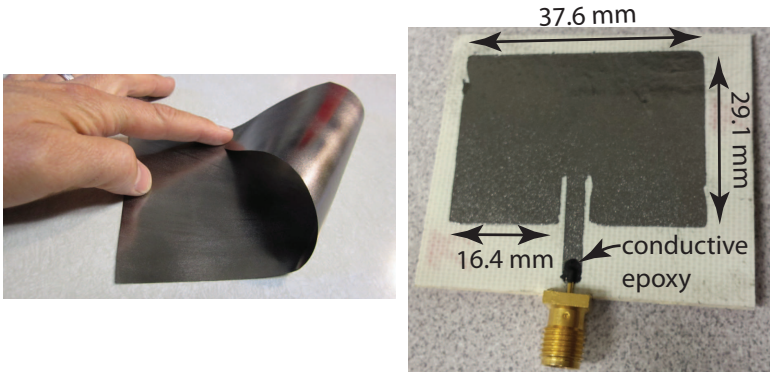

Figure 3.1. (a) Photograph of the commercially available flexible graphene-based conducting material and (b) a photograph of the prototype (with dimensions) of the fabricated graphene-based patch antenna.

3.1. The Manufacturing Process

Several steps are required to prepare the graphene-based conductor material in Figure 3.1(a) for manufacturing of a conformal microstrip antenna. Initially, the temporary spray adhesive (Sulky KK 2000 [45]) shown in Figure 3.3 is applied to the top surface of a 100 μm thick sheet of paper [46] and bonded to the bottom surface of the graphene-based conducting material (Figure 3.2). Next, the same spray adhesive is applied to the bottom surface of a 100-μm thick transparency film and bonded to the top surface of the graphene-based conducting material (also shown in Figure 3.2). As a result, the three layers are bonded together for manufacturing, giving the 3-layer structure

shown in Figure 3.2. The 3-layer structure is then placed on the adhesive cutting mat shown in Figure 3.3. The graphene-based conducting layer is now ready for cutting out the shape of the microstrip patch. It should be noted that the three layers were pressed together by hand and the temporary adhesive was cured at room temperature for 2 - 3 minutes before cutting. This allowed for the separation of the three layers after the cutting process was completed. Finally, the layout of the patch is defined in the software included with the micro-cutter, which is discussed at the end of this section.

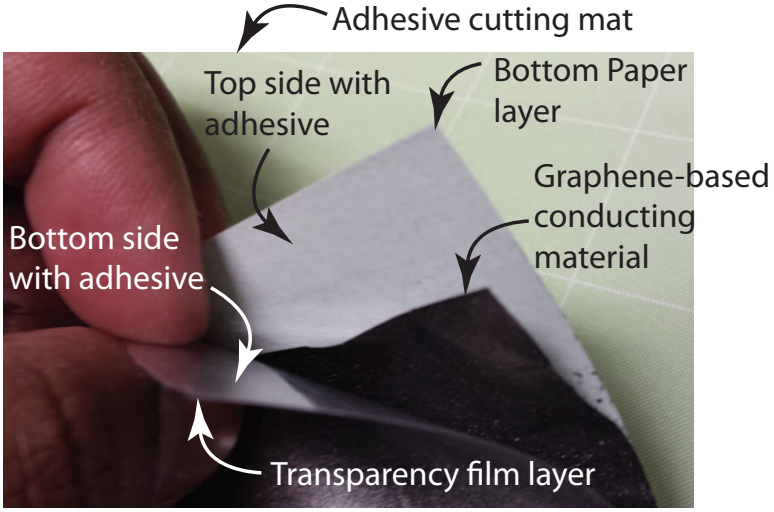

Figure 3.2. Photograph of the flexible graphene-based conductors placed in between different layers to fabricate the antenna.

Figure 3.3. Photograph of the commercial micro-cutter [47] and the temporary adhesive spray [45].

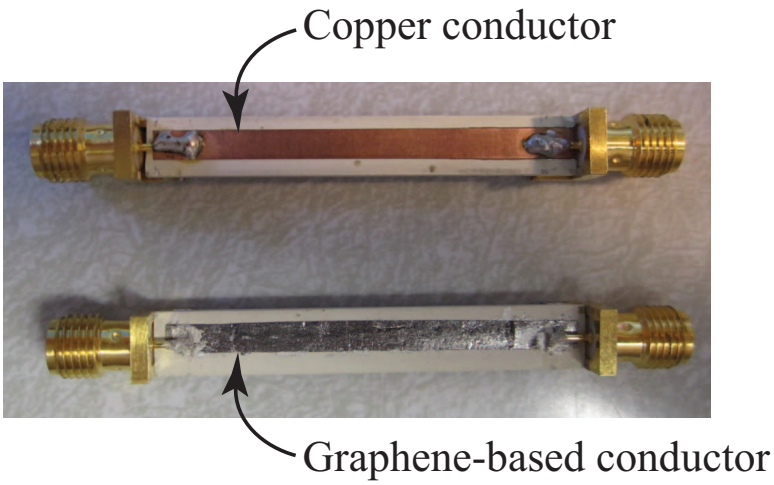

Figure 3.4. (top) Printed microstrip transmission line on a TMM4 substrate with a copper conductor and (bottom) printed microstrip transmission line on a TMM4 substrate with graphene-based conductors.

3.2. Extracting the Conductivity of the 97% Carbon Content Graphene-based Materials and Validation

3.2.1. Microstrip transmission line prototypes

For this extraction, the two geometrically similar printed microstrip TLs shown in Figure 3.4 were designed and evaluated in a manner to determine the conductivity of the graphene-based conductors. The top TL consisted of a printed copper conductor and the bottom TL had the copper conductor removed and replaced by the graphene-based conductors material in Figure 3.1(a). The SMA connectors were edge mounted, and wire glue conductive epoxy [48] (item number 0400) was used to attach the center pin to the surface of the graphene-based conductors. The top TL had 0.5-oz copper, and the thickness of the graphene-based conductors was measured to be 25 μm. Both TL prototypes have the same geometry (conductor width $W = 3.0$ mm and length $L = 41.0$ mm). The substrate is a 1.27 mm thick TMM4 material ($\varepsilon_r = 4.5$ and $\tan\delta = 0.002$), and both prototypes have identical copper ground planes on the bottom side. By choosing two geometrically similar designs, the attenuation constant of the graphene-based conductors could be determined in a well-known environment. Finally, it should be mentioned that the prototype TL with the copper conductor in Figure 3.4(top) was designed in ADS to have a characteristic impedance of $Z_o = 50$ Ω and the graphene-based conductor was attached to the TMM4 substrate with double-sided tape.

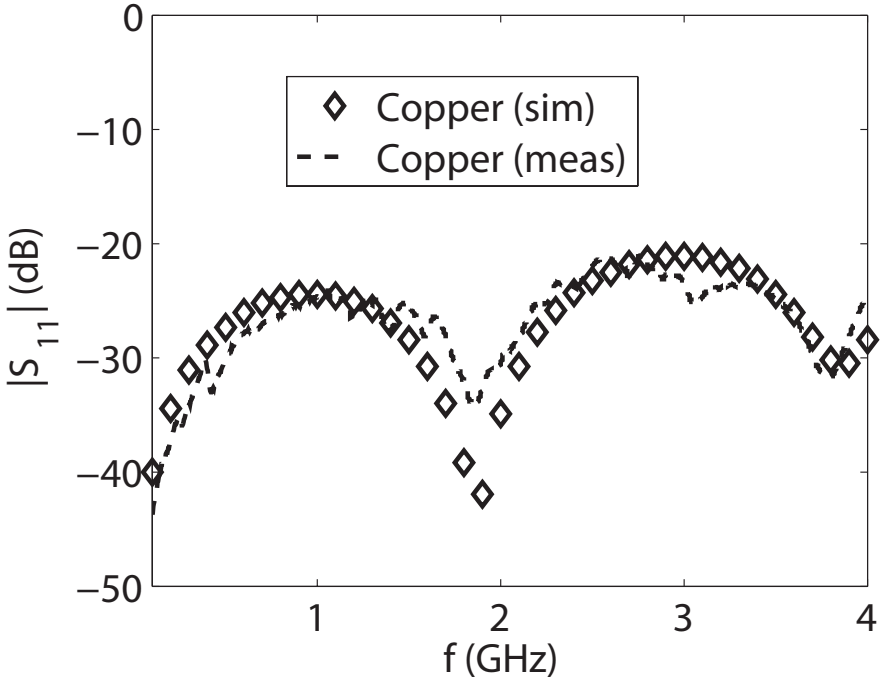

Figure 3.5. Simulated and measured $|S_{11}|$ values of the copper microstrip TL.

3.2.2. Conductivity extraction

First, the insertion loss introduced by the graphene-based conductors was demonstrated by comparing the measured S-parameters of the prototypes in Figure 3.4. The results from these measurements are shown in Figures 3.5 - 3.8. For both prototypes, the $|S_{11}|$ measurements in Figures 3.5 and 3.7 show a -10 dB BW from 100 MHz to 4.0 GHz. Next, of particular interest is the comparison between the $|S_{21}|$ values of the copper and graphene-based conductors TLs. The measurements in Figure 3.6 show that $|S_{21}| < 0.5$ dB for the copper TL and that $|S_{21}| < 1.0$ dB for the graphene-based TL. Using this additional 0.5 dB of loss over the band of interest, and the known length and width of the TL, the attenuation constant was computed to be $\alpha_c = 1.5$ Np/m [49]. Then using sheet resistance,

$$R_s = \alpha_c ZoW \tag{3.1}$$

and

$$R_s = \sqrt{\omega\mu_0/2\sigma}, \tag{3.2}$$

the conductivity was determined to be $\sigma = 1.94 \times 10^5$ S/m.

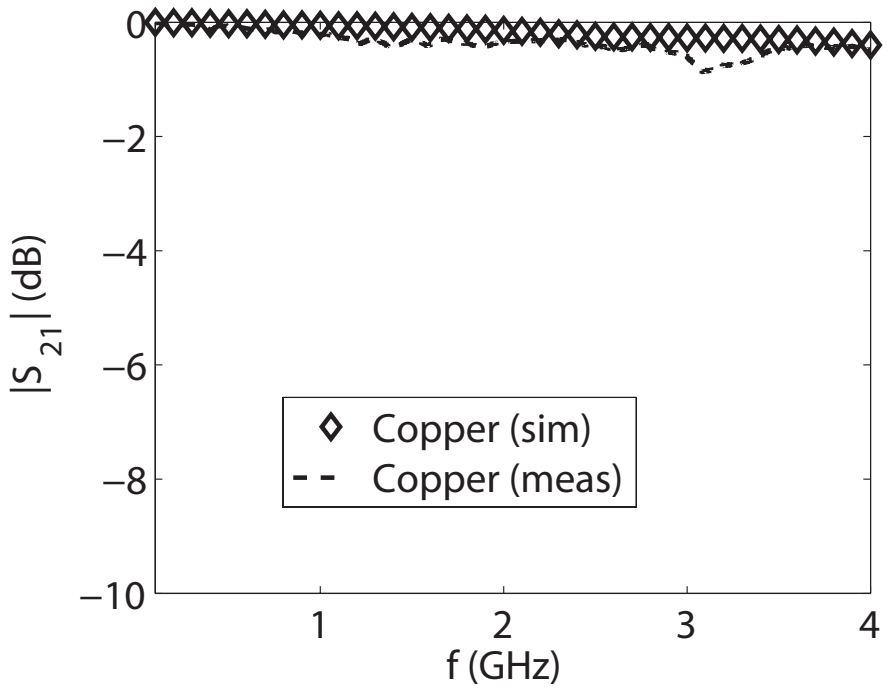

Figure 3.6. Simulated and measured $|S_{21}|$ values of the copper microstrip TL.

Next, using the conductivity extracted from analytical computations and measurements, the graphene-based TL was modeled in ADS. The simulated results for both the copper and graphene-based TLs are also shown in Figures 3.5 - 3.8. The simulation results in Figure 3.8 compute the extra 0.5 dB of loss introduced by the graphene-based conductors; indicating a good model in ADS.

3.2.3. Microstrip patch antenna prototoypes

Two prototype microstrip patch antennas for operation at 2.57 GHz were designed (on the same grounded 0.5 oz copper TMM4 substrate as the TLs) to further validate the extracted conductivity of the graphene-based conductors. In a manner similar to the TLs, a prototype with a copper conductor and a geometrically similar patch with graphene-based conductors was designed in ADS, manufactured and tested. The prototype antennas are shown in Figure 3.9. Again, by using similar geometries, the introduction of the graphene-based conductors into the design could be examined. The main properties of interest for these experiments were the $|S11|$ values and the gain at 2.57 GHz. The simulated and measured $|S_{11}|$ values are shown in Figures 3.10 and 3.11 for the copper and graphene-based conductors conductors, respectively. Good agreement is shown overall.

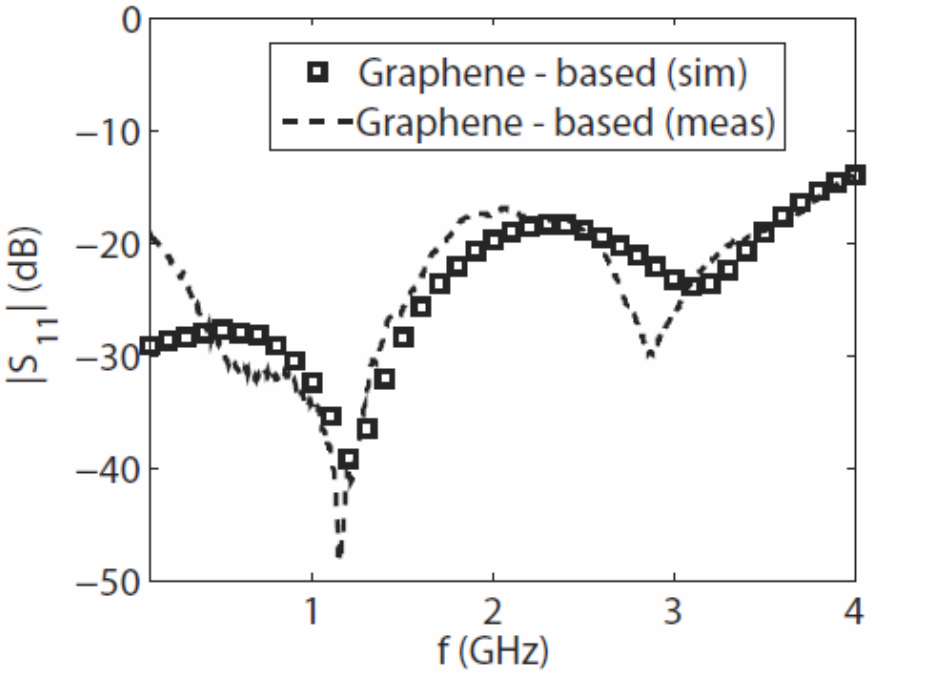

Figure 3.7. Simulated and measured $|S_{11}|$ values of the graphene-based conductors microstrip TL.

Then, the gain of the prototype antenna with the graphene conductor was computed in ADS and compared to the measured gain in the full anechoic chamber. The simulated gain was G_{sim} = 2.87 dBi and measured to be G_{meas} = 2.5 dBi. A good comparison validated the graphene-based conductor model in ADS.

3.3. Design and Evaluation of the Prototype Microstrip Patch Antenna

To develop the patch antenna in Figure 3.1, the conductive properties of the graphene-based material [44] were determined by measuring the S-parameters of a known printed microstrip transmission line that used the graphene-based conductors instead of copper. The conductivity was determined to be $\sigma = 1.94\times10^5$ S/m for a thickness of 25 μm. Next, this thickness and conductivity were used in the commercial simulation software ADS [50] to determine the geometry of the patch antenna shown in Figure 3.1(b). The simulated S-parameters are shown in Figure 3.13. The resonant frequency was predicted to be 2.4 GHz and the grounded FR4 substrate was 1.5 mm thick with ε_r = 4.5 (the bottom layer of the FR4 was 0.5 oz copper). Then, this geometry was drawn in the software included with the micro-cutter and used to cut out the graphene-based conducting layers shown in Figure 3.12. As a final step, the graphene-based conducting patch was removed

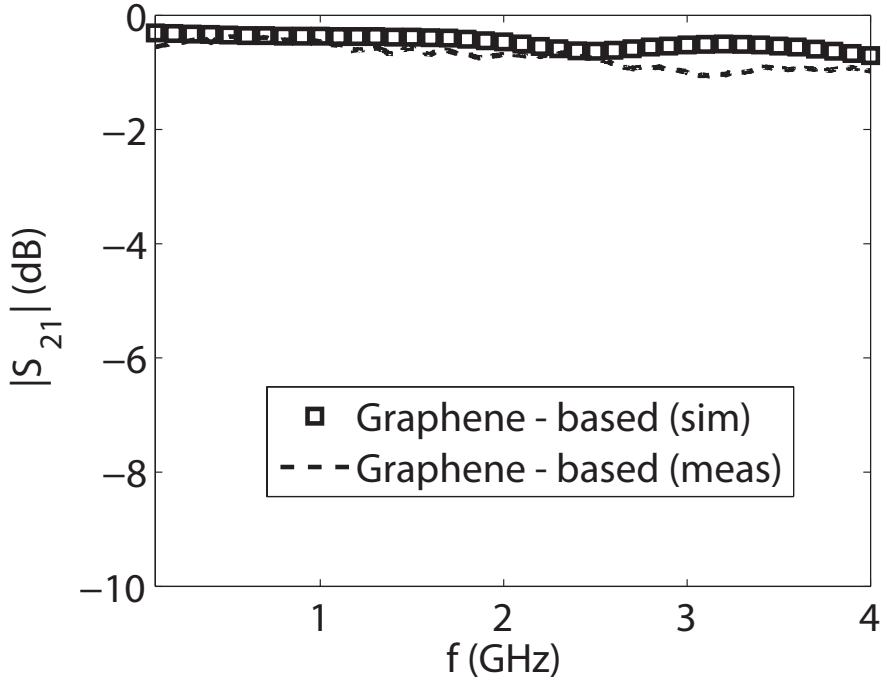

Figure 3.8. Simulated and measured $|S_{21}|$ values of the graphene-based conductors microstrip TL.

from the 3-layer structure and attached to the FR4 substrate. The result was the manufactured prototype shown in Figure 3.1(b). The center conductor of the SMA connector was attached to the patch with conductive epoxy. Next, the $|S_{11}|$ values of the prototype were measured in an anechoic chamber and are shown in Figure 3.13. The resonant frequency was 2.6 GHz.

3.4. Discussion

Several comments can be made about the results in Figure 3.1(b) and 3.13. Closer observation of the edges in Figure 3.1(b) shows that the micro-cutter blade tends to wobble slightly during cutting, which may be the cause of the differences in the S-parameters in Figure 3.13. This behavior could be due to the blade depth setting and further exploration has been planned for the near future. On the other hand, the results in Figure 3.13 show that a new patch antenna can be developed using this flexible graphene-based material, which may otherwise be difficult to otherwise manufacture with the existing PCB techniques.

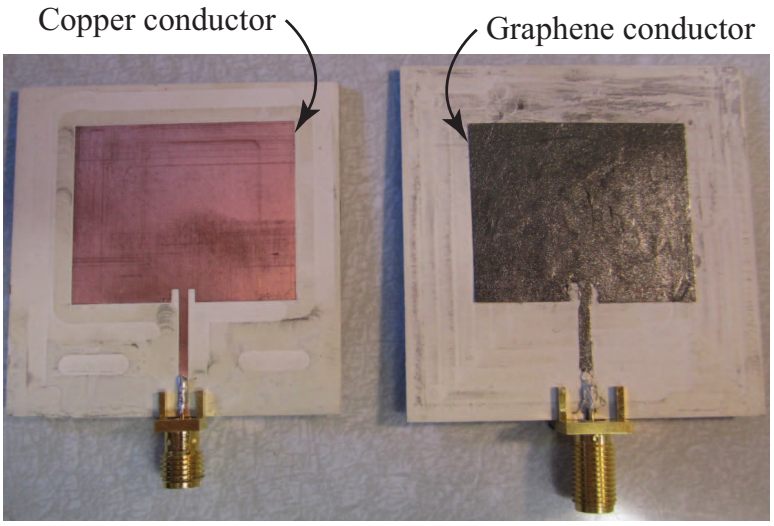

Figure 3.9. (left) Printed microstrip patch antenna on a TMM4 substrate with a copper conductor and (right) printed microstrip patch antenna on a TMM4 substrate with a graphene-based conductor.

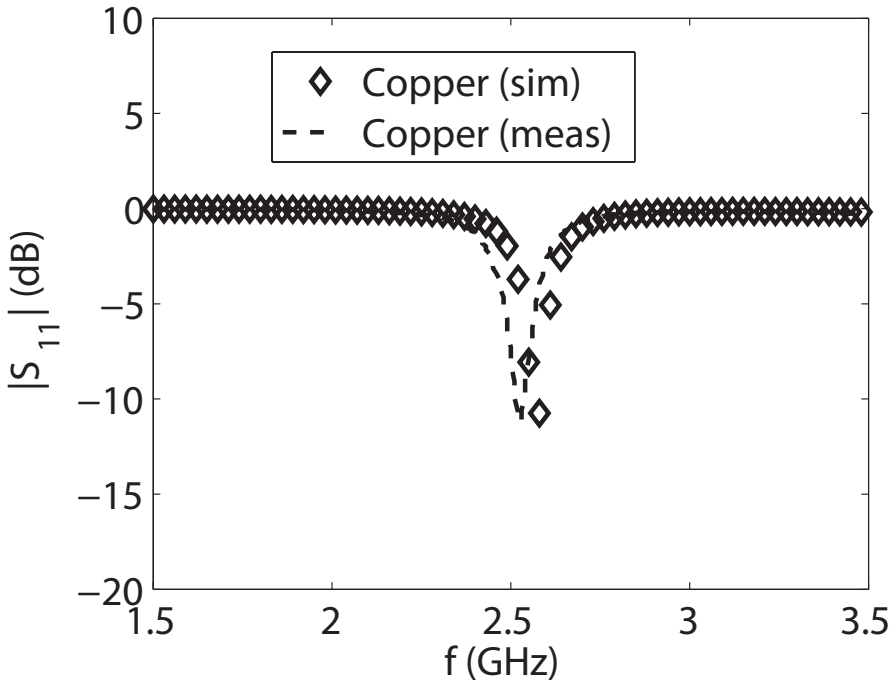

Figure 3.10. Measured and simulated $|S_{11}|$ values of the prototype microstrip patch antenna with the copper conductor.

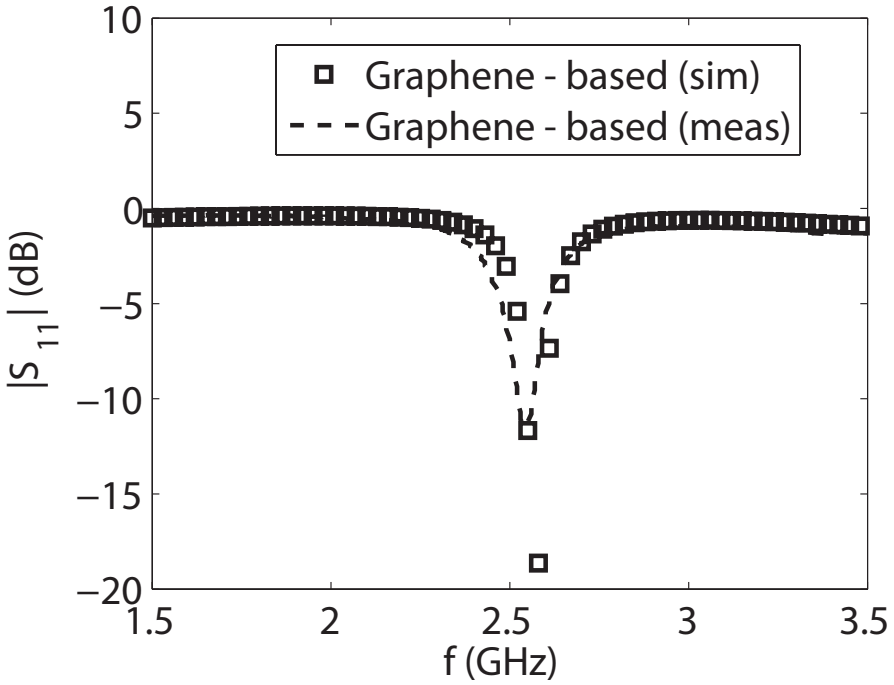

Figure 3.11. Measured and simulated $|S_{11}|$ values of the prototype microstrip patch antenna with the graphene conductor.

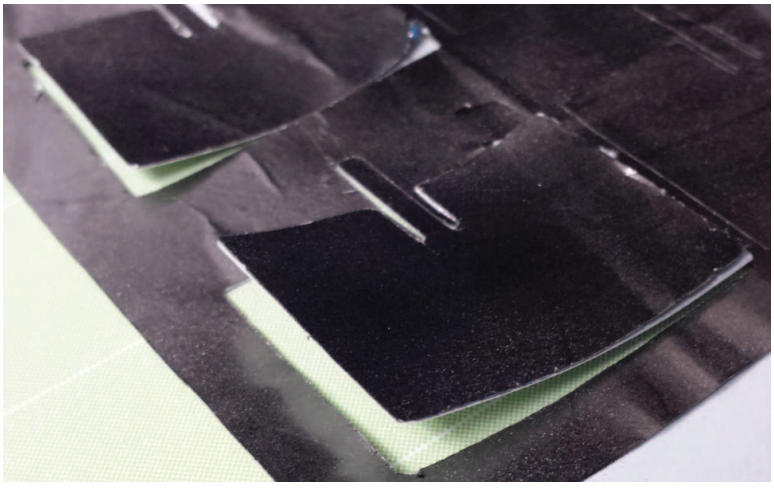

Figure 3.12. Fabrication step to separate the flexible graphene-based conducting layer of the patch from the protected layers.

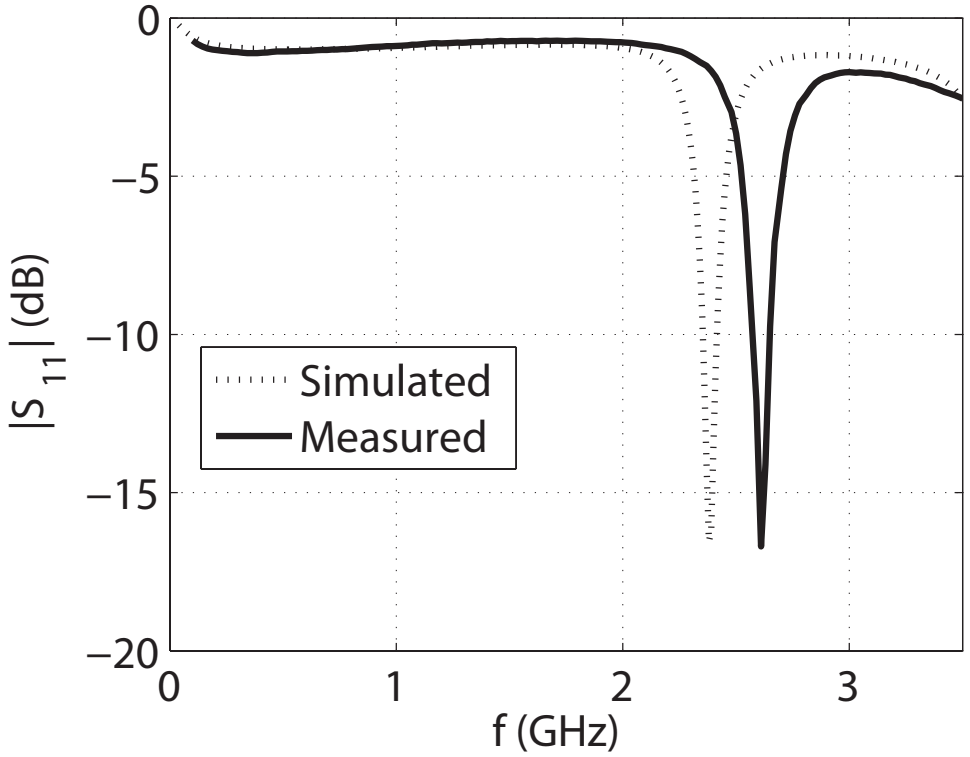

Figure 3.13. Measured and simulated $|S_{11}|$ values of the prototype graphene-based antenna.

4. DETERMINING PROPAGATION CHARACTERISTICS OF THE 97% CARBON CONTENT GRAPHENE-BASED CONDUCTORS

Microstrip antennas are the promising candidates for microwave applications, where the emphasis is on reducing the volume and weight, especially when conformal antenna arrays are needed. These antenna arrays, however, show gain and efficiency limitations due to ohmic and dielectric losses in the feed network caused by the unwanted coupling within it, and due to surface wave excitation in the dielectric substrate [51, 21]. This unwanted coupling between TLs in the long and complicated feed network has been a serious design issue as the efficiency limitations are most severe in large arrays due to high losses at high frequencies. As reported in [52], reducing the losses in the feed network of these antenna arrays significantly improves the gain and overall efficiency. Copper microstrip TLs have been the preferred choice when designing the feed network for antenna arrays, but, besides other drawbacks, they tend to fail and crack in conformal applications [8]. The demand for various new composite materials with structural strength and high electrical conductivity has hence been increasing to fill this gap. The 97% carbon content graphene-based conducting (GBC) sheet is flexible and provides good electrical conductivity [13]; therefore it is considered to be a good candidate for conformal applications [1].

4.1. Flat Transmission Line(TL) Comparison

Here, replacing the copper conductors with 97% carbon content graphene-based conductors (GBC) [44] as shown in Figure 4.1(a) for TLs has been investigated. Also the coupling between a conventional copper microstrip and a GBC TL, as well as two parallel GBC TLs manufactured on the same substrate have been studied and analyzed. The results show that the GBC TLs can be used as an alternative to copper TL with some limitations but are more flexible, light weight, and give better results for unwanted coupling at high frequencies.

[1] A part of the materials in this chapter was co-authored by Sayeed Z. Sajal. He was involved with this work and he was responsible for the fabrication, simulation and measuring the prototype. Sayeed Sajal was the one of the key developers of this work and some of his ideas were implemented in this work.

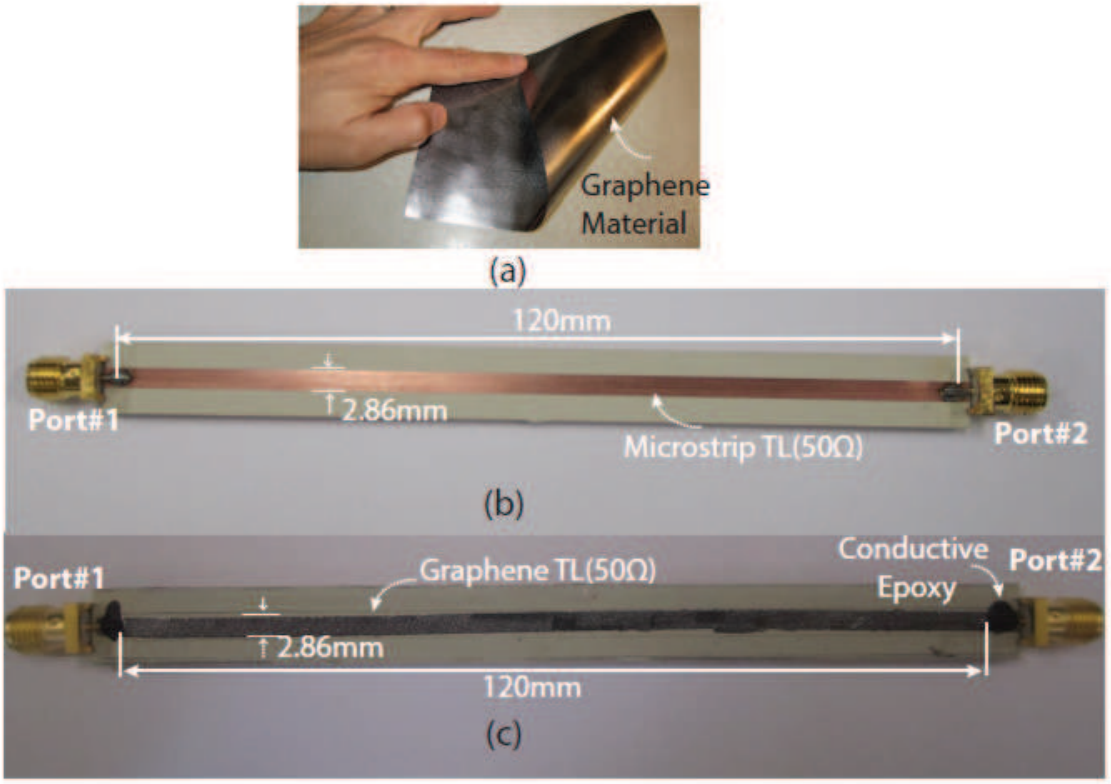

Figure 4.1. (a) Commercially available graphene-based conducting material, (b) conventional microstrip transmission line (TL) and (c) graphene-based conductors (GBC) TL.

4.1.1. Prototypes of the conventional copper and graphene-based conductors (GBC) transmission lines (TLs) on a flat surface

As illustrated in Figure 4.1(b) and (c), two similar 50 Ω TLs (a conventional microstrip and a GBC) were first fabricated on TMM4 substrate ($\varepsilon_r \approx 4.5$, tan δ= 0.0020 and thickness, T_s = 1.52 mm) with copper ground plane on the bottom side. The S-parameters of the microstrip TL were first simulated using commercially available full-wave simulator Keysight's Advanced Design System (ADS) [50] and later measured in an anechoic chamber with a calibrated vector network analyzer, E5071C. Simulated and measured results agreed well with the simulations and served as a reference in designing the GBC TL. The manufacturing process of GBC TL was adapted from the method reported in [53]. A 2.86-mm wide and 120-mm long graphene-based conductor was first glued on the top surface of the substrate and then connected to the 50-Ω SMA connector using conductive epoxy.

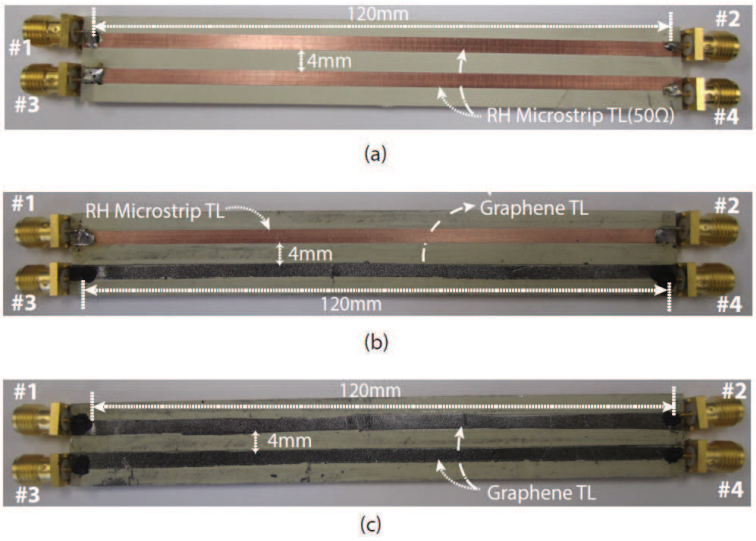

Figure 4.2. Detailed pictures of (a) two 50-Ω microstrip TLs, (b) a microstrip Cu and a GBC TL, (c) and two GBC TLs.

For the comparison of unwanted coupling measurements, three prototypes as shown in Figure 4.2(a), (b) and (c), were manufactured and tested. Similar geometries were used on the same substrate (with copper ground plane) for all the prototypes to investigate the unwanted coupling.

In order to measure the near-end coupling, port 2 and 4 were terminated with the 50 Ω load, while the other two ports (1 and 3) were connected with the network analyzer for measurements. Similarly, far-end coupling was measured by terminating ports 2 and 3, while measurements were taken at ports 1 and 4.

4.1.2. Results and discussion

Results of the matching performance and wave propagation of microstrip and GBC TLs are shown in Figure 4.3 and Figure 4.4, respectively. Compared to the microstrip TL, it can be observed from Figure 4.3 that the GBC TL also has a good matching performance up to 8.5 GHz. Figure 4.4 shows the wave propagation of the simulated and measured microstrip TLs and the measured GBC TL. As illustrated, the $-3\ dB$ point (50% power loss)of the GBC TL was at 7 GHz, which shows its limitations at high frequencies.

Figure 4.5 shows the comparison of the simulated and measured near-end coupling between the two microstrips TLs, measured microstrip−GBC TLs as well as the two GBC TLs. It was

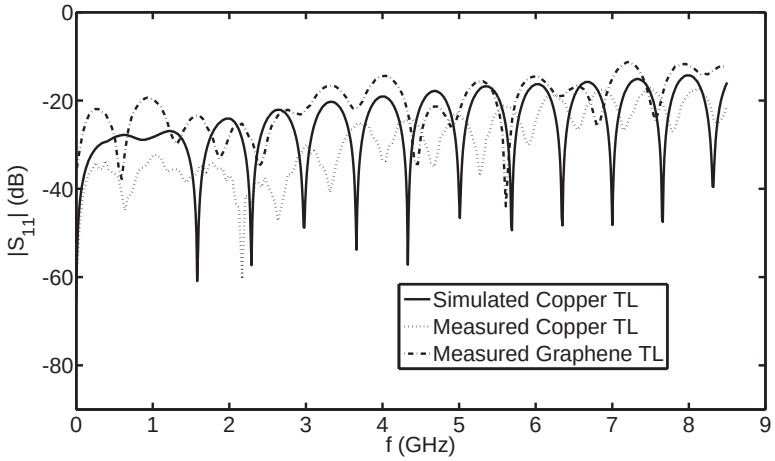

Figure 4.3. Matching performance ($|S_{11}|$(dB)) of the microstrip Cu and GBC TLs.

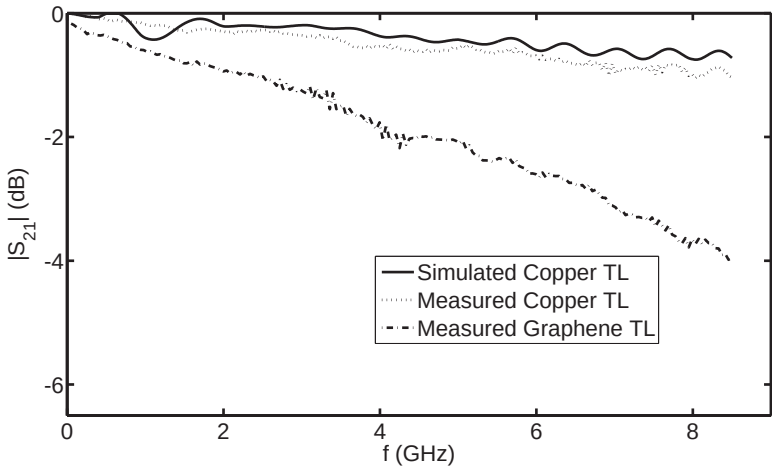

Figure 4.4. Magnitude of forward transmission ($|S_{21}|$(dB)) of the microstrip Cu and GBC TLs.

observed that the two parallel GBC TLs have better isolation up to 8.5 GHz, which is much better than the two equally spaced conventional microstrip TLs and conventional microstrip−GBC TLs.

The far-end coupling in terms of $|S_{41}|$ (dB) for the prototypes was depicted in Figure 4.6. This result shows that the far-end coupling does not exhibit any oscillations for the case of microstrip−microstrip TLs, microstrip−GBC TLs and the two parallel GBC TLs. In the case of two parallel microstrip TLs, the magnitude of the sine function is not large enough to cause oscillations [54], this phenomenon may occur for two parallel GBC TLs too. Hence it is argued that the microstrip−GBC TLs and the two parallel GBC TLs exhibit similar behavior to that of the two parallel microstrip TLs.

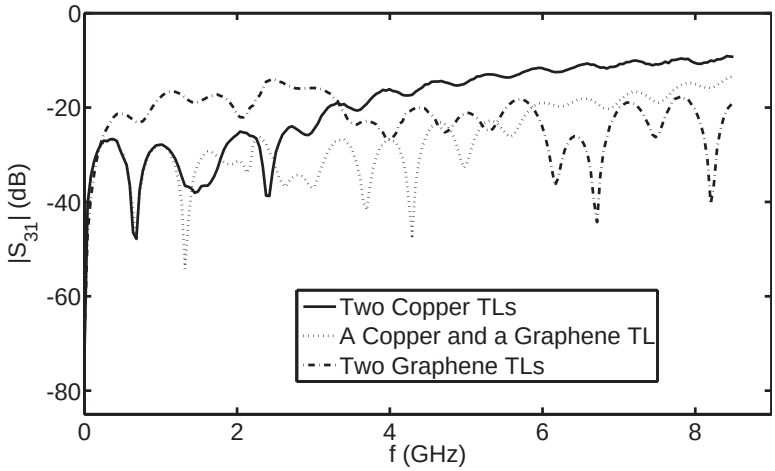

Figure 4.5. Magnitude of near-end coupling ($|S_{31}|$(dB)) between the microstrip Cu and GBC TLs.

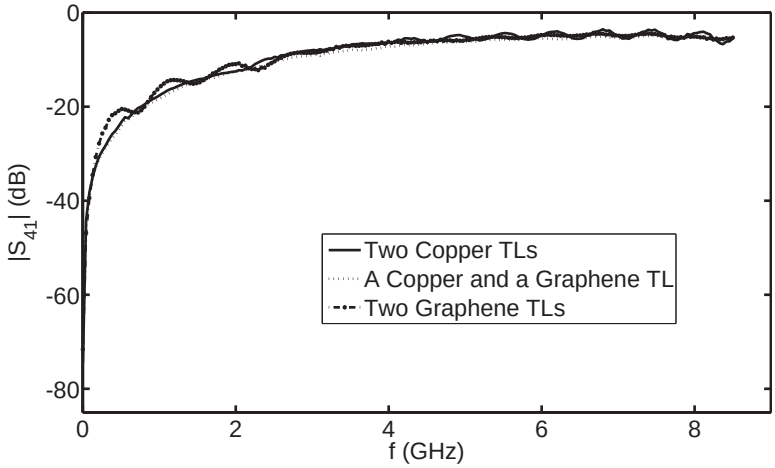

Figure 4.6. Magnitude of $|S_{41}|$(dB) (far-end crosstalk) of microstrip Cu and GBC TLs.

Carbon microfiber TLs were investigated for feed network in arrays [55], but it was observed that GBC TLs have better potential to be used as an alternative to the conventional TLs for conformal feed network applications. Finally, the DC resistances of the fabricated microstrip and GBC TLs, as shown in Figure 4.1 (b) and (c) have been measured using a *GW Instek*-819 *LCR* meter and found to be 0.0471 Ω and 1.44 Ω, respectively.

4.2. Conformal Transmission Line(TL) Comparison

Graphene-based conformal TL behavior was investigated in an experimental study [56]. Here, the near-field and far-field coupling were investigated on any conformal shapes of a microstrip copper TLs and 97% carbon content graphene-based TLs.

4.2.1. Prototypes of the conventional copper and graphene-based conductors (GBC) transmission lines (TLs) on a conformal surface

The conformal transmission line prototype was fabricated on a flexible Rogers RT duroid 6002 substrate (thickness = 0.508 mm; $\varepsilon_r \approx 2.94$; $\tan\delta = 0.0012$) with 35 μm copper cladding on both sides. 50-Ω TL is designed for both copper and 97% carbon content graphene-based conductive (GBC) materials. Then, both the TLs were fabricated using LPKF [57], and the GBC trace was precisely cut using the technique mentioned in [53]. Then the GBC trace was glued on the flexible substrate using conductive glue [45], and an SMA connector was connected using conductive epoxy [48]. The designed length and width of the TL are 78 mm and 1.3 mm. The fabricated prototype is shown in Figure 4.7.

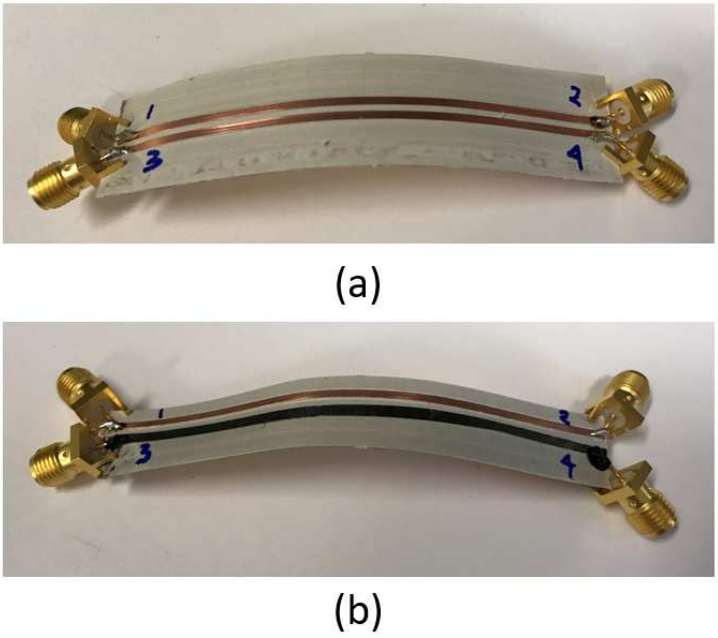

Figure 4.7. Detailed pictures of (a) two 50-Ω microstrip copper TLs on a conformal surface, (b) a microstrip copper and a GBC TL on a conformal surface.

4.2.2. Results and discussion

Here, the S-parameters of the TLs were measured on conformal shapes using a calibrated vector network analyzer (VNA). Results of the matching performance and wave propagation of copper microstrip TL and GBC TLs on a corformal surface are shown in Figure 4.8 and Figure 4.9,

respectively. Comparing to the microstrip TL, it can be observed from Figure 4.3 that the GBC TL also has a good matching performance from 100 MHz to 4 GHz. Figure 4.9 shows the wave propagation of the simulated and measured microstrip TLs and also the measured GBC TL on a conformal surface. As illustrated, it were almost identical except in the 2.5 GHz to 3 GHz range.

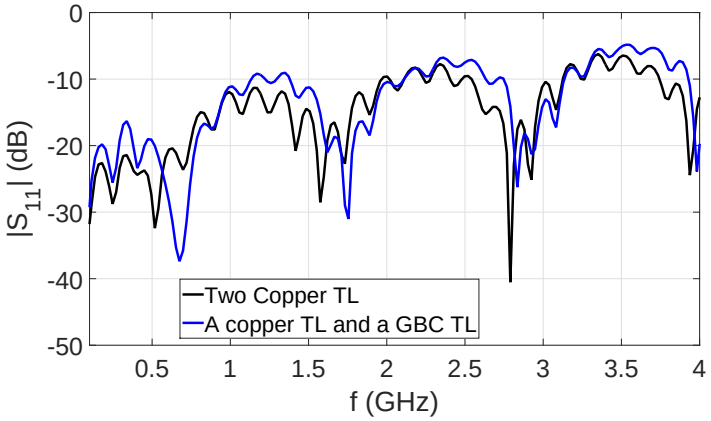

Figure 4.8. Matching performance ($|S_{11}|$(dB)) of the microstrip copper and GBC TLs on a conformal surface.

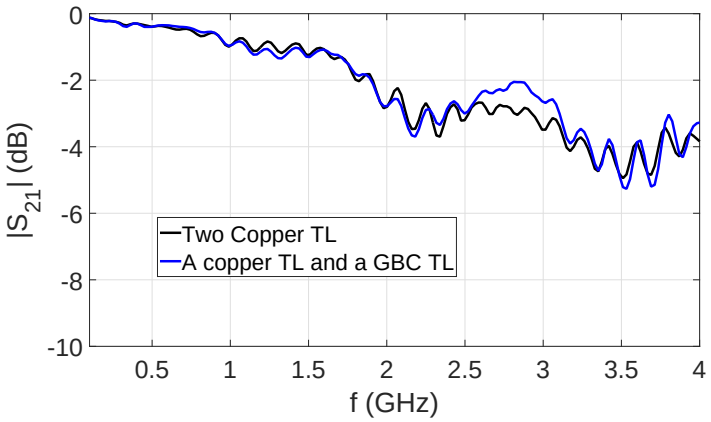

Figure 4.9. Magnitude of forward transmission ($|S_{21}|$(dB)) of the microstrip copper and GBC TLs on a conformal surface.

Figure 4.10 shows the comparison of the simulated and measured near-end coupling between the two microstrip copper TLs, measured microstrip copper−GBC TLs. It can be seen that the

results did not match completely, but did follow a similar trend.

The far-end coupling in terms of $|S_{41}|$ (dB) for the prototypes on a conformal surface is depicted in Figure 4.11. This result shows that the far-end coupling did not exhibit any oscillations in the case of copper−copper TLs and copper−GBC TLs. The results are only around 5 dB off from each other. It is hence argued that the copper−copper TLs and microstrip copper−GBC TLs exhibited similar behavior on a conformal surface. Overall, in both cases (flat TLs and conformal TLs), 97% carbon content graphene-based conductive material exhibited superior elecrical properties compared to copper.

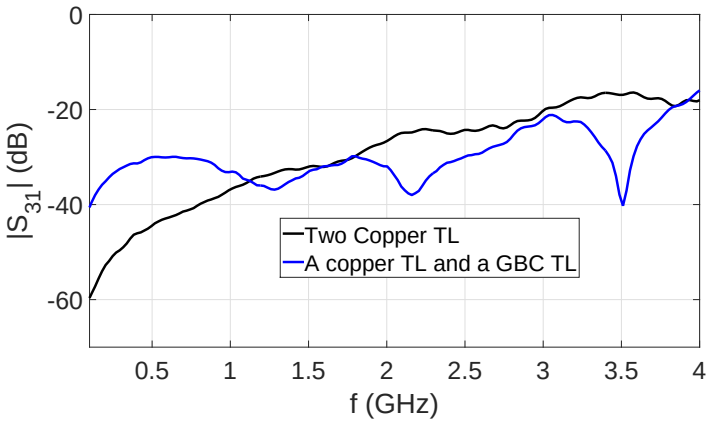

Figure 4.10. Magnitude of near-end coupling ($|S_{31}|$(dB)) between the microstrip copper and GBC TLs.

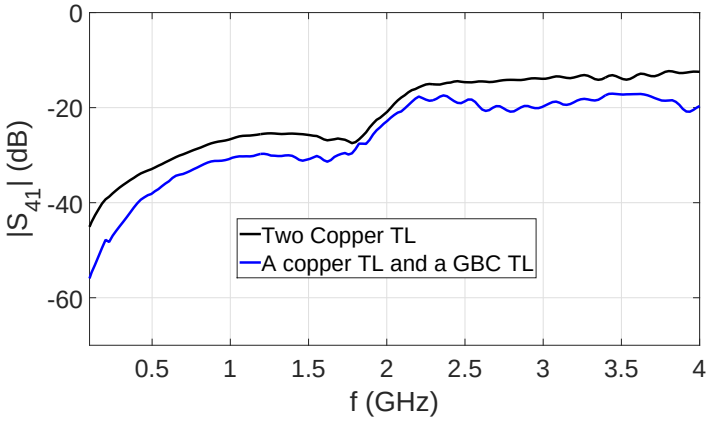

Figure 4.11. Magnitude of $|S_{41}|$(dB) (far-end crosstalk) of microstrip copper and GBC TLs.

5. MECHANICAL PROPERTIES OF 97% CARBON CONTENT GRAPHENE-BASED CONDUCTORS

Though many flexible substrates are being developed, conductive materials tend to be fragile and unable to withstand repetitive bending. Therefore, understanding the bending characteristics of different conductive materials is an important area to study. Here, the study of bending characteristics of different conductive materials in particular copper, aluminum, and 97% carbon content graphne-based conductive materials as transmission lines is presented. A fixture was developed to experimentally determine the bending characteristics of different TLs. In the experiment copper, aluminum, and ghaphene-based conductive materials were tested. The results were that on average, after 57 iterations the aluminum connection failed; after 74 iterations the copper connection failed; but no failure was observed in the graphene-based conductors even after 750 iterations which demonstrates the additional mechanical benefits of the graphene-based conductors. It was also shown that all the materials agreed on S-parameters in full wave simulation. Graphene-based conductive materials showed its superior reliability without compromising the performance on the TL.

5.1. Motivation

Conformal transmission lines, as well as conformal antennas, have been used for many years when needed on surfaces that are not flat [58, 59, 60, 61, 62, 63, 64]. Bending is present for any conformal application such as wearables [65, 66]. One of the challenges of the conformal transmission line, or antenna, is to ensure flexible substrates and conductive materials. Much research has been done to investigate flexible substrates [67, 68]. But bending on a specific spot could degrade the quality of connections in a transmission line. To test the bending characteristics, it is very important to study the reliability of the connections on transmission lines with different conductive materials. Here to understand and demonstrate the capabilities of a conformal surface, three materials (aluminum, copper, and graphene-based) have been studied. A full-wave simulation was also used to validate the transmission quality of the three conductive materials.

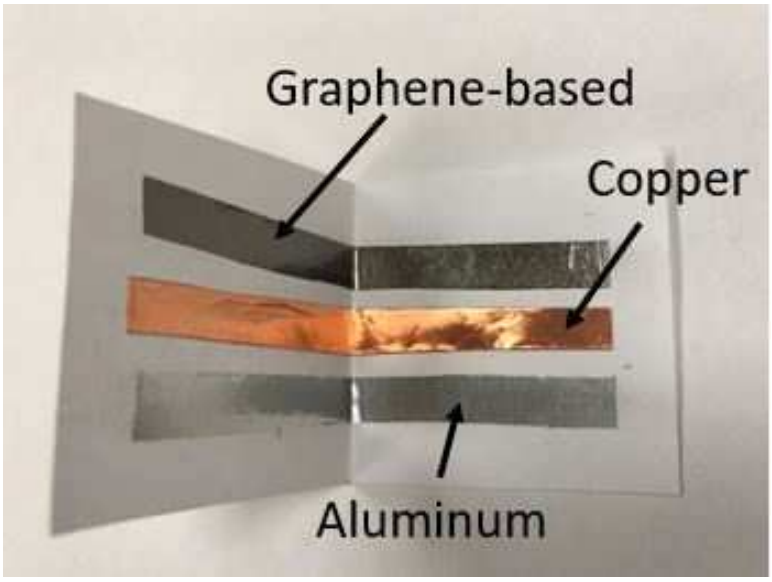

Figure 5.1. Layout of the TL on paper for bending experiment.

5.2. Simulation Results on Transmission Lines

Here we studied the three conductive materials as a transmission line (TL) shown in Figure 5.1. To study the transmission line S-parameters, Rogers TMM4 [69] was used as the substrate (ϵ= 4.5 and tan δ= 0.002). Three different conductive materials such as aluminum (σ =3.69×10^7 S/m, thickness of 25 μm), copper(σ =5.85×10^7 S/m, thickness of 25 μm) and graphene-based [44] (σ =1.94×10^5 S/m, thickness of 25 μm) were used to show the S-parameter agreement. These transmission lines were modeled in ADS [50]. The $|S_{11}|$, $|S_{12}|$, $|S_{21}|$, $|S_{22}|$ values of the TLs using different conductive materials are shown in Figures 5.2, 5.3, 5.4 and 5.5, respectively. The length of the TL was 65 mm and width was 2.86 mm. The frequency sweep was performed from 500 MHz to 4.5 GHz. It was found that all the S-parameter results agreed well. In the S-parameter analysis, the graphene-based and aluminum overlapped in a way that we hardly can see three lines for three conductive materials.

5.3. Development of Test Fixture and Measurement Results

The mechanical properties of the three conductors were experimentally studied. A text fixture was developed for bending experiments, consisted of two planar surfaces connected on one edge with a pivoting hinge, as shown in Figure 5.6. Next, three samples made of aluminum, copper and the graphene-based conductors were attached to the test fixture. The length of each sample

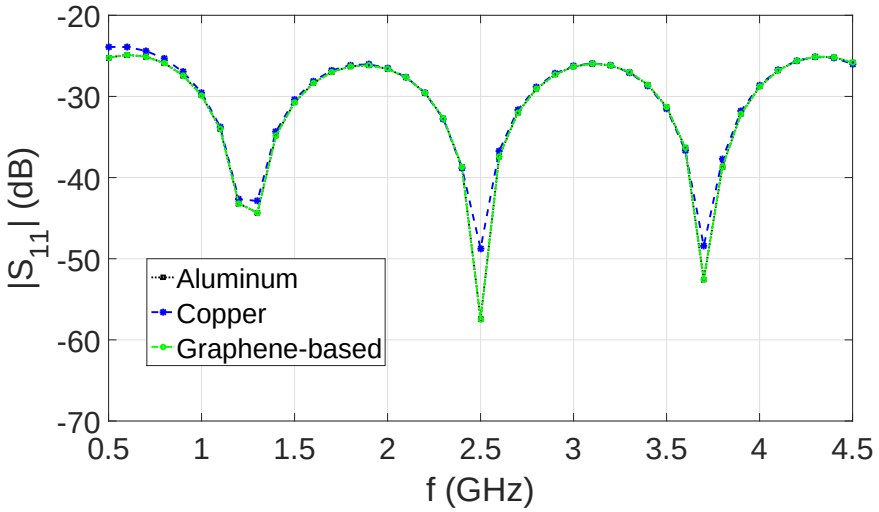

Figure 5.2. A comparison of $|S_{11}|$ values of the 50-Ω transmission line on three different conductive materials (aluminum, copper and graphene-based) using full-wave simulations in ADS.

was 65 mm and the width was 2.86 mm. The thickness of all conductive layers was 25 μm. The angle θ was varied from 0 to 110 degrees at a rate of approximately 37 bends/min. The experiment was conducted on 3 samples. On average, after 57 iterations, the aluminum connection failed, as shown in Figure 5.7; after 74 iterations, the copper connection failed, as shown in Figure 5.8. Then, the fixture conducted 750 iterations on the graphene-based conductors and no failure was observed; showing the additional mechanical benefits of the graphene-base conductors.

5.4. Discussion

In this chapter, we investigated three different conducive materials to study the bending characteristics. We found that all three conductive materials (aluminum, copper, and graphene-based) agreed on S-parameter results. In bending experiments, we found that graphene-based material is more than 13 times reliable compared to aluminum and 10 times more reliable than copper in terms of bending iterations. Overall, the electrical performance of the graphene-based conductor was comparable to that of the aluminum conductor and the copper conductor for the designs investigated in this work, indicating that the graphene-based conductors have the potential to be used in the development of more robust conformal antennas without the trade-off of electrical performance. This opens the door to investigate many applications where we can use the superior reliability of graphene-based conductors as an alternative to aluminum and copper conductors.

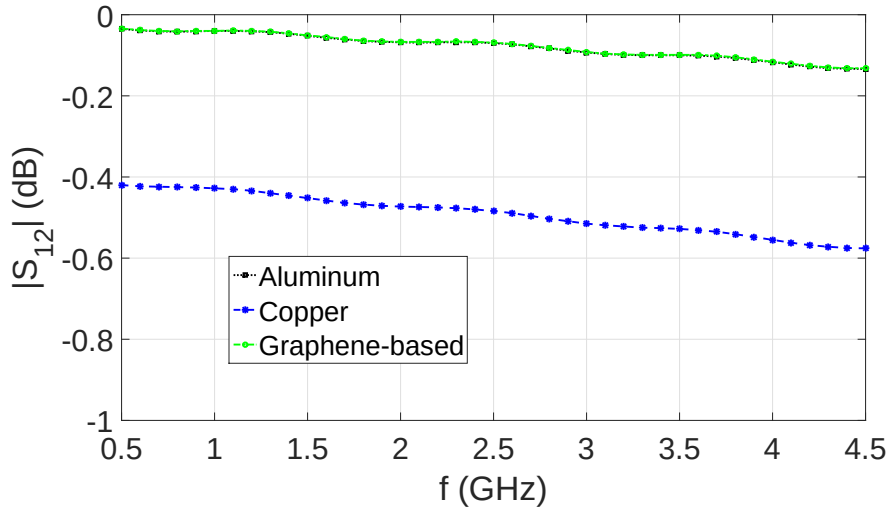

Figure 5.3. A comparison of $|S_{12}|$ values of the 50-Ω transmission line on three different conductive materials (aluminum, copper and graphene-based) using full-wave simulations in ADS.

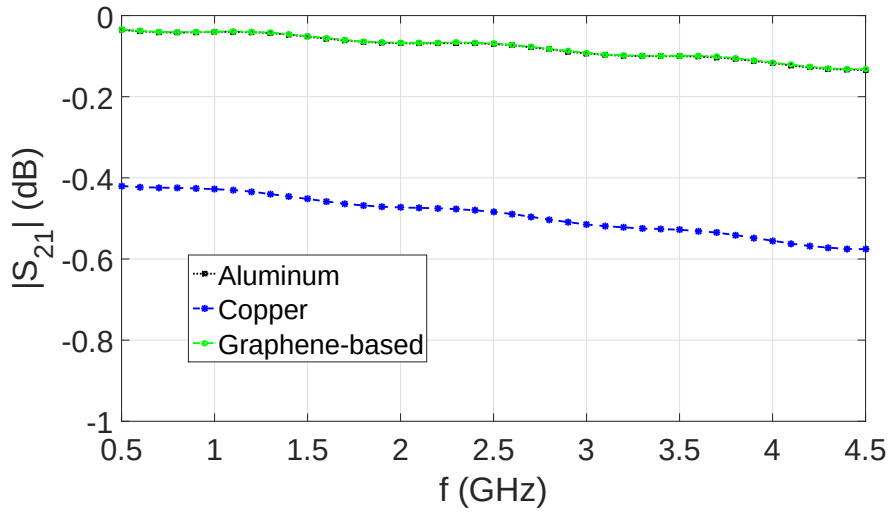

Figure 5.4. A comparison of $|S_{21}|$ values of the 50-Ω transmission line on three different conductive materials (aluminum, copper and graphene-based) using full-wave simulations in ADS.

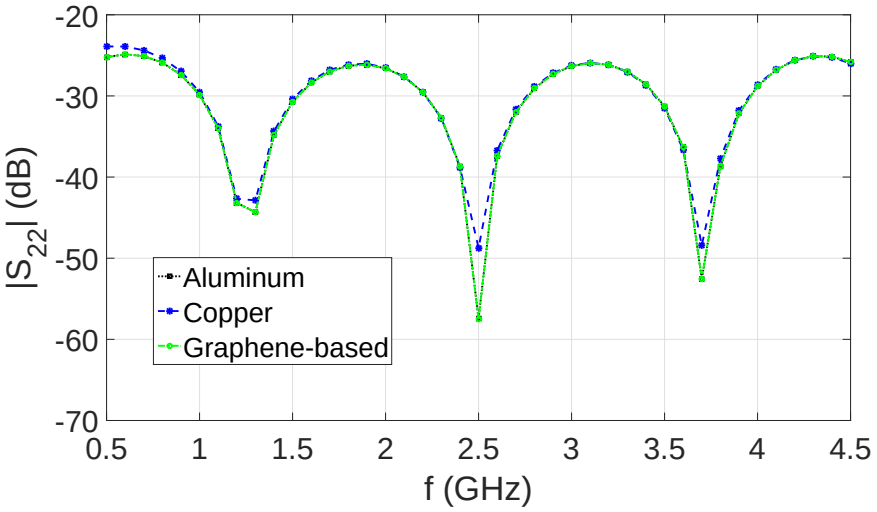

Figure 5.5. A comparison of $|S_{22}|$ values of the 50-Ω transmission line on three different conductive materials (aluminum, copper and graphene-based) using full-wave simulations in ADS.

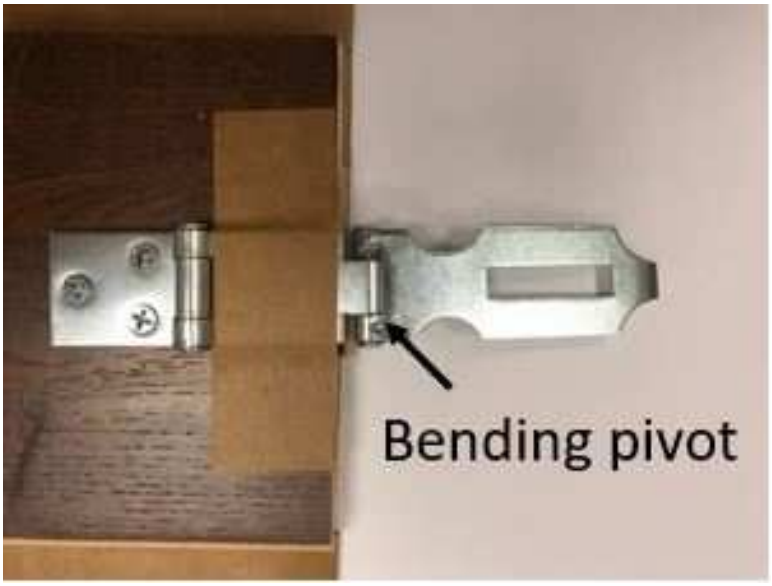

Figure 5.6. Developed test fixture for bending experiment.

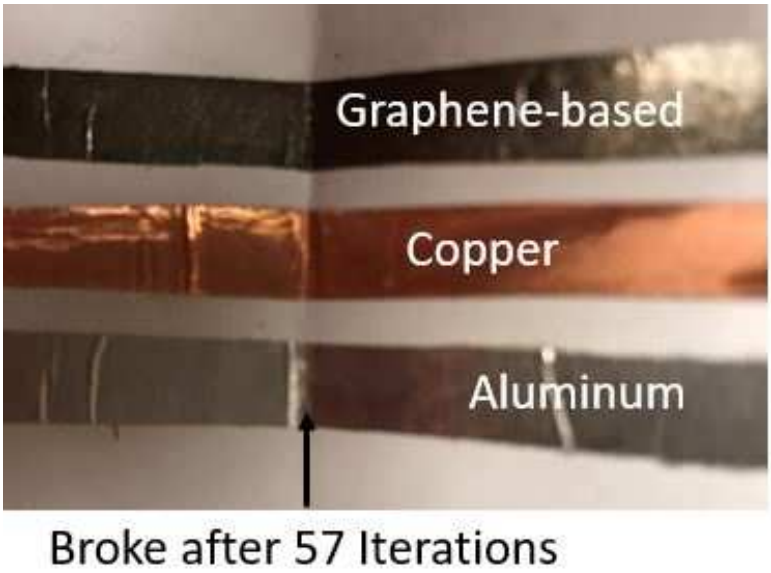

Figure 5.7. Breakdown of aluminum after 57 bending iterations.

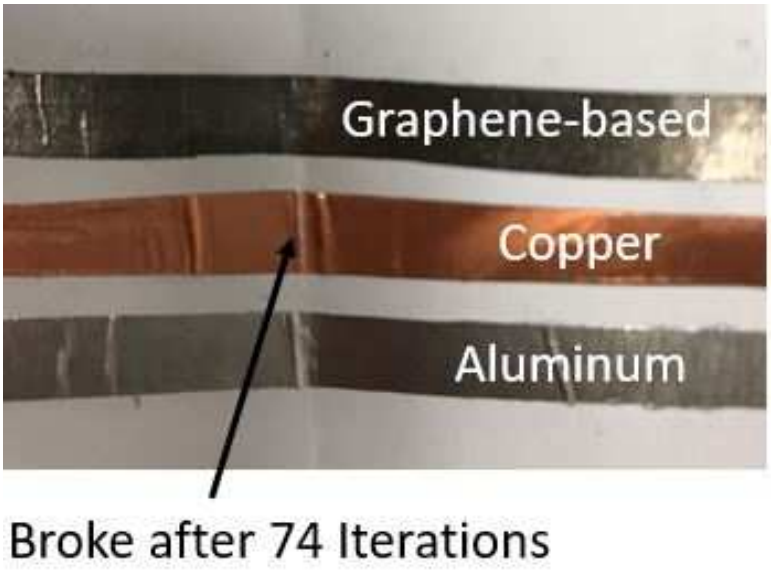

Figure 5.8. Breakdown of copper after 74 bending iterations.

6. STUDY OF ANTENNA ELEMENTS ON FLEXIBLE SUBSTRATES OF CONFORMAL ARRAY APPLICATIONS

6.1. Design of a Conformal Monopole Antenna on a Paper Substrate Using the Properties of 97% Carbon Content Graphene-Based Conductors

Two key components, among several, in the design of a conformal antenna are planar conductors and flexible substrates. In this chapter, a new approach using graphene-based conductors instead of copper conductors in the design of a conformal antenna is presented. As shown earlier, to determine the conductivity properties of a graphene-based conductor, the copper conductors in a well-known micro-strip transmission line (TL) and microstrip antenna were replaced with graphene-based conductors and were analytically evaluated, simulated in a full-wave simulation software and experimentally tested. Overall, it was shown that these graphene-based conductors have a conductivity high enough for designing a useful micro-strip TL and micro-strip antenna. In particular, a conductivity of $\sigma = 1.94 \times 10^5$ S/m for a 25-μm thick graphene-based conductor was determined from 100 MHz to 4.0 GHz. Finally, the conformity of graphene-based conductors was demonstrated using a mechanical test fixture and by designing a monopole antenna on a 100-μm thick paper substrate. In summary, the results in this chapter show that the graphene-based conductors provide an alternative to the more fragile copper conductors traditionally used to design conformal antenna elements.

6.1.1. Motivation

Conformal antennas are gaining popularity because they can enable the embedding of wireless systems into the design of complex geometries. This is because in certain scenarios, such as aircrafts and wearable garments, there may be little opportunity to place an antenna on a flat surface. Furthermore, this antenna placement can be complicated by the fact that the surface on which the antenna is placed could be vibrating or changing shape with time [8, 25, 60, 70]; and one of the drawbacks of conformal antennas is that the copper conductors used to fabricate the antenna tend to fail and crack as the surface changes shape [8, 60]. Recently, new composite ma-

terials with structural strength and high electrical conductivity have been designed by embedding graphene-based materials into them [13, 71]. Antenna fabrication [53] and related graphene-based materials studies [72, 73, 74, 75, 76] have been investigated where graphene-based conductors were used as conducting materials. The graphene-based materials [44] provide the electrical conductivity in these composites and when isolated they are very flexible, making them possible for conformal antenna applications. Therefore, the objective of this section is to develop the modeling approach of using graphene-based materials in the design of a conformal antenna element instead of copper conductors. In this work, replacing the copper conductors with graphene-based conductors in the conformal monopole antenna design shown in Figure 6.1(a) is studied. In particular, the conductors of the monopole design consist of the graphene-based materials shown in Figure 6.1(b) and the layout was chosen for operation at 2.57 GHz on a paper substrate. Initially though, the conductivity of the graphene-based materials in Figure 6.1(b) was determined by evaluating the well-known geometry of a printed micro-strip transmission line (TL) that used the graphene-based materials as the TL conductor instead of copper. By analyzing the micro-strip TL first, analytical computations, ADS simulations [50] and measurements were each used to extract the conductivity of the graphene-based materials. Then, this conductivity was used to design a micro-strip patch antenna prototype in ADS that used the graphene-based materials as the conductor for the radiating portion of the design (i.e., top layer conductor). The prototype was manufactured and measured for accuracy in a full anechoic chamber for further conductivity validation. Once the conductivity of the graphene-based materials was determined and validated with two known designs, the new conformal monopole antenna in Figure 6.1(a) was designed on a paper substrate with the conductors made of the graphene-based material in Figure 6.1(b). The simulation and experimental results show that the much more robust graphene-based conductors can be used to manufacture more reliable conformal antennas.

The work reported here differs from the research in [72, 73, 74] by (1) presenting the new design of conformal monopole antennas on paper substrates using 97% carbon content graphene-based conductors (2) showing the mechanical benefits of 97% carbon content graphene-based conductors over traditional copper conductors. These conductors can be applied to load bearing antennas, wearable antennas, conformal antennas affixed to the sides of military equipment and aircraft [8, 25, 60, 70, 71, 13]. and related works on paper substrate [75, 76, 77].

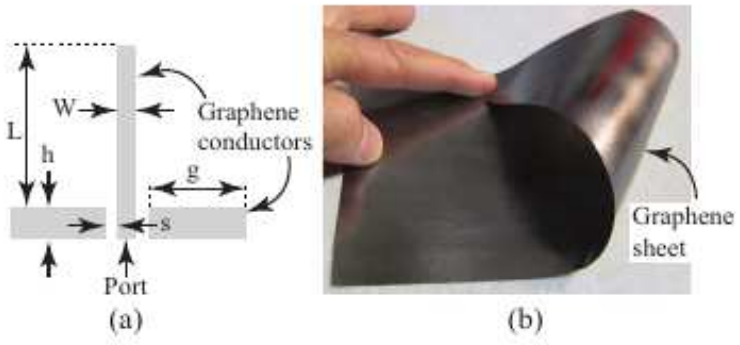

Figure 6.1. (a) Topology of the conformal monopole design on the paper substrate (g = 16.0 mm, h = 10.0 mm, L = 39.0 mm, W = 2.2 mm and s = 1.1 mm). and (b) photograph of the graphene sheet used as the conductors in the conformal monopole antenna design.

Therefore, the objective of this work is to develop an approach of using 97% carbon content graphene-based conductors in the design of a conformal antenna instead of copper conductors. Introducing this new material into the design of conformal antennas is beneficial because the graphene-based conductors are not as prone to cracking as copper based conductors are.

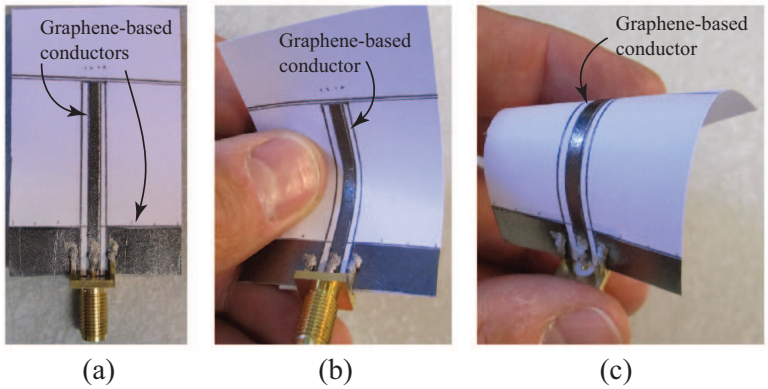

Figure 6.2. (a) Manufactured prototype conformal monopole antenna on a paper substrate and graphene-based conductors conductors, and (b) and (c) photographs illustrating the conformal properties of the monopole.

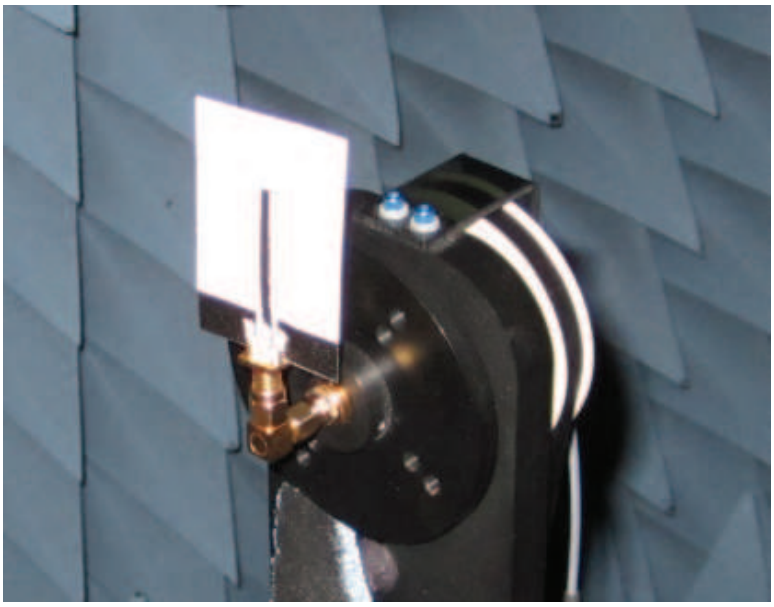

Figure 6.3. Photograph of the prototype conformal monopole being measured in the full anechoic chamber.

6.1.2. The conformal 97% carbon content graphene-based monopole antenna on paper substrate

6.1.2.1. Prototype design

Next, to illustrate the conformal properties of the graphene-based conductors, the design of the conformal monopole antenna shown in Figure 6.1(a) is presented. Again, instead of copper, the graphene-based conductors material in Figure 6.1(b) was used in the design for the conductors. The extracted conductivity was used in ADS to model the graphene-based conductors, and the monopole was designed on a 100-μm thick paper substrate ($\varepsilon_r = 3.0$). A picture of the manufactured prototype is shown in Figure 6.2(a). The pictures in Figures 6.2 (b) and (c) illustrate the conformal properties of the design.

6.1.2.2. Simulation and measurement results

To measure the $|S_{11}|$ and gain values, the prototype was placed in a full anechoic chamber shown in Figure 6.3. The measured $|S_{11}|$ of the conformal monopole is shown in Figure 6.4 and the gain was determined to be - 0.1 dBi. For comparison, the simulated $|S_{11}|$ values in ADS are also shown in Figure 6.4 and the gain was computed to be 1.0 dBi, which is slightly deviated from the measured gain of a monopole; however, it still compares well with the measured gain. This design

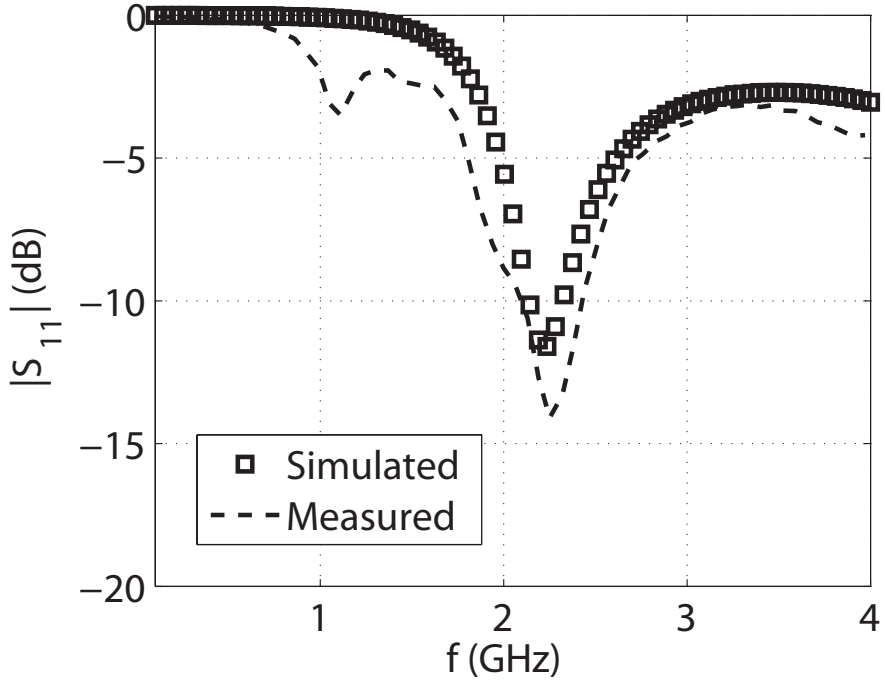

Figure 6.4. Measured and simulated $|S_{11}|$ values of the prototype conformal monopole with the graphene-based conductors.

further validates the ADS model of graphene-based conductors. It also illustrates the benefits of using graphene-based conductors for conformal antenna designs.

6.1.3. On the mechanical properties of the 97% carbon content graphene-based conductors for antennas

Finally, a comparative study on the mechanical properties of the graphene-based and copper conductors was experimentally conducted. The test fixture consisted of two planar surfaces connected on one edge with a pivoting hinge, as shown in Figure 6.5. Next, two samples made of copper and the graphene-based conductors were attached to the test fixture (also shown in Figure 6.5). The length of each sample was 75 mm and the width was 5.0 mm. The thickness of both was 25 μm. The angle θ was varied from 0 to 110 degrees at a rate of approximately 37 bends/min. The experiment was conducted on 3 samples. On average, after 74 iterations, the copper connection failed, as shown in Figure 6.6. Then, the fixture conducted 750 iterations on the graphene-based conductors and no failure was observed; showing the additional mechanical benefits of the graphene-based conductors. Though this experiment was done separately, the results are

very similar to the results mentioned in chapter 5. It should be mentioned that a further study on these mechanical properties would be beneficial and that will help future research.

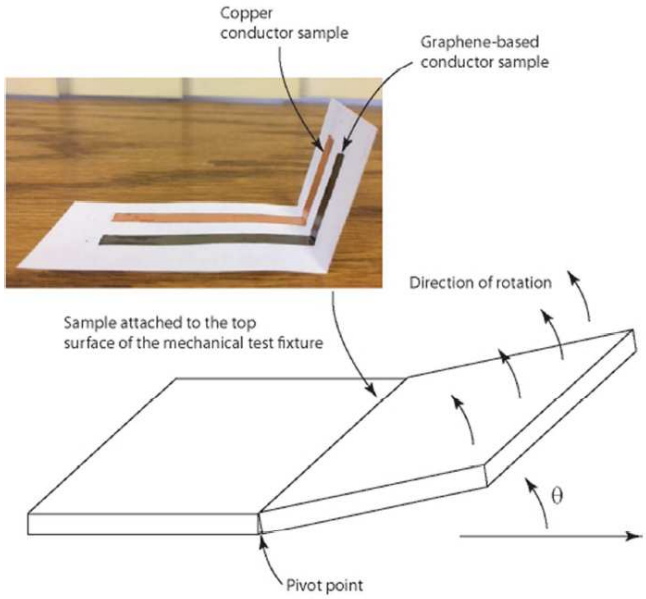

Figure 6.5. An illustration of the test fixture used to compare the mechanical properties of the graphene-based and copper conductors.

6.1.4. Results and discussion

A method for implementing graphene-based conductors as conductors in a conformal monopole on a paper substrate was presented in this section. The conductivity of the graphene-based conductors was determined by analytically evaluating, simulating and measuring microstrip transmission lines and microstrip antennas on a TMM4 substrate; which are well known problems and useful for extracting conductivity. It was shown that a conductivity of $\sigma = 1.94 \times 10^5$ for 25 μm thick graphene-based conductors from 100 MHz to 4.0 GHz could be used to model the graphene-based conductors in ADS. Overall, the electrical performance of the graphene-based conductors was comparable to the copper conductor for the designs investigated in this work, indicating that graphene-based conductors have the potential to develop more robust conformal antennas without the trade-off of electrical performance.

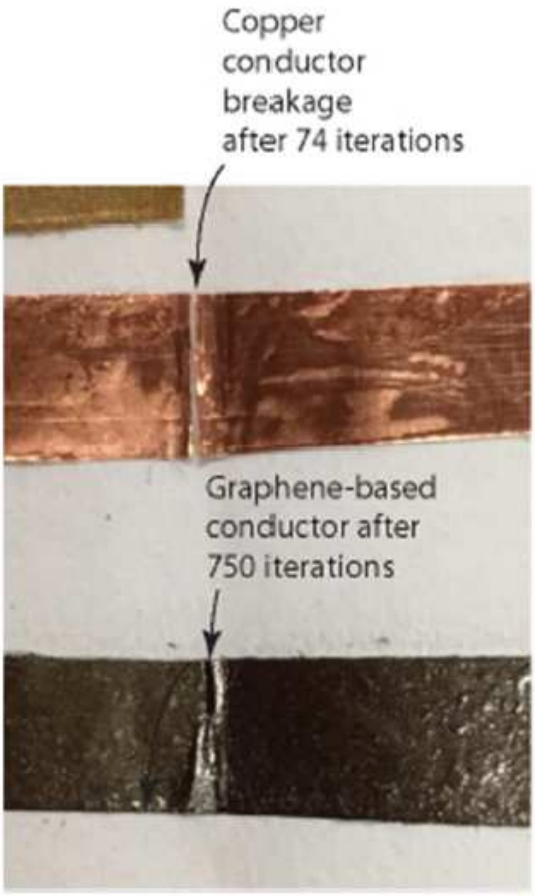

Figure 6.6. A photograph of the breakage of the copper conductor at the pivot point.

6.2. A Conformal Antenna on a Passive UHF RFID Tag Using 97% Carbon Content Graphene-Based Conductors and Paper Substrates

Passive UHF radio frequency identification (RFID) systems are being applied to many different industries. Because of this, these systems are now increasingly required to operate in complex electromagnetic environments. This may require tags to operate on different surface types or time varying shapes. This section presents a conformal antenna design that can be used on a passive UHF RFID tag with a paper substrate. More specifically, instead of copper conductors for the antenna, commercially available 97% carbon content graphene-based material is used to mitigate conductor failure; which has been observed in copper-based conformal antenna designs. Simulations and read-range measurements(2.1 meters) of this prototype UHF passive RFID tag

with graphene-based conductors are competitive to commercially available copper-based RFID. Moreover, the overall dimensions and size are also competitive.

6.2.1. Motivation

A passive radio frequency identification (RFID) tag typically consists of three major components, namely an IC, antenna and substrate. There has been extensive research conducted on different ICs [78], antenna layouts (i.e., compact designs) for different applications [79], and different thin substrates for attachment to various conformal surfaces [80]. However, in much of the earlier work reported on RFID antenna designs, the material used was copper. It is well known that copper is a good conductor; however, the properties of this material can be altered if it is attached to a conformal surface that changes shape with time [81]. The objective of this section is to present the new design shown in Figure 6.7 that uses graphene-based conductors instead of copper as a method to develop a conformal antenna on a passive UHF RFID tag with a paper substrate. A graphene-based conductor has been shown in previous chapters of this dissertation to be less vulnerable to surface changes and is a material that can be used in UHF antenna designs on conformal surfaces.

6.2.2. Development of the graphene-based conductor antenna

The layout of the proposed antenna is shown in Figure 6.7(a). A meandering line design was chosen to reduce the overall size of the antenna [79] and hence the tag. Then, instead of using copper, the commercially available 97% carbon content graphene-based material shown in Figure 6.7(b) was used as a conductor.

6.2.2.1. Simulations of the graphene-based antenna

Initially, the antenna was modeled in HFSS [82] on a 0.1 mm thick paper substrate with $\varepsilon_r = 2.19$ and $\tan\delta = 0.035$. The dielectric properties of the paper substrate were measured using a RF Impedance/Material Analyzer E4991A (1MHz-3GHz) [83]. According to the data sheet, the thickness of the graphene-based layer was 25 μm and had conductivity of $\sigma = 1.94 \times 10^5$ determined earlier in chapter 3. For the prototype, an Alien Higgs 2 IC [84] was chosen for demonstration purposes only. At 915 MHz, the input impedance of the IC was $13.8 - j143.6\ \Omega$. With the dimensions shown in Figure 6.7(a), the input impedance computed in HFSS was $8.61 + j143$ at 915 MHz. The real and imaginary parts of the simulated values are shown in Figure 6.8. It should also be noted that a pattern similar to a dipole was observed.

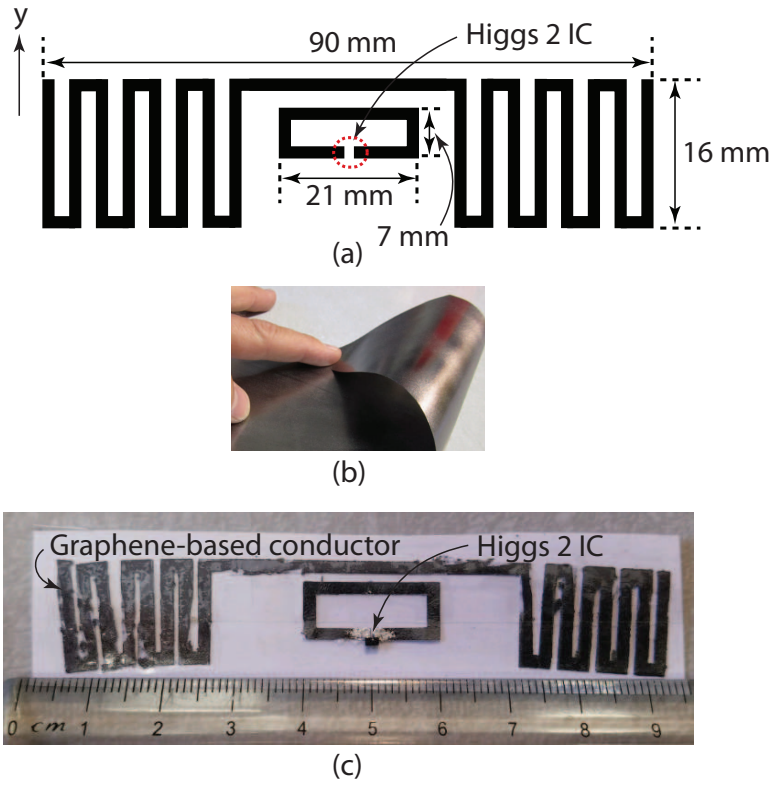

Figure 6.7. (a) Topology and dimensions of the antenna on the UHF RFID tag; (b) Photograph of the commercially available 97% carbon content graphene-based material used for the antenna and (c) Photograph of the prototype UHF RFID tag with graphene-based conductors and a paper substrate.

6.2.2.2. Measurements of the prototype

Next, a prototype of a passive RFID tag with the design in Figure 6.7(a) was manufactured. This was done using the procedure reported in [53]. In summary, the antenna manufacturing technique consisted of a three-layer structure. The bottom layer was 0.1 mm thick paper, the middle layer was the graphene-based material shown in Figure 6.7(b) and the top layer was transparency film. The graphene material was lightly adhered to the paper layer and the transparency film was used to hold down the graphene-based material during cutting. Then, a micro-cutter [47] was used to cut out the shape of the antenna. The cutter went through all three layers. Then, the paper and transparent layers were removed by hand and the graphene-based material in the shape of the antenna remained. This antenna was then attached to the paper substrate to form the prototype passive tag shown in Figure 6.7(c). The Higgs 2 IC was attached to the port using conductive silver epoxy.

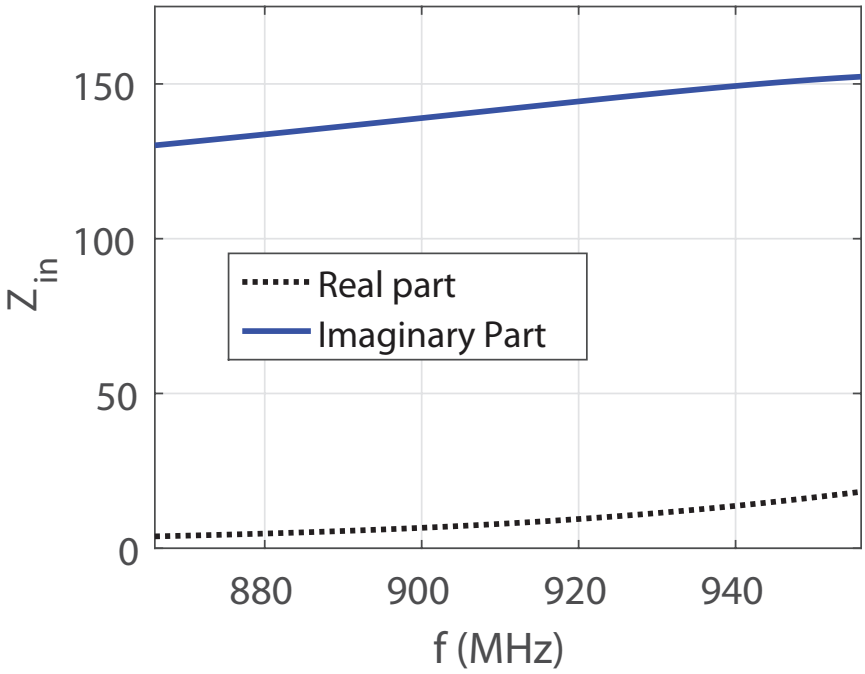

Figure 6.8. Simulated input impedance of the antenna with graphene-based conductors.

Then, the read range of the prototype was measured in a full anechoic chamber. An Alien 9780 reader [84] (with a maximum output power of 1 W) connected to a CP antenna with a gain of 6 dBi was used for these measurements as shown in Figure 6.9(a). The prototype tag was attached to a styrofoam block and is shown in the chamber in Figure 6.9(b). The read-range was found by moving the tag away from the reader antenna until reading ended. It was shown that a read-range of 2.1 m could be achieved and verified the simulation results in Figure 6.8.

6.2.3. Results and discussion

An antenna design that uses commercially available 97% carbon content graphene-based conductors instead of copper for passive UHF radio frequency identification (RFID) tags has been presented in this section. It has been demonstrated that the conducting properties and additional benefit of conformality of graphene-based conductors could be used to develop a passive UHF RFID tag. Measurements show that useful read-ranges of 2.1 meters could be achieved for tags on thin conformal paper substrates.

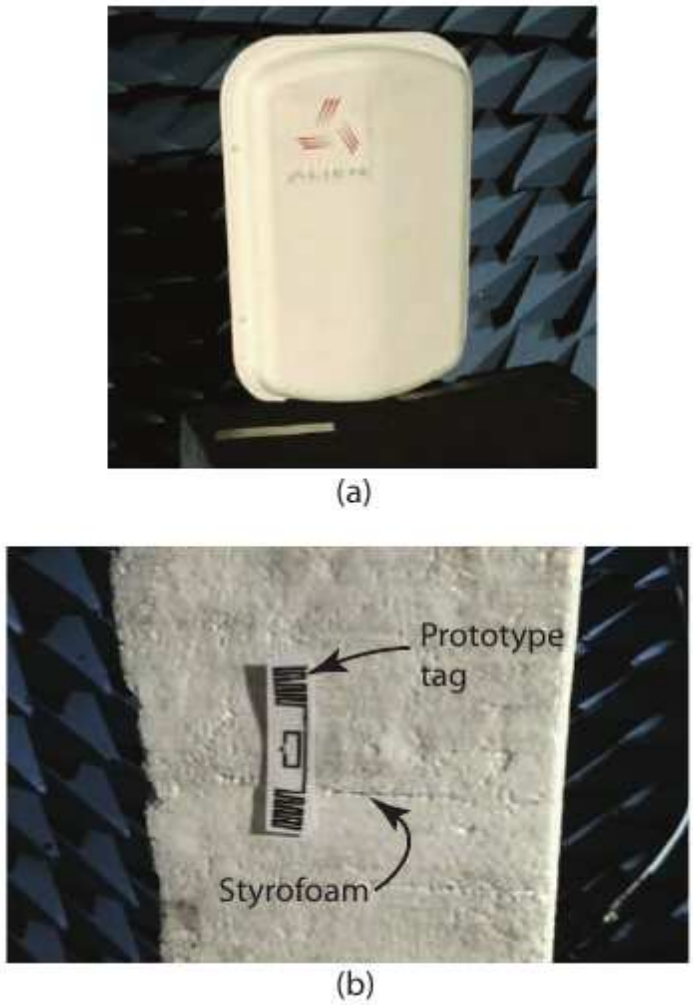

Figure 6.9. (a) Photograph of the antenna on the RFID reader in the full anechoic chamber during read-range measurements and (b) photograph of the read-range of the prototype tag being measured in the full anechoic chamber.

6.3. Design of a coplanar waveguide fed (CPW-fed) Graphene-Based Conformal Monopole on a Paper Substrate

Here, a coplanar waveguide fed (CPW-fed) conformal monopole antenna was designed on a flexible low-cost multi-purpose paper substrate with a thickness of 0.1 mm, and flexible graphene-based conductive material shown in Figure 6.10(b) was used as an alternative to copper. The antenna was designed for 3.6 GHz applications with a size of 24 mm $\times$ 6 mm. The design shown in Figure 6.10(a), was simulated in HFSS, a full-wave simulation tool; a prototype was manufactured using a micro-cutter; and measured in a full anechoic chamber. Overall, it was shown that the

S-parameter simulations agreed well with the measurements, and that the electrical benefits of the flexible graphene-based conductor can be utilized to design a CPW-fed conformal monopole antenna.

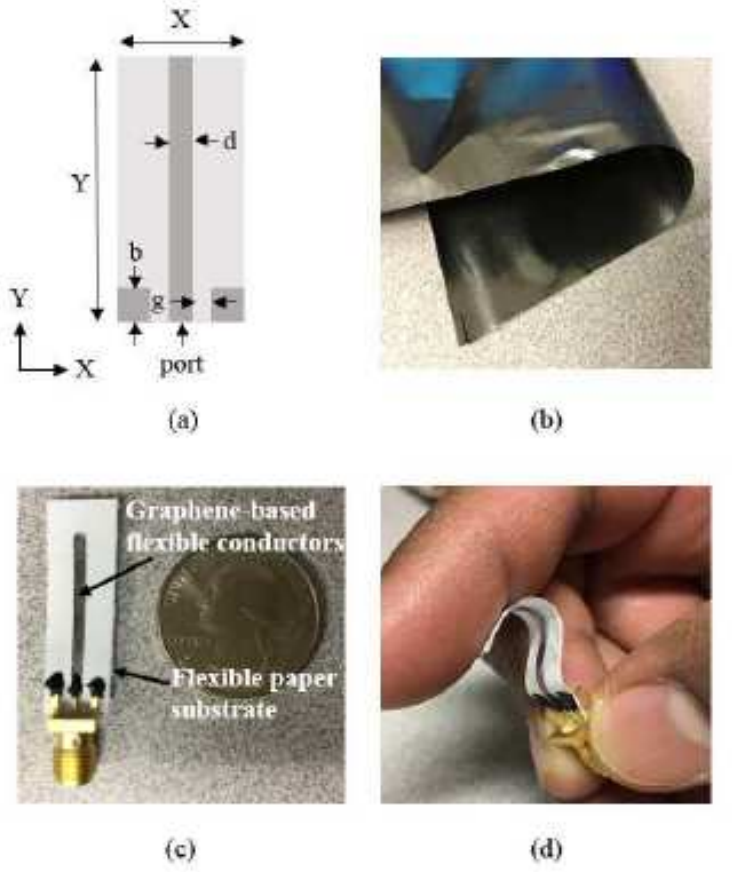

Figure 6.10. (a) Dimension of the conformal graphene-based monopole antenna; (b) Photograph of the graphene-based material from [44]; (c) Photograph of the manufactured prototype antenna with flexible graphene-based materials on a paper substrate and (d) Photograph illustrating the conformal properties of the prototype (b = 2.0 mm, d = 1.0 mm, g = 1.0 mm, X = 6.0 mm and Y = 24.0 mm).

6.3.1. Simulation of CPW-fed graphene-based conformal monopole

A CPW 50-Ω graphene-based microstrip transmission line (TL) was used for the feed network on a 0.1 mm thick paper substrate. A conductivity of $\sigma = 1.94\times10^5$ S/m [14] (for a thickness of 25 μm) for the graphene-based conductive material as determined in section 3.2.2 was used in the HFSS [82] simulations. The relative permittivity ($\varepsilon_r \approx 2.19$) and loss tangent ($tan\delta \approx 0.035$)

of the 0.1 mm thick paper substrate were measured with the help of a RF Impedance/Material Analyzer E4991A (1MHz-3GHz) [83]. The graphene-based conductive material was precisely cut using the Cricut Explore Air [47] following the procedure reported in [53].

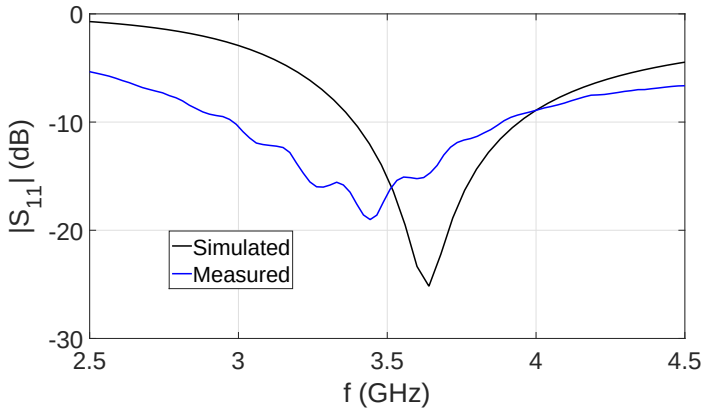

Figure 6.11. Measured and simulated $|S_{11}|$ values of graphene-based antenna prototype.

6.3.2. Results and discussion

The HFSS simulation results of the CPW-fed graphene-based conformal monopole are shown in Figure 7.4 and an image of the HFSS geometry is shown in Figure 6.12(a). The resonant frequency was 3.6 GHz, which was designed in simulation. Next, a prototype of the CPW-fed graphene-based monopole on paper was manufactured, and is shown in Figure 6.10(c). An illustration of the conformal nature of the prototype is also shown in Figure 6.10(d). Conductive glue was used to attach the SMA connector. The $|S_{11}|$ values of the prototype were then measured in a full anechoic chamber and agreed well with the simulations as shown in Figure 7.4. The measured resonant frequency was 3.45 GHz, a 4.16 % deviation from simulation results. Finally, the total gain of the prototype was simulated in HFSS and determined to be 1.9 dB at 3.6 GHz. These values are shown in Figure 6.12(b) and a pattern similar to a monopole was achieved.

A CPW-fed graphene-based monopole antenna was simulated in HFSS using the graphene-based material, and a prototype was manufactured and measured in a full anechoic chamber. Overall, good agreement with small deviations between the $|S_{11}|$ values were observed, and it was shown that a good gain can be achieved using graphene-based conductors and a low-cost paper substrate.

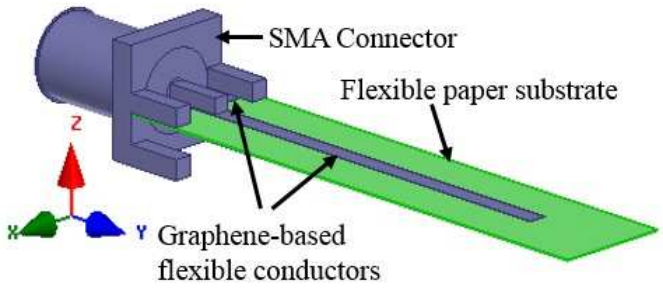

(a)

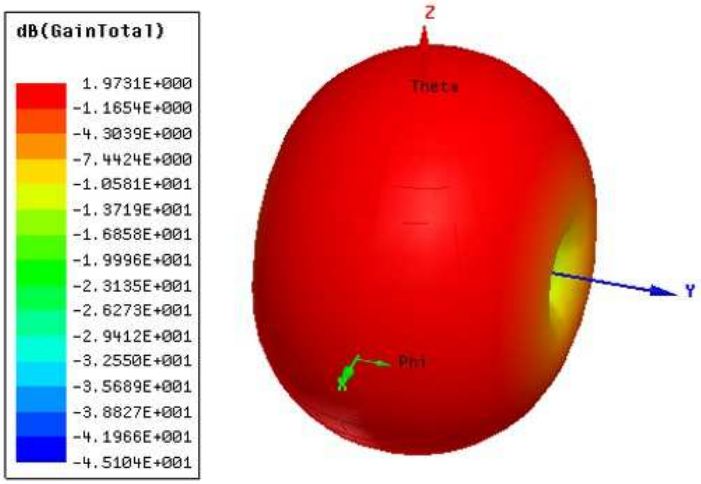

(b)

Figure 6.12. (a) Model in HFSS and (b) simulated total gain.

This will open up a new avenue for conformal antenna designs on paper substrates, which, in addition to being flexible are also, in many cases, affordable.

7. ANALYSIS OF AN ARRAY WITH 97% CARBON CONTENT GRAPHENE-BASED CONDUCTORS

In this chapter, an array with graphene-based conductive material and an array with the same layout with traditional copper were studied and compared. More specifically, the antenna array with graphene-based conductors shown in Figure 7.1 was designed, simulated, and fabricated for the first time. Both the copper and graphene-based antenna array prototypes were designed and simulated at 1.99 GHz. A Rogers TMM4 substrate (thickness = 1.52 mm; $\varepsilon_r \approx 4.5$; tan δ = 0.002) was used for both cases. Next, both the prototypes were measured in an anechoic chamber and the performance (i.e; gain, S-parameters) of both prototypes was analyzed. The simulation and measurement results in both cases were found to be in good agreement. Thus graphene-based conductors have the potential to be a better alternative to copper-based conductors, especially for conformal designs.

7.1. Motivation

Antenna design on graphene-based materials has been progressive because of its unique properties. To mention a few among the many breakthroughs, S. Stankovich and his team developed graphene-based composite materials [13], and J. Y. Kim and his team developed transparent material with high dielectric values [85]. The comparison between graphene-based transmission lines (TL) and traditional copper TLs also were investigated in previous work [73]. Furthermore, Ignacio Llatser and his team developed graphene-based nano-patch antennas for terahertz radiation, photonics and nano-structures [43].

7.2. Design, Simulation and Fabrication

To develop the graphene-based antenna array in Figure 7.1, the conductive properties of the graphene-based material were utilized from section 3.2.2. A conductivity of $\sigma = 1.94\times10^5$ S/m for a thickness of 25 μm was used in the simulation [14]. For the copper antenna array, the conductive properties of copper ($\sigma = 5.8\times10^7$ S/m for a thickness of 17.5 μm) were used in simulation. The effect of the SMA connector was not considered in the simulation and the S-parameters were determined in ADS [50] for the both designs. The frequency ranged from 1.5 GHz to 2.5 GHz. In

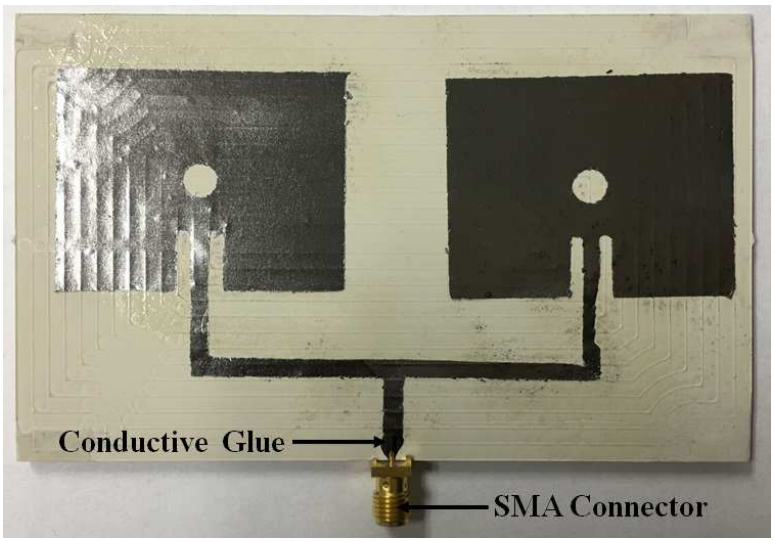

Figure 7.1. First prototype of a graphene-based antenna array.

both cases, the double sided Rogers TMM4 [69] substrate (thickness = 1.52 mm; $\varepsilon_r \approx 4.5$; tan δ = 0.002) was used as a dielectric material. In the case of copper, a LPKF Model S63 [57] milling machine was used to mill the copper antenna array, and mill one side of the double sided Rogers TMM4 to attach the graphene layer on the empty surface of the dielectric substrate.

Again, the graphene layer was fabricated separately using a Cricut Expression [47] printer. The fabrication process was reported in [53]. The connection between the graphene layer and SMA connector was made using conductive glue [48]. The dimensions of the antenna array are shown in Figure 7.2. The flexible graphene-based sheet after fabrication process is shown in Figure 7.3.

7.3. Results and Discussions

The ADS simulation of the graphene-based conductor(GBC) antenna array as well as the copper antenna array are shown in Figure 7.4. Next, the fabricated copper array shown in Figure 7.2 and the GBC array shown in Figure 7.1 were measured in an anechoic chamber using a network analyzer Agilent E5071C [86]. The measurement results are also shown in Figure 7.4. We found that the resonant frequency of the fabricated copper antenna array was 1.94 GHz and GBC antenna array was 1.99 GHz. Simulation and measurement results agree for the GBC array antenna, whereas the copper array measures are below the simulations by 2.5%. The gains of both the antenna arrays were measured in an anechoic chamber as well. The gain was 9.04 dBi for the copper antenna array at 1.94 GHz, and 8.72 dBi for the GBC antenna array at 1.99 GHz.

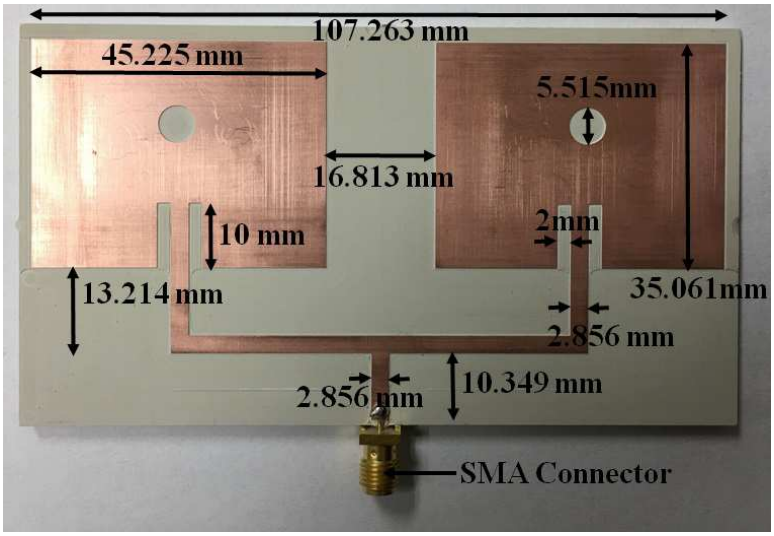

Figure 7.2. The dimensions of the copper antenna array (107.26 mm X 58.62 mm).

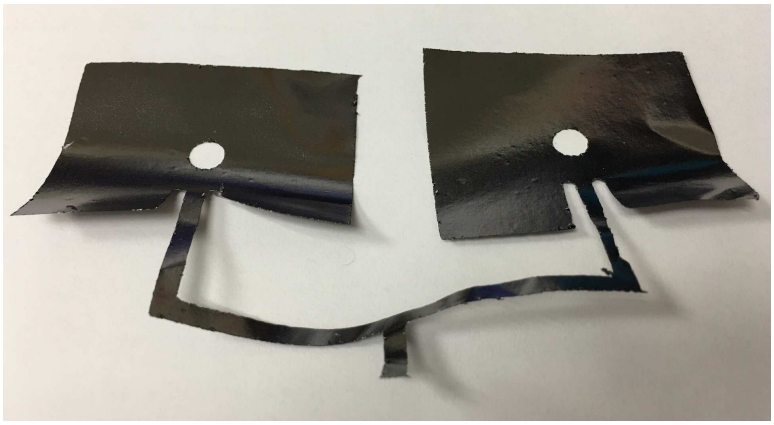

Figure 7.3. Flexible 97% carbon content graphene-based sheet after fabrication.

An initial investigation to compare the graphene-based antenna array with a copper antenna array was performed in this chapter. The design was simulated in ADS using extracted material properties, both the prototypes were fabricated following different fabrication processes, and tested in an anechoic chamber. Overall, good agreement between the $|S_{11}|$ values and gain were observed. It was demonstrated that using graphene-based conductors in an antenna array can achieve performance similar to a copper antenna array design.

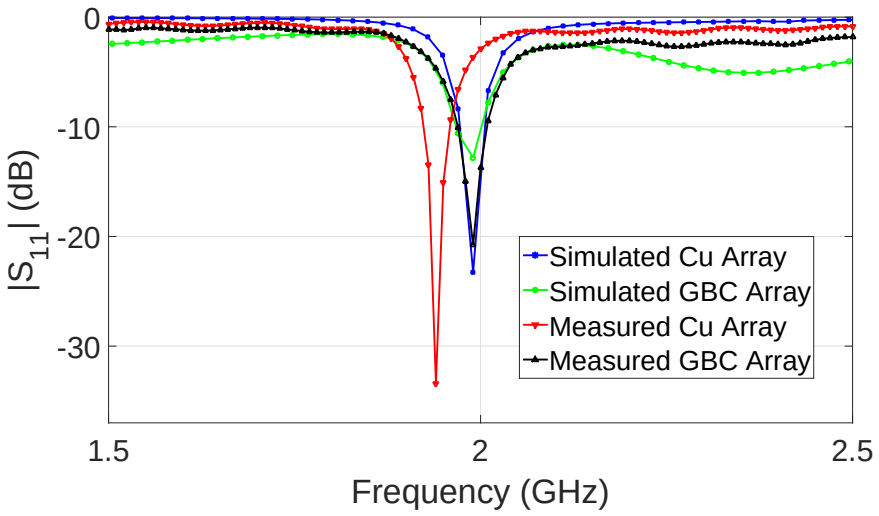

Figure 7.4. Measured and simulated $|S_{11}|$ values of graphene-based antenna array and copper antenna array.

8. MODEL ON THE 97% CARBON CONTENT GRAPHENE-BASED CONDUCTIVE MATERIALS WITH ADHESIVE LAYER FOR REDUNDANCY APPLICATIONS

8.1. Motivation

Becasue of the additional benefits of 97% carbon content graphene-based conductive(GBC) materials, we can use graphene-based material for antenna development. We can use 97% carbon content graphene-based conductive materials in many applications such as ultra wideband antennas [87] and MIMO planar antennas [88]. In this chapter, a model has been shown and redundancy [89, 90, 91, 92] techniques were implemented using graphene-based materials.

8.2. Model Development

To develop a model, the single patch antenna shown in Figure 8.1 was initially designed using a full wave simulator HFSS [82] and Rogers TMM4 [69] substrate (thickness = 1.52 mm; $\varepsilon_r \approx 4.5$; $\tan\delta = 0.002$). It was simulated with copper conductive materials only. Then, a split was made on the feeding transmission line of the antenna. Next, 97% carbon content graphene-based conductors were precisely cut according to [53] and adhered to the top of the broken transmission line like a band aid. An expanded view of the connection is shown in Figure 8.2 and the HFSS simulation setup is shown in Figure 8.3.

8.3. Results

Next, two samples were fabricated using the LPKF milling machine [57]. One sample was made of only Copper conductive materials and other sample was developed with an extra layer of 97% carbon content graphene-based conductor on the top of the broken copper layer. The graphene-based conductors were cut precisely using a Cricut micro-cutter [47] before adhering on the copper transmission lines. A picture of the two samples before the graphene-based conductor addition is shown in Figure 8.4 where (a) is a single antenna with no breakage or cracking, and (b) is a single antenna with breakage or cracking. Again, the picture of the two samples after the graphene-based conductor addition is shown in Figure 8.5 where (a) is a single antenna with no

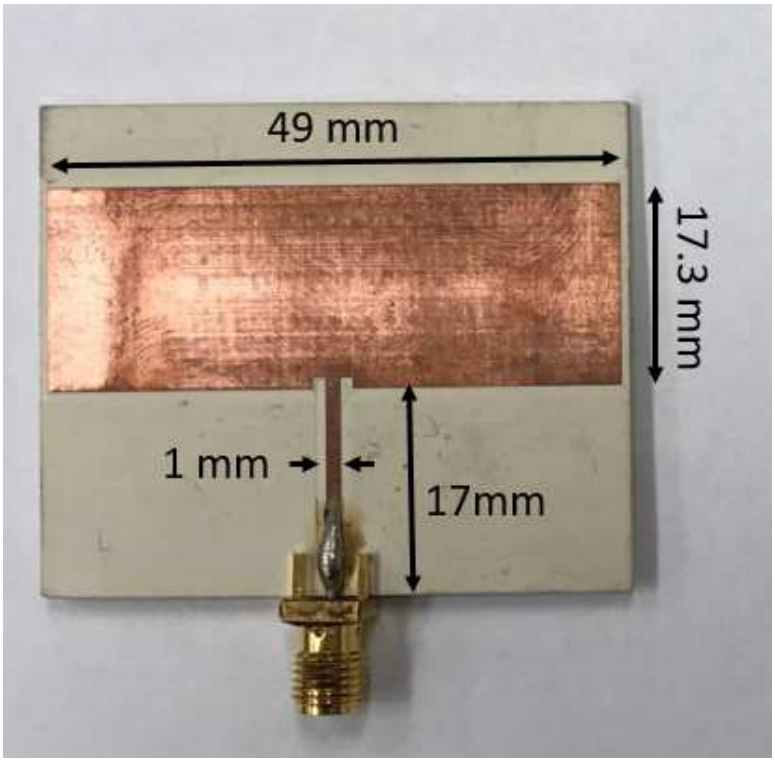

Figure 8.1. The dimension of the antenna simulated in HFSS.

breakage or cracking, and (b) is a single antenna with breakage or cracking covered by graphene-based layer.All the S-parameters and gain measurement were determined in an anechoic chamber as shown in Figure 8.6 and with a calibrated network analyzer. The $|S_{11}|$ values of the antenna were shown in Figure 8.7 based on five different scenarios as mentioned below.

(a) Copper TL with a break

(b) Only Copper TL without GBC layer

(c) Only Copper TL without GBC layer (HFSS)

(d) Copper TL with a break covered by GBC TL

(e) Copper TL with a break covered by GBC TL (HFSS)

To measure the gain, one horn antenna and one sample patch antenna were set-up at a distance of 158 cm. The horn antenna acted as a reference for all the measurements. The horn antenna was at position 1 and the patch antenna samples were on position 2. The $|S_{21}|$ values were

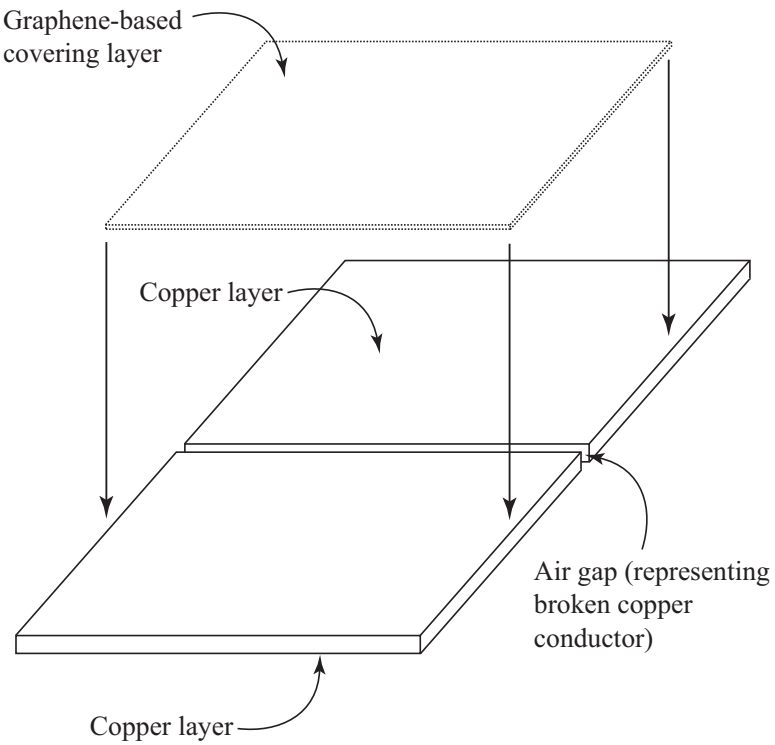

Figure 8.2. Expanded view of connection between 97% carbon content graphene-based conductors on copper.

measured using an Agilent E5071C network analyzer [86] and the results were shown in Figures 8.8. The frequency was swept from 100 MHz to 4.5 GHz. It was determined that the gain of the antenna, in both cases, was measured to be 4.0 dBi at 3.7 GHz. In HFSS simulations, the gain was computed as 7.3 dBi at 3.7 GHz in both cases.

8.4. Discussion

It was found that adding a layer over the broken section of copper was a great redundancy technique without impacting the S-parameters and gain of the antenna. We can use similar models on flat, conformal applications and commercial applications. This will open-up new avenues for creating redundancy antennas that do not compromise performance.

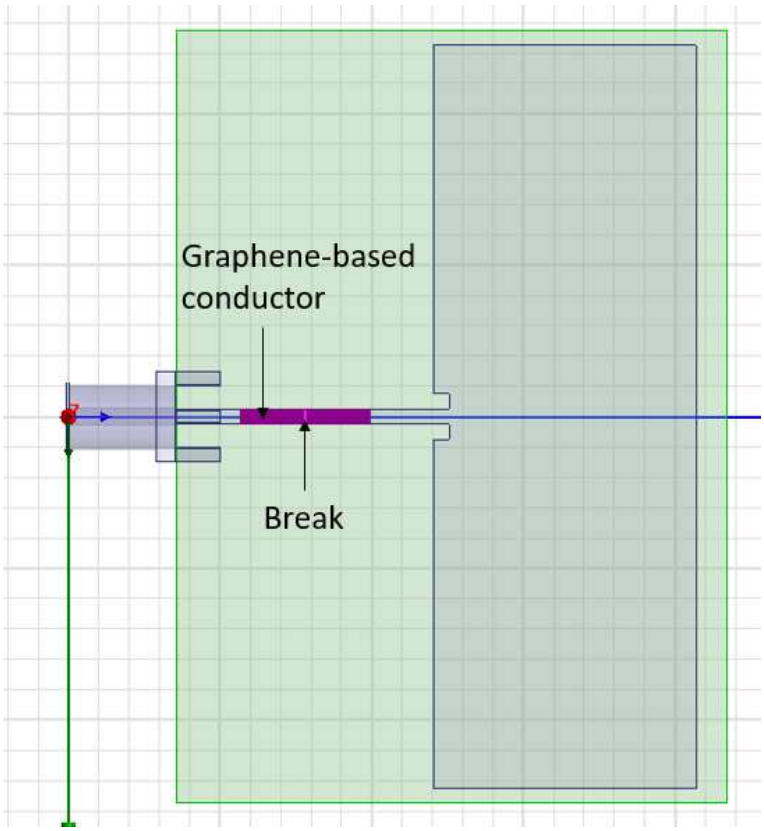

Figure 8.3. Full wave HFSS simulation of the antenna.

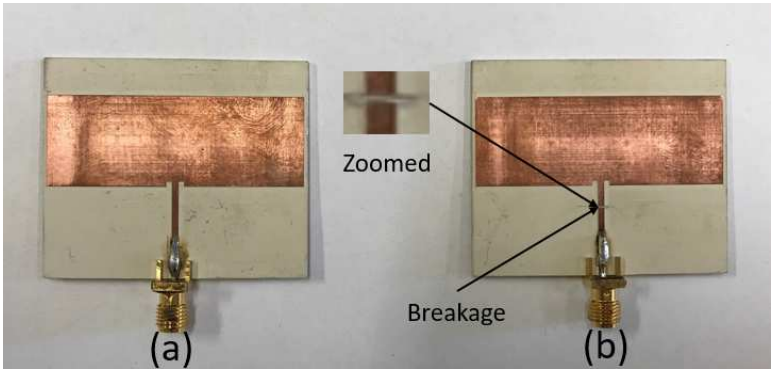

Figure 8.4. Before adding the graphene-based layer: (a) A single antenna with no breakage or cracking (b) A single antenna with breakage or cracking.

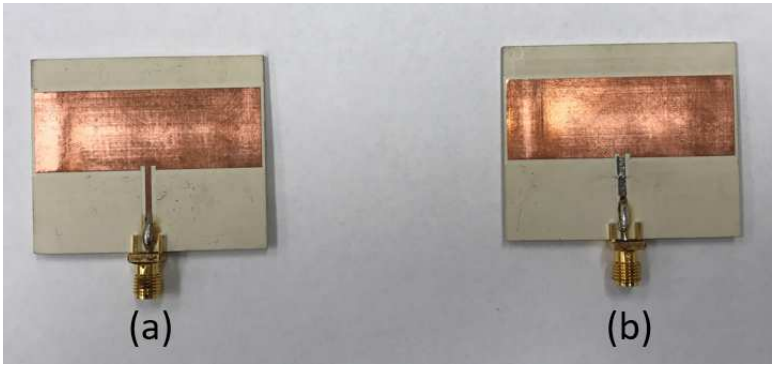

Figure 8.5. After adding the graphene-based layer: (a) A single antenna with no breakage or cracking (b)A single antenna with breakage or cracking covered by graphene-based layer.

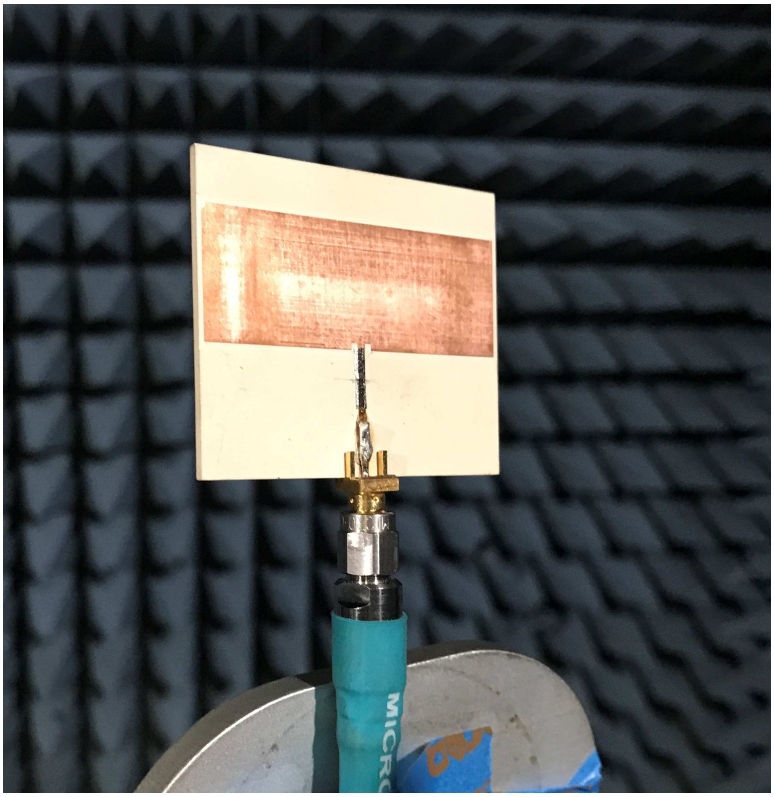

Figure 8.6. $|S_{11}|$ values and gain measurement in an anechoic chamber.

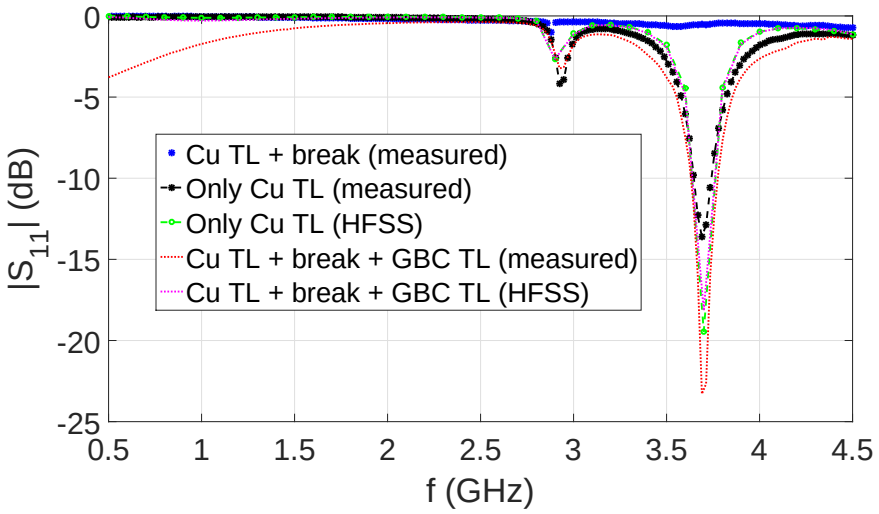

Figure 8.7. Simulated and measured $|S_{11}|$ values of the antenna.

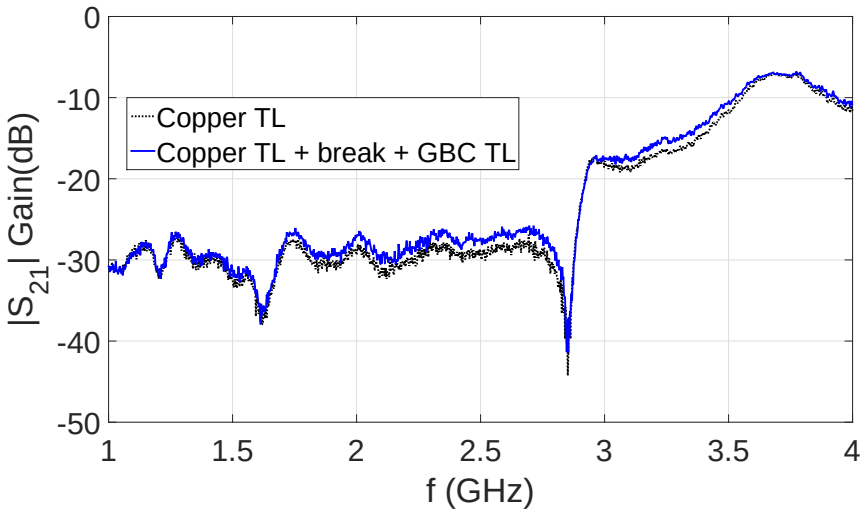

Figure 8.8. Measured $|S_{21}|$ values in order to calculate gain of the antenna.

9. ANALYSIS ON CONFORMAL 97% CARBON CONTENT GRAPHENE-BASED ANTENNA ARRAY ON ITERATIVE BENDING EVENTS

9.1. Motivation

There are many benefits of using antenna arrays [15, 16, 17, 18, 19, 20, 21]. These benefits will be negatively impacted when the conductive materials of the antenna arrays experience breakage or cracking on the transmission lines or antenna radiators due to iterative bending applications. Copper has been most commonly used but copper has been shown to be prone [75] to breakage or cracking when several iterative bending actions occur on a specific point of the antenna array. Here, analysis on conformal 97% carbon content graphene-based (GBC) antenna array are studied on iterative bending events.

9.2. Simulation, Fabrication and Measurement

A 2 $\times$ 1 antenna array design was simulated using a full wave simulator ADS [50]. A thin Rogers RT/duroid 6002 [69] substrate (thickness = 0.508 mm; $\varepsilon_r \approx 2.94$; tan $\delta = 0.0012$) was used to design this conformal 2 $\times$ 1 antenna array. The antenna array dimensions are shown in Figure 9.1. Next, the antenna array was manufactured using a LPKF S63 milling machine [57]. An SMA connector was attached to the antenna array at the port and the fabricated conformal 2 $\times$ 1 antenna array is shown in Figure 9.2. The $|S_{11}|$ and gain of manufactured antenna array was measured in an anechoic chamber shown in Figure 9.3. The simulated and measured $|S_{11}|$ values of the manufactured antenna array are shown in Figure 9.4. The simulated gain was 6.6 dBi at 2.5 GHz and the measured gain was 5.5 dBi.

9.3. Iterative Bending Experiment

To study the iterative bending experiment, the 2 $\times$ 1 antenna array was bent iteratively on two specific spots (right and left)of the antenna array. These spots are shown in Figures 9.5 and 9.6. Only after 5 iterations on the right side of the antenna array, the copper layer was broken. The broken copper is shown in Figure 9.5. Next, only the left side of the antenna array was bent iteratively and the copper broke on the left side after just 6 iterations. The broken

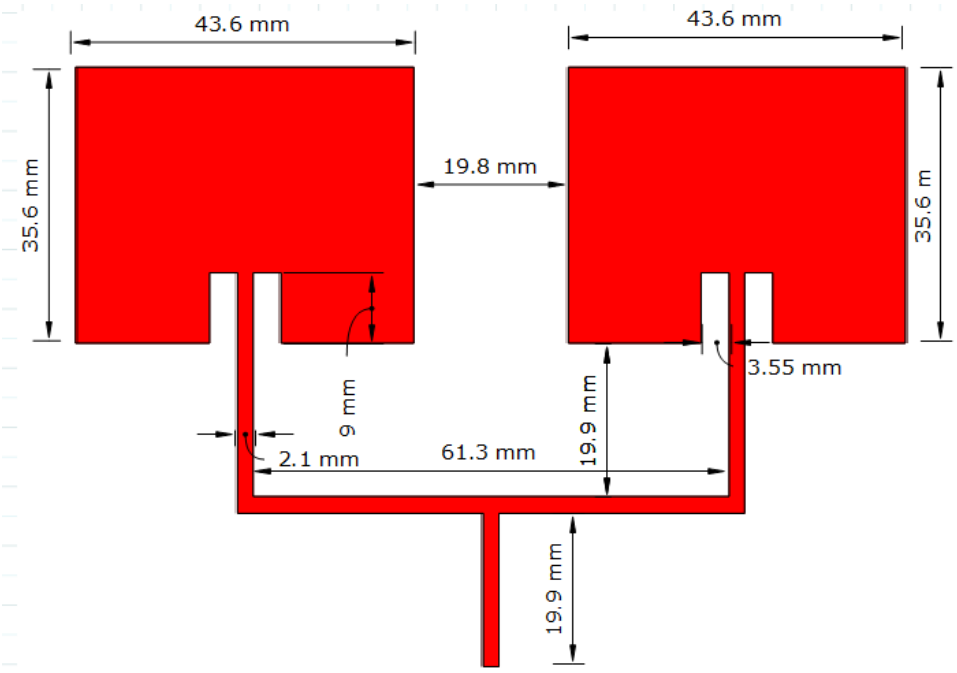

Figure 9.1. The dimension of the 2 × 1 antenna array.

copper is shown in Figure 9.6. In both cases, the discontinuity of the conductive layer was checked using a digital multimeter. Then, the 97% carbon content graphene-based layer was precisely cut applying the process mentioned in [53] and adhered on top of the broken copper layer. Part of the adhesive process is shown in Figure 9.7. After 60 iterations, the second layer of 97% carbon content graphene-based conductive TL was added on top of the copper layer. Then 130 bending iterations were performed to investigate the impact of the extra layers of graphene-based conductors. 1 layer and 2 layers of the 97% carbon content graphene-based conductors are shown in Figure 9.8 and Figure 9.9, respectively.

9.4. Results and Discussion

$|S_{11}|$ values of the 2 × 1 antenna array at 8 different bending iterations were plotted and shown in Figure 9.10. The 8 different scenarios are given below.

(a) 0 GBC layer (5 iterations and Cu broke on right side)

(b) 0 GBC layer (6 iterations and Cu broke on left side)

(c) 1 GBC layer (6 iterations)

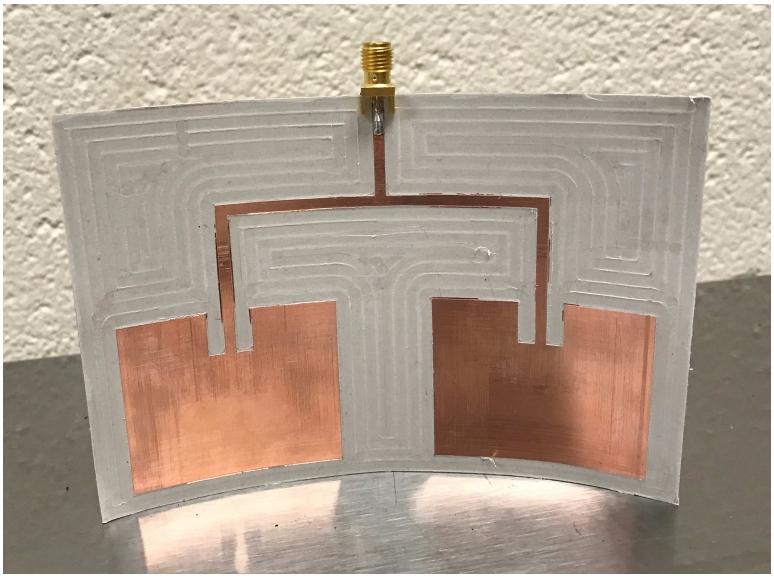

Figure 9.2. The conformal 2 × 1 antenna array.

(d) 1 GBC layer (30 iterations)

(e) 1 GBC layer (60 iterations)

(f) 2 GBC layer (90 iterations)

(g) 2 GBC layer (120 iterations)

(h) 2 GBC layer (130 iterations)

Based on this plot, we observed that, after 5 and 6 iterations, both the right and left side of the antenna array were broken. After close observation, after 5 iterations, the antenna array was resonating at 2.5 GHz (approx) and after 6 iteration on the left side, the antenna was not resonating at all, because the feed network was disconnected from both sides of the antenna array radiators. Then, the additional 1 layer and 2 layers of the 97% carbon content graphene-based conductor on top of the copper layers made the antenna array immune to the iterative bending events. It acted as a reliable antenna array as we used the additional layers of graphene-based conductor as redundancy techniques in sensitive antenna array applications.

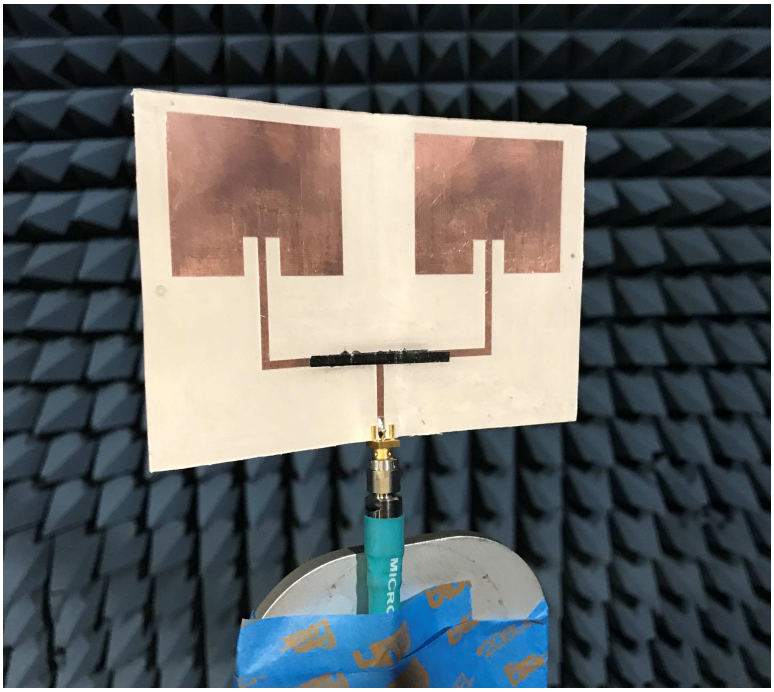

Figure 9.3. S-parameter and gain measurement in an anechoic chamber.

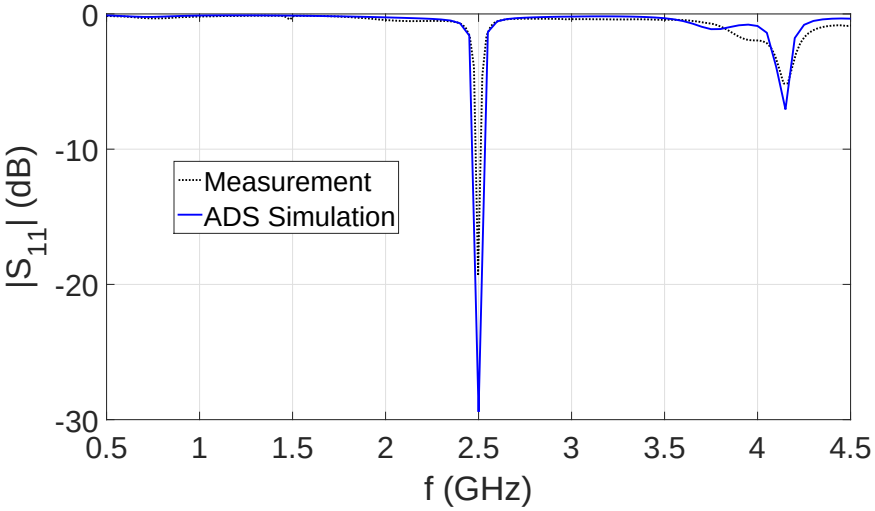

Figure 9.4. Simulated and measured $|S_{11}|$ values of the 2×1 antenna array.

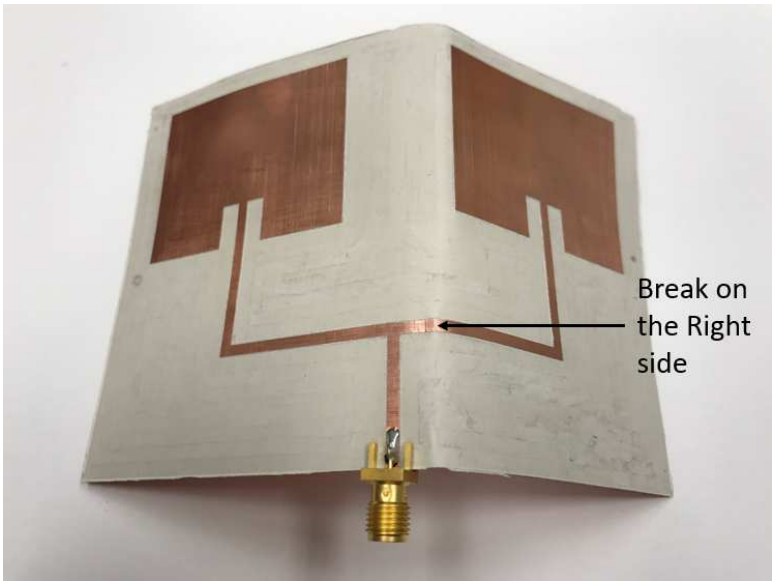

Figure 9.5. The break on the right side of the 2 × 1 antenna array.

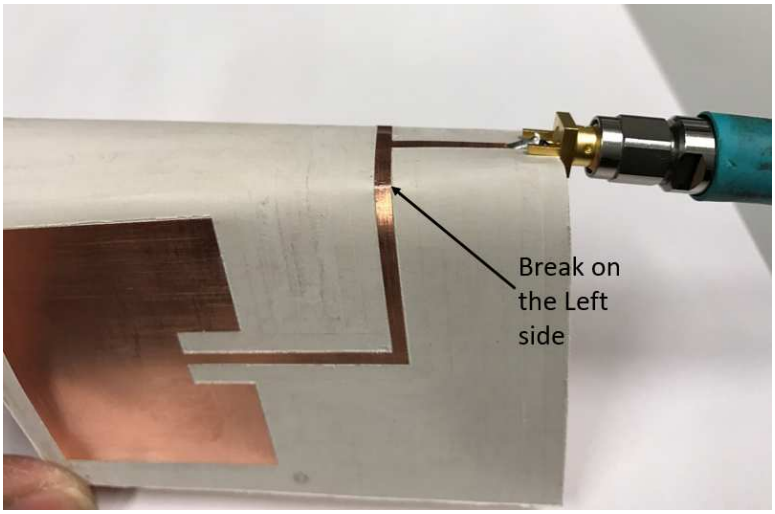

Figure 9.6. The break on the left side of the 2 × 1 antenna array.

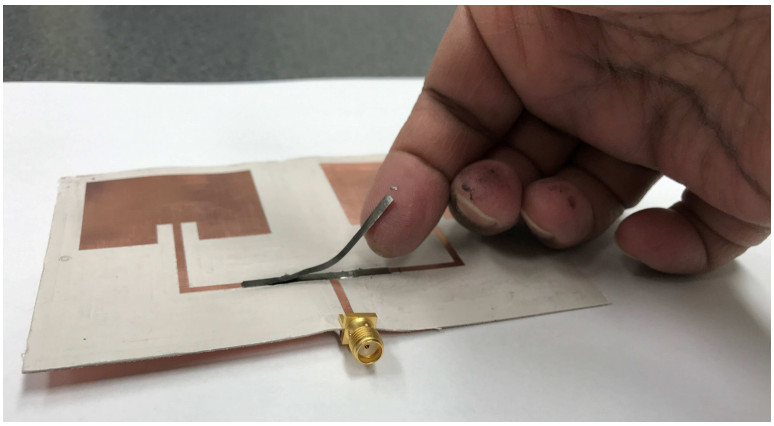

Figure 9.7. Adhesion process of 97% carbon content graphene-based conductor on copper TL.

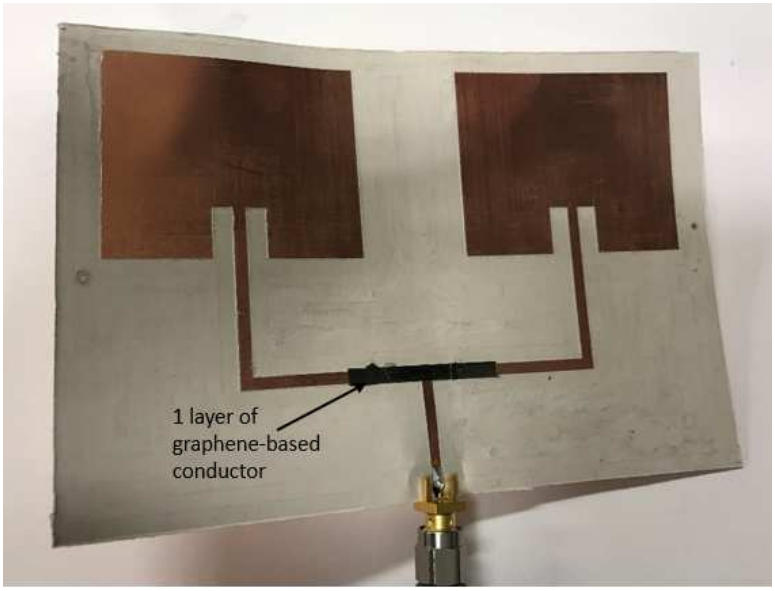

Figure 9.8. 1 layer 97% carbon content graphene-based conductor on copper.

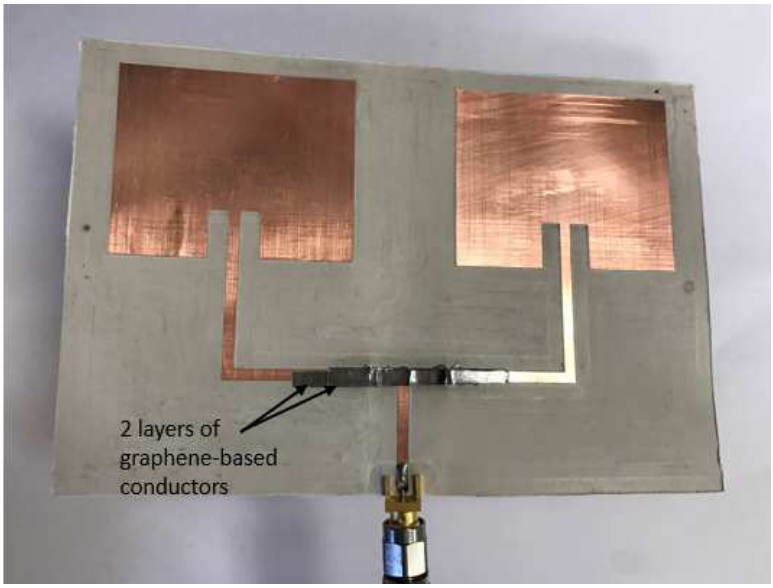

Figure 9.9. 2 layer 97% carbon content graphene-based conductor on copper.

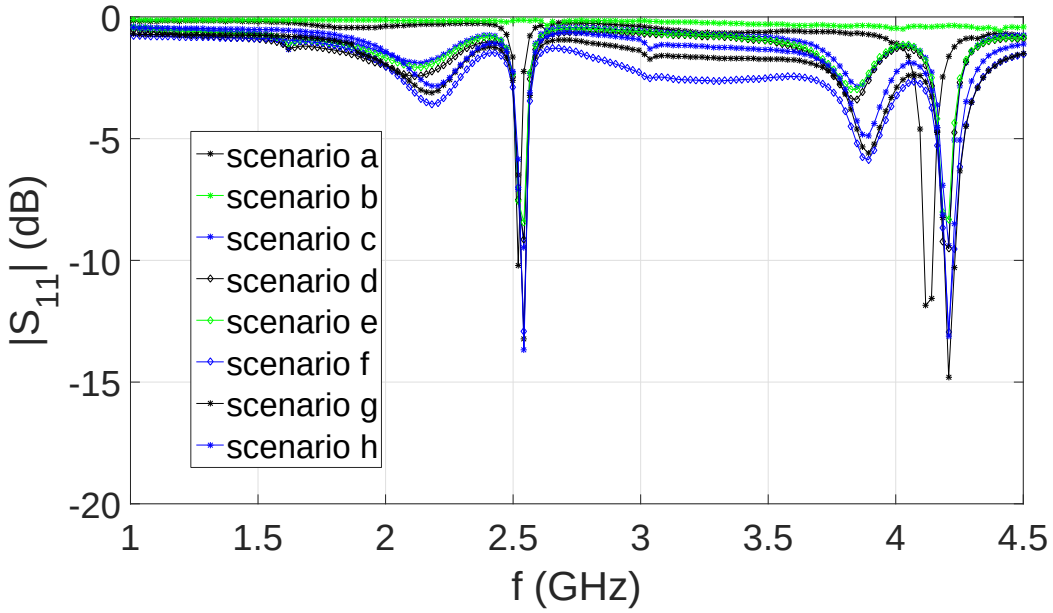

Figure 9.10. $|S_{11}|$ values of the 2×1 antenna array at 8 different bending iterations.

10. IMPLEMENTATION OF REDUNDANCY TECHNIQUES USING 97% CARBON CONTENT GRAPHENE-BASED CONDUCTORS

10.1. Motivation

In this chapter, a technique where 97% carbon content graphene-based conductors that can be used redundantly [89, 90, 91, 92] is shown for the first time. It was studied in chapter 5 of this dissertation and was found that graphene-based conductors are more than 10 times more reliable [75] than traditional copper conductors which are widely used in transmission lines and antenna radiators. Here, conductor failure was imitated on both flat and conformal surfaces to investigate the advantages of using 97% carbon content graphene-based conductors.

10.2. Antenna on a Flat Surface

A patch antenna was designed on a Rogers 5880 [69] substrate (thickness = 1.575 mm; $\varepsilon_r \approx 2.2$; $\tan \delta = 0.004$) and simulated in HFSS [82] at 2.45 GHz. The antenna dimensions are shown in Figure 10.1. Four patch antennas are fabricated using a LPKF S63 [57] milling machine. The fabricated four antennas are shown in Figure 10.2. The purpose of using four antennas was to investigate the breaking or cracking on the radiator part of the antenna. All four antennas were measured in an anechoic chamber and measurements were compared.

To understand the impact of cracking on the radiator surface of the antenna, a crack or break was made manually using a exacto blade at a 10 mm distance from the top of the radiator surface. A digital multimeter was used to ensure the discontinuation of the radiator surface. Similar cracks or breaks were made on two out of the four samples. The graphene layer [44] was cut according to the size of the radiator using the method described in [53] and was adhered on top of the copper surface of the radiator of the two samples (one with crack or break and another without crack and break) using an adhesive material [48]. The assembly part of the process is shown in Figure 10.3. An expanded view is drawn in Figure 10.4.

Next, four samples were manufactured for the experiment. The samples are described below in (a) to (d) and the fabricated antennas are shown in Figure 10.5.

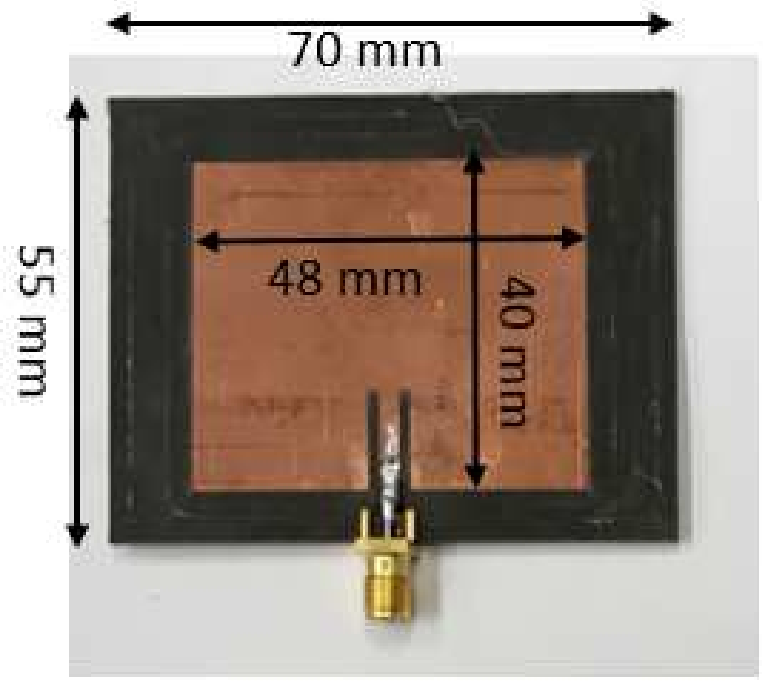

Figure 10.1. The dimension of the antenna.

(a) Single patch antenna with a copper only layer without break.

(b) Single patch antenna with a copper only layer with a break.

(c) Single patch antenna with both copper and graphene-based layers without a break.

(d) Single patch antenna with both copper and graphene-based layers with a break.

10.2.1. Results

All the four antennas were measured next in an anechoic chamber using a network analyzer Agilent E5071C [86]. The measurement results are also shown in Figure 10.6. The frequency was swept from 100 MHz to 4.5 GHz. It was found that the resonant frequency of the fabricated samples (a), (c) and (d) were 2.45 GHz and sample (b) was resonated at 3.15 GHz.

To measure the gain, one horn antenna and one sample patch antenna were set-up at a distance 158 cm and the picture is shown in Figure 10.7. The horn antenna acted as a reference for all the measurements. In the picture in Figure 10.7, the horn antenna was on position 1 and patch antenna samples were on position 2. The $|S_{21}|$ was measured using a network analyzer Agilent E5071C [86] and the results are shown in Figure 10.8. The frequency was swept from 500 MHz to

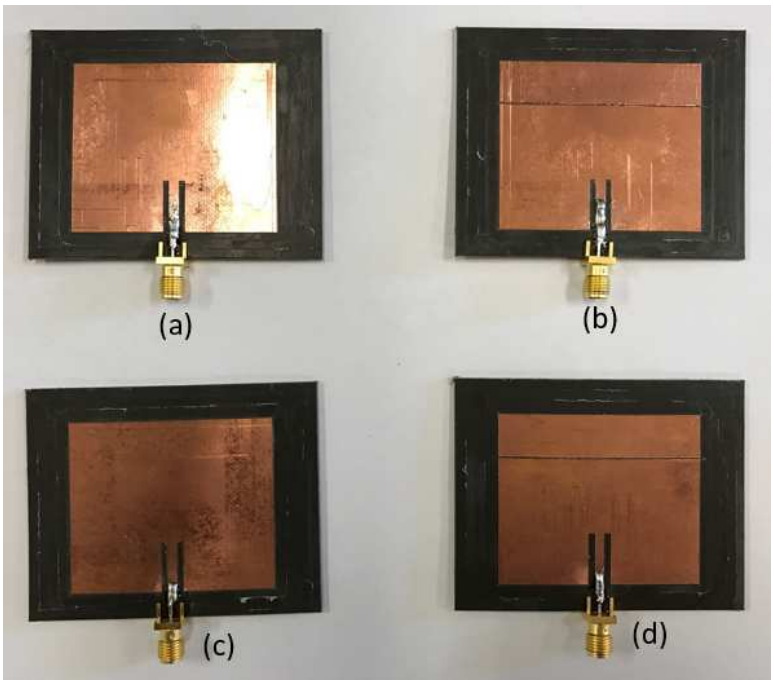

Figure 10.2. Four different scenarios before the graphene-based layer was added; (a) only copper layer without break; (b) only copper layer with a break; (c) only copper layer without a break; (d) only copper layer with a break.

4 GHz. It was computed and found that the gain of all the three samples (a), (c) and (d) were about 4.9 dBi at 2.45 GHz. The gain of the sample (b) was measured 1.3 dBi at 3.15 GHz.

10.3. Antenna on a Conformal Surface

A patch antenna was designed next on a flexible Rogers RT/Duroid 6002 [69] substrate (thickness = 0.508 mm; $\varepsilon_r \approx 2.94$; $\tan\delta = 0.0012$) and simulated in HFSS[82] at 2.45 GHz frequency. The antenna dimension is shown in Figure 10.9. Two conformal patch antennas were fabricated using a LPKF S63 [57] milling machine. The fabricated two antennas are shown in Figure 10.10. The purpose of using two antennas was to investigate the breaking or cracking on the radiator part of the antenna. Both of the antennas were measured in an anechoic chamber and measured results were well matched with the simulation results. Both of the antennas resonated at 2.45 GHz.

To understand the impact of cracking on the radiator surface of the antenna, a crack or break was made manually using a exacto blade at 10 mm distance from the top of the radiator surface. A digital multimeter was used to ensure the discontinuation of the radiator surface. Similar cracks or breaks were made on both of the samples. Next, the graphene layer [44] was cut according

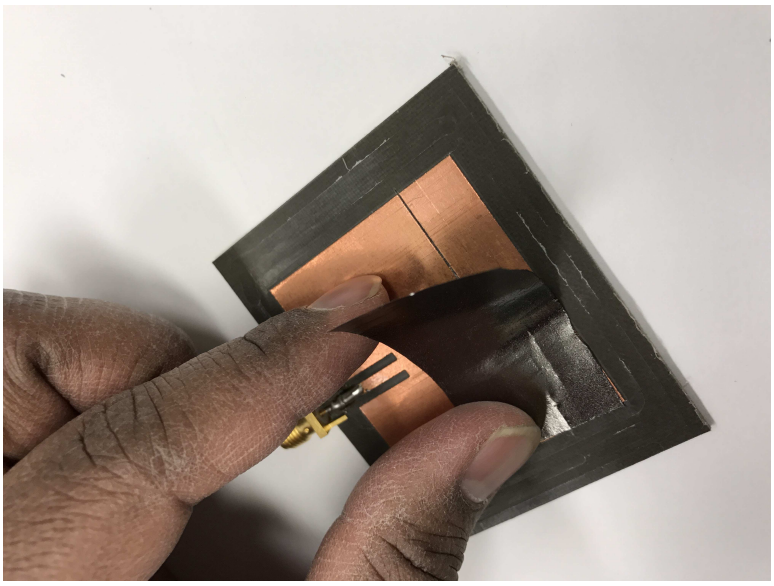

Figure 10.3. The part of the process of antenna fabrication.

to the size of the radiator using the method described in [53] and pasted on top of the copper surface of both antennas. The part of the process is shown in Figure 10.11. The two antenna samples are described below in (a) and (b). The fabricated antennas are shown in Figure 10.12

(a) Single conformal patch antenna with both copper and graphene-based layers with a break.

(b) Single conformal patch antenna with both copper and graphene-based layers without a break.

10.3.1. Results

Both antennas were measured again in an anechoic chamber using a network analyzer Agilent E5071C [86]. The measurement results are also shown in Figure 10.13. The frequency was swept from 100 MHz to 4.5 GHz. It was found that the resonant frequency of the fabricated sample (a) was 2.45 GHz and sample (b) resonated at 2.5 GHz. A slight frequency shift was observed in the $|S_{11}|$ results.

To measure the gain, one horn antenna and one sample patch antenna were set-up at a distance of 158 cm as shown in Figure 10.14. The horn antenna acted as a reference of all the measurements. In the picture in Figure 10.14, the horn antenna was at position 1 and the patch antenna samples were on position 2. The $|S_{21}|$ was measured using a network analyzer Agilent E5071C [86] and the results were shown in Figure 10.15. The frequency was swept from 500 MHz

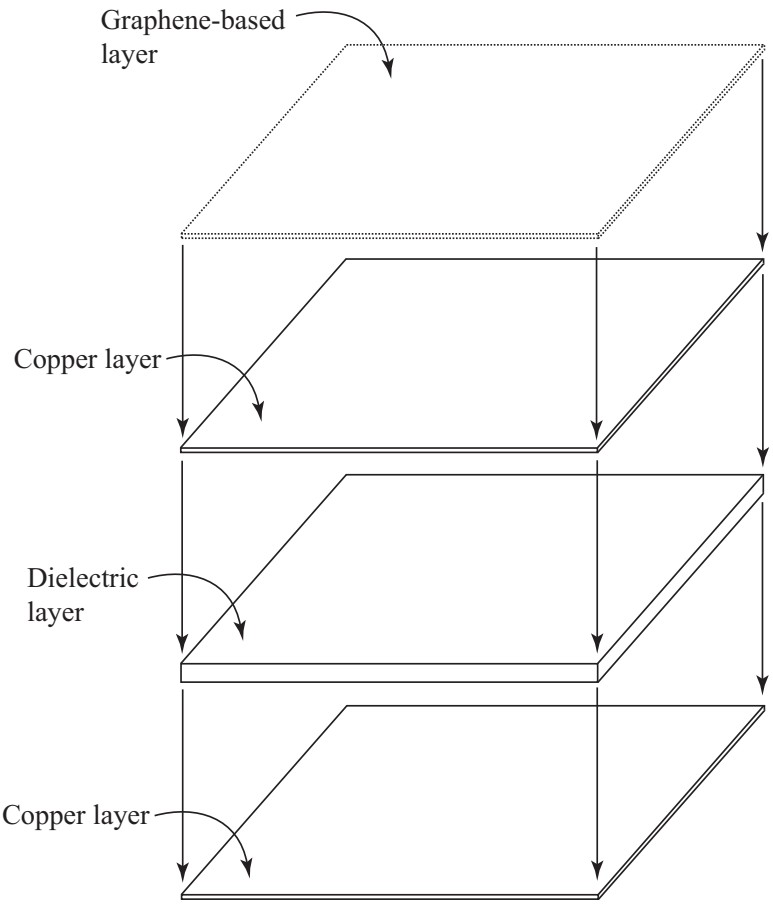

Figure 10.4. The extended view of the process of adhering graphene-based conductors.

to 4 GHz. It was computed that the gain of antenna (a) was measured to be -3.0 dBi at 2.45 GHz. The gain of the antenna (b) was measured as -5.3 dBi at 2.5 GHz.

10.4. Discussion

With this experiment, the cracking or breakage on the reflector of the antennas was investigated in both the cases (flat and conformal antenna). A thicker substrate was used for the flat antenna and a comparatively thin substrate was used for conformal application.

In the case of the flat antennas, only the antenna (b) with a break without graphene-based layers behaved differently. Because of the cracking on the antenna conductive material, it shifted the resonant frequency from 2.45 GHz to 3.15 GHz, which is expected according to antenna theory [49]. All other three antenna samples behaved the same though they were constructed differently. More specifically, in Figure. 10.5, the sample antenna (d) had a crack like (b) and one extra layer of graphene-based conductor was added on top of the copper layer. This extra layer of graphene

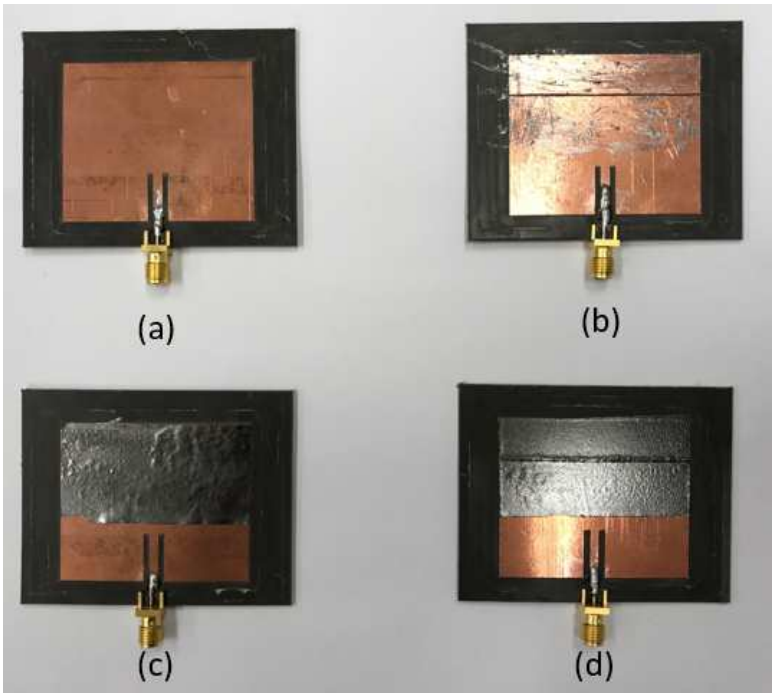

Figure 10.5. Four different scenarios after the graphene-based layer addition; (a) only copper layer without break; (b) only copper layer with a break; (c) both copper and graphene-based layers without a break; (d) both copper and graphene-based layers with a break.

mitigated the cracking and breaking effect of the iterative bending and acted in a similar manner to the antenna without cracking or breakage.

In the case of the conformal antennas, one antenna had a break or crack and the other was without any crack or break. When an extra layer of graphene-based conductive layer was added on top of the copper layer, the $|S_{11}|$ results and Gain of the both cases were similar. This extra layer made this conformal antenna mitigate the effect of repeated bending.

Overall, the graphene-based conductive material performed very well in relieving the problem of cracking or breaking in both flat and conformal antennas. It also served acted as a technique to provide redundancy antenna applications where the likelihood of cracking or breaking degenerative is an important factor to be considered.

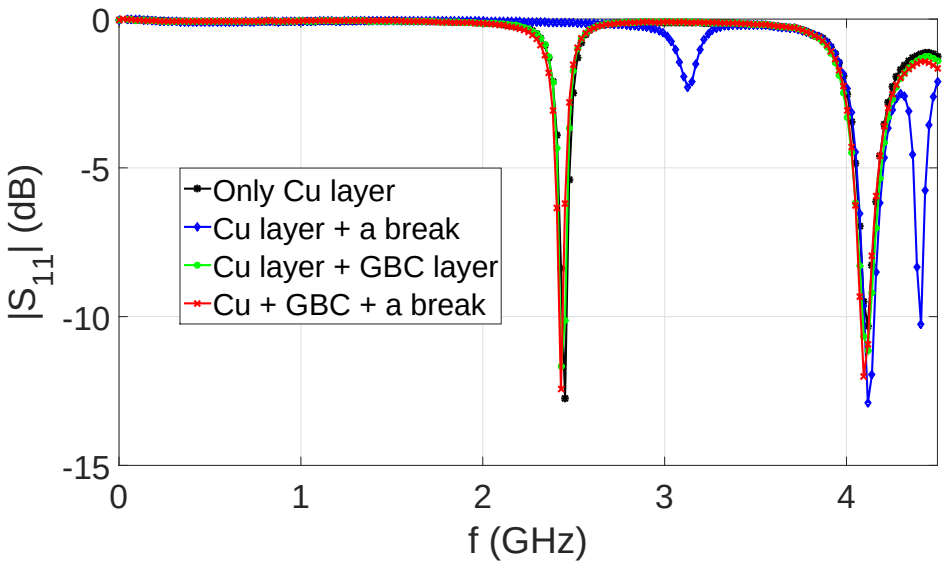

Figure 10.6. Comparison of the $|S_{11}|$ parameters in 4 different scenarios.

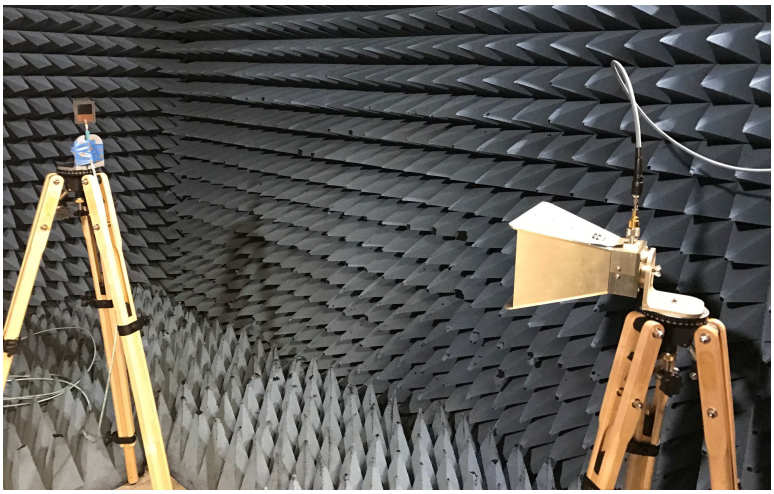

Figure 10.7. The gain measurement setup in an anechoic chamber.

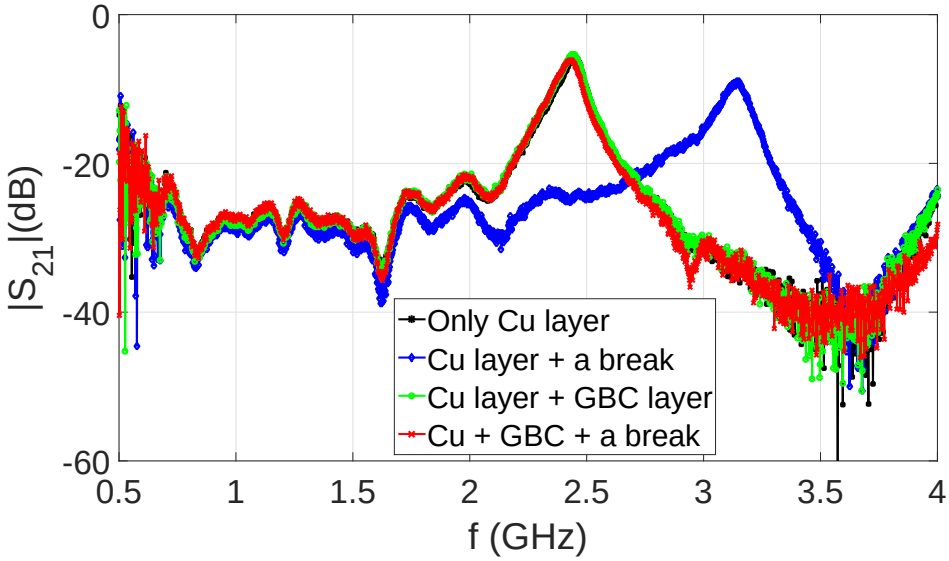

Figure 10.8. Comparison of the antenna gain in 4 different scenarios.

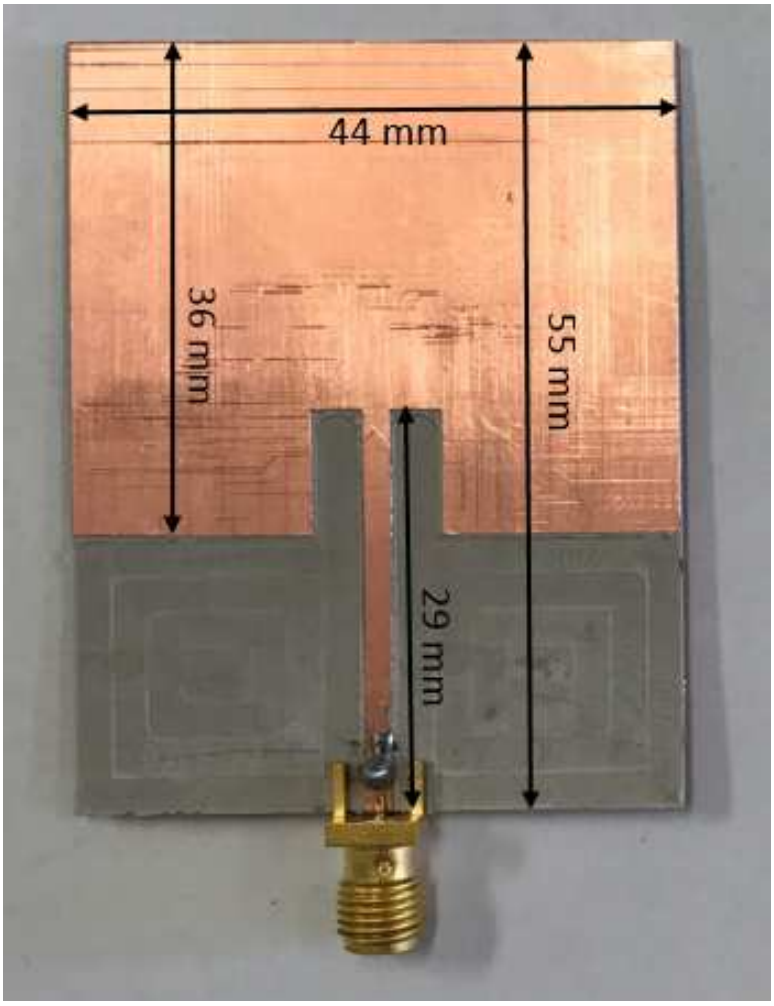

Figure 10.9. The dimension of the conformal antenna.

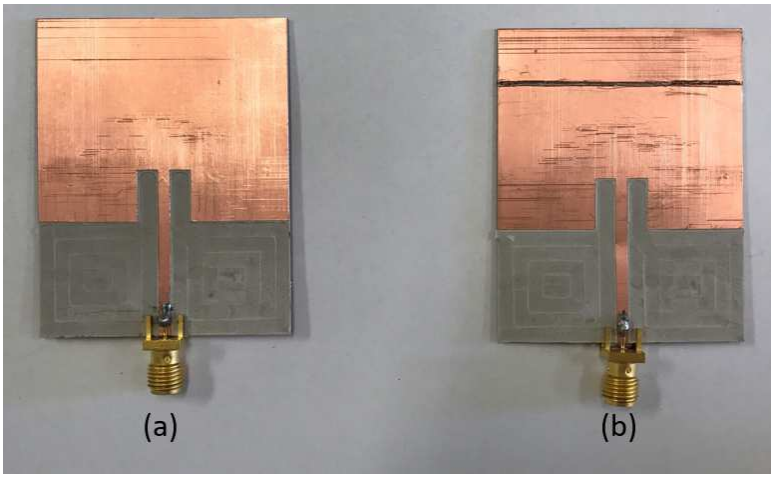

Figure 10.10. Two different scenarios before the graphene-based layer addition on conformal surface; (a) Only copper layer without a break; (b) Only copper layer with a break.

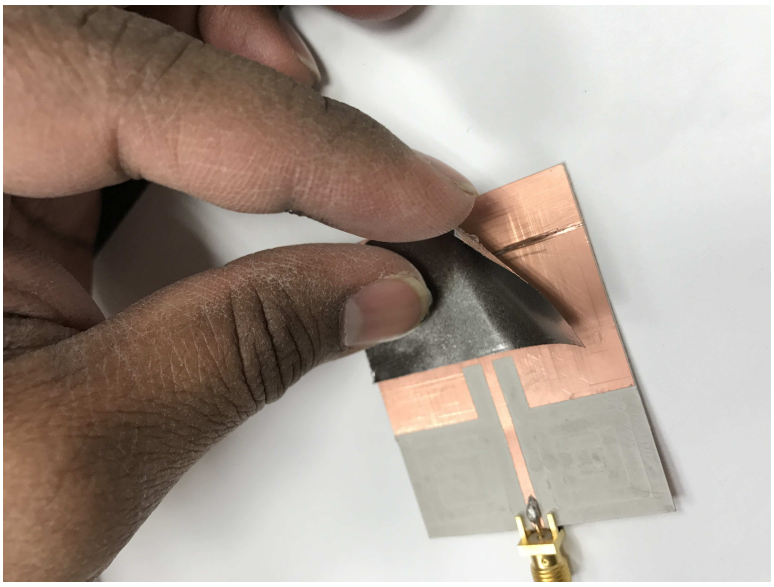

Figure 10.11. The part of the fabrication process on conformal antenna.

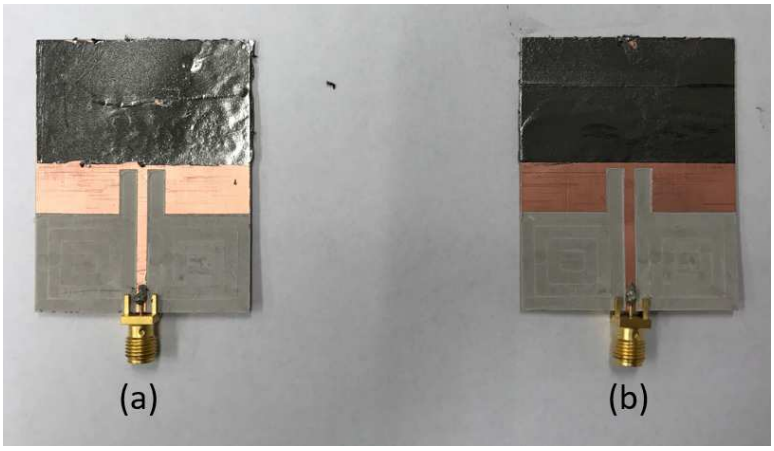

Figure 10.12. Two different scenarios after the graphene-based layer addition; (a) both copper and graphene-based layers without a break; (b) both copper and graphene-based layers with a break.

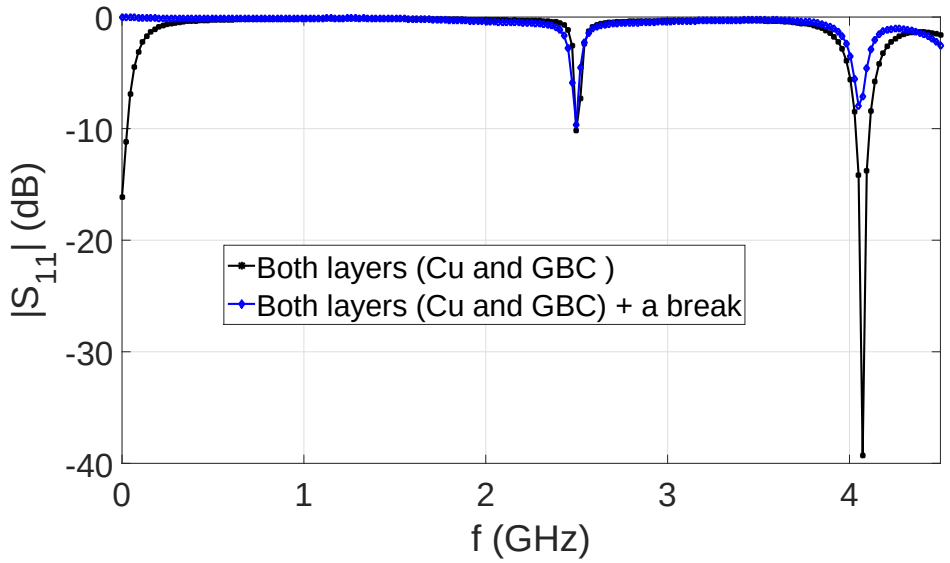

Figure 10.13. Comparison of the $|S_{11}|$ parameters in both scenarios on conformal surface.

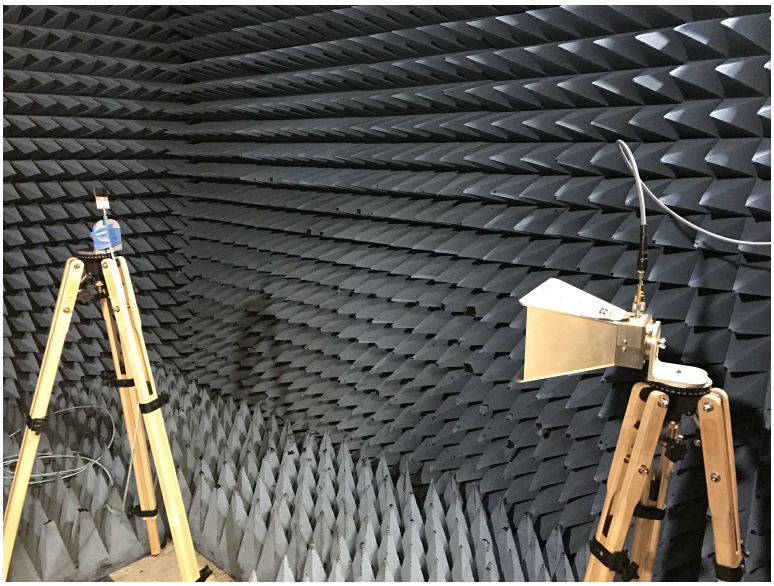

Figure 10.14. The gain measurement setup in an anechoic chamber.

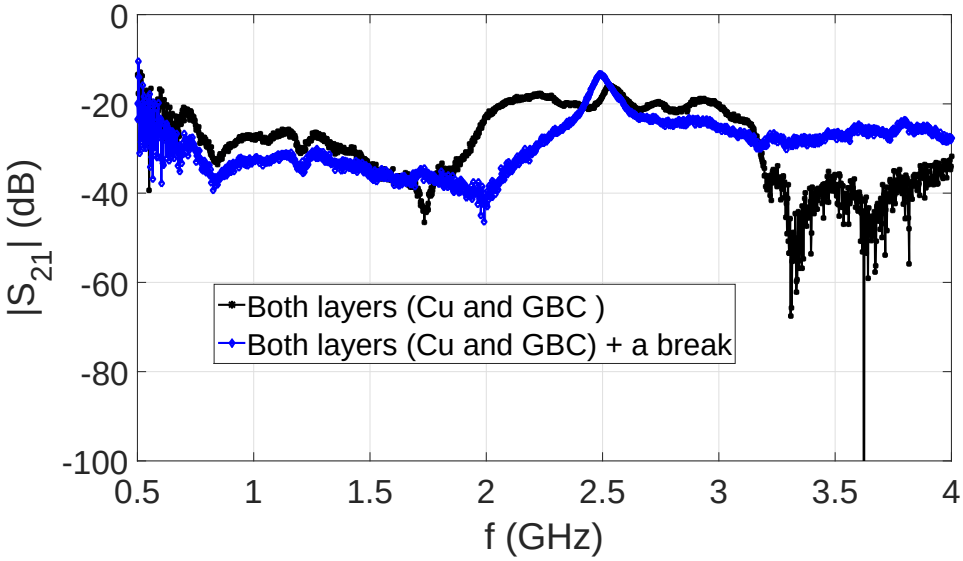

Figure 10.15. Comparison of the antenna gain in both scenarios on conformal surface.

11. CONCLUSION

We have investigated the electrical and mechanical properties of 97% carbon content graphene-based conductors (GBC).We determined the conductivity of the GBC is 1.94 $\times 10^5$ S/m which is less than Copper. But the S-parameter and gain results, which are the most important parameters in antenna design, found in the experiments were very competitive. Additionally, we found that GBC is at least 10 times more resilient to iterative bending than copper is. A unique process for manufacturing graphene-based antennas was also presented.

It was found that 97% carbon content graphene-based conductors are an alternative to traditional copper conductors. We constructed a conformal monopole antenna, a GBC RFID antenna and a CPW-fed conformal antenna on paper utilizing competitive advantages of using GBCs. We then tested them and found that all the simulated and measured results matched using the determined conductivity of the GBC.

Finally, we introduced novel techniques for creating redundancy using the unique electrical and mechanical properties of 97% carbon content graphene-based conductors. To do this, we first developed a GBC model with an adhesive layer. Then we conducted an iterative bending experiment on a conformal 2 $\times$ 1 array. We found the results to be as expected. Next, we implemented redundancy techniques using 97% carbon content graphene-based conductors (GBC) on flat and conformal antennas.

Overall, in order to implement the novel redundancy technique of using graphene-based conductors on transmission lines and antenna radiator surfaces. This work focused on solving the following technical challenges:

(a) How to fabricate GBC antenna

(b) How to obtain the benefits of GBC in antenna design

(c) How to merge the benefits of copper and GBC

(d) How to merge the benefits of GBC and conformal antennas

(e) How to know the trade-off for obtaining the benefits of redundancy techniques

In closing, and to summarize, though much more work is yet to be done, the research and techniques presented here show that 97% graphene-based conductors are a viable alternative to copper in antenna and antenna array applications, and that they have much potential value for redundancy in copper antenna applications where the antenna and/or the transmission line is subject to repeated bending. Its competitive characteristics and its superior resiliency against structural fatigue strongly suggest it as a functional and low-cost candidate for a multitude of functions where wearability or conformity to irregular geometric surfaces is desirable. We envision that upon further research and testing, production for a variety of these applications will lead us to the next level in mobility and aesthetic electronic design.

REFERENCES

[1] G. K. Geim and K. S. Novoselov, "The rise of Graphene," *Nature Mater.* 6,183-191 (2007).

[2] Wang, Han; Nezich, D.; Kong, Jing; Palacios, Tomas, "Graphene Frequency Multipliers," *Electron Device Letters,* IEEE , vol.30, no.5, pp.547,549, May 2009.

[3] Llatser, I.; Kremers, C.; Chigrin, D.N.; Jornet, J.M.; Lemme, Max C.; Cabellos-Aparicio, A.; Alarcon, E., "Characterization of graphene-based nano-antennas in the terahertz band," *Antennas and Propagation (EUCAP), 2012 6th European Conference on,* vol., no., pp.194,198, 26-30 March 2012.

[4] Bayram, Y.; Yijun Zhou; Bong Sup Shim; Shimei Xu; Jian Zhu; Kotov, N.A.; Volakis, J.L., "E-Textile Conductors and Polymer Composites for Conformal Lightweight Antennas," Antennas and Propagation, *IEEE Transactions on,* vol.58, no.8, pp.2732,2736, Aug 2010.

[5] Morton, T.E.; Pasala, K.M., "Pattern synthesis of conformal arrays for airborne vehicles," *Aerospace Conference, 2004. Proceedings. 2004 IEEE,* vol.2, no., pp.1030,1039 Vol.2, 6-13 March 2004.

[6] K. Dickerson, "The first viable product made with 'wonder material' graphene is about to hit stores", *Business Insider, 2015*[online]. Available: http://www.businessinsider.com/first-graphene-light-bulb-hits-stores-2015-3; Last accessed: March 1st, 2017.

[7] Constantine A. Balanis, *Antenna Theory: Analysis and Design,* Harper and Row, Publishers, New York, 1982.

[8] B. D. Braaten, M. A. Aziz, S. Roy, S. Nariyal, I. Irfanullah, N. F. Chamberlain, M. T. Reich and D. E. Anagnostou, "A Self-Adapting Flexible (SELFLEX) Antenna Array for Changing Conformal Surface Applications," *IEEE Trans. Antennas Propag.,* vol. 61, no. 2, Feb., 2013, pp. 655 - 665.

[9] J. S. Gomez-Diaz and J. Perruisseau-Carrier, "Microwave to THz Properties of Graphene and Potential Antenna Applications," *Proc. of ISAP2012,* OCT. 29 - Nov. 2, 2012, Nagoya, Japan, pp. 239 - 241. 0 GBC layer (6 iterations and Cu broke on left side)

[10] J. Perruisseau-Carrier, "Graphene for Antenna Applications: Opportunities and Challenges from Microwaves to THz," *2012 Loughborough Antennas and Propag. Conf,* Nov. 12 - 13, Loughborough, UK.

[11] A. K. Geim, "Graphene: Status and Prospects," *Science 19 June 2009,* Vol. 324 no. 5934 pp. 1530-1534.

[12] Ranjbartoreh, Ali R. and Wang, Bei and Shen, Xiaoping and Wang, Guoxiu, "Advanced mechanical properties of graphene paper," *Journal of Applied Physics,* 109, 014306 (2011).

[13] S. Stankovich, D. A. Dikin, G. H. B. Dommett, K. M. Kohlkaas, E.J. Zimney, E. A.Stach, R. D. Piner, S.T.Nguyen and R.S. Ruoff, "Graphene-Based Composite Materials", *Nature,* 442, Jul. 20, 2006, pp. 292-286.

[14] B. D. Braaten, T. Tolstedt, S. Asif, M. J. Schroeder and M. S. Khan, "On Using the Electrical Characteristics of Graphene-Based Conductors for Designing a Conformal Monopole on a Transparent Substrate", *2015 IEEE International Symposium on Antennas and Propagation,* Jul. 19 - 25, 2015, Vancouver BC, Canada, pp. 2435-2436.

[15] R.E. Munson,"Conformal microstrip antennas and microstrip phased arrays," *IEEE Transactions on Antennas and Propagation,* Vol. 22, Issue 1, January 1974, pp. 74-78.

[16] R. E. Munson,"Microstrip phased array antennas," *22nd Annual USAF Antenna Symposium,* Oct. 1972.

[17] E. Fubini. J. McDonough, and R. Malech,"Stripline radiators," *IRE Conference,* Rec., Pt. 1, p. 51, 1955.

[18] J. McDonough, R. Malech. and J. Kowalsky,"Recent developments in the study of printed antennas," *IRE Conference,* Rec., Pt. 1 , p. 173. 1957.

[19] J. R. James and C. J. Wilson,"Radiation characteristics of stripline antennas," in *Proc. 4th European Microwave Conference,* Sept. 1974, pp. 484-488.

[20] E. V. Byron, "A new flush-mounted antenna element for phased array application," in *Proc. Phased Array Antenna Symposium,* 1970. pp. 187-192, reprinted in Phased Array Antennas. A. A. Oliner and G. H. Knittel, Eds. Dedham, MA: Artech House. 1972.

[21] R. Mailloux, J. McIlvenna and N. Kernweis, "Microstrip array technology," in *IEEE Transactions on Antennas and Propagation,* vol. 29, no. 1, pp. 25-37, Jan 1981.

[22] R. Collings, U.S. Patent 3 680 136, July 1972.

[23] H. Schippers, G. Spalluto, and G. Vos, Radiation analysis of conformal phased array antennas on distorted structures, in *Proc. 12th Int. Conf. Antennas and Propagation,* Mar. 31- Apr. 3 2003, pp.160-163.

[24] H. Schippers, J. Verpoorte, P. Jorna, A. Hulzinga, A. Meijerink, C. Roeloffzen, R. G. Heideman, A. Leinse, and M. Wintels, Conformal phased array with beam forming on airborne satellite communication, in *Proc. Int. ITG Workshop on Smart Antennas,* Feb. 26-27, 2008, pp.343-350.

[25] H. Schippers, P. Knott, T. Deloues, P. Lacomme, and M. R. Scherbarth,Vibrating antennas and compensation techniques research in NATO/RTO/SET 087/RTG 50, in *Proc. IEEE Aerospace Conf.,* Mar. 3-10,2007, pp. 1-13.

[26] P. Jorna, H. Schippers, and J. Verpoorte, Beam synthesis for conformal array antennas with efficient tapering,presented at the *5th Eur. Workshop on Conformal Antennas,* Bristol, U.K., Sep. 11-12, 2007.

[27] P. Knott,Deformation and vibration of conformal antenna arrays and compensation techniques,in *Proc. Meet. RTO-MP-AVT-141,* 2006, pp. 1-12, paper 19.

[28] R. C. Hansen, *Phased Array Antennas.* Hoboken, NJ, USA: Wiley, 1998.

[29] R. L. Haupt, *Antenna Arrays: A Computational Approach.* Hoboken,NJ, USA: Wiley, 2010, pp. 287-315.

[30] L. Josefsson and P. Persson, *Conformal Array Antenna Theory and Design.* Hoboken, NJ, USA: Wiley, 2006.

[31] M. Klemm and G. Troester, Textile UWB antennas for wireless body area networks, *IEEE Trans. Antennas Propag.,* vol. 54, no. 11, pp.3192-3197, Nov. 2006.

[32] T. F. Kennedy, P. W. Fink, A. W. Chu, N. J. Champagne, G. Y. Lin, and M. A. Khayat, Body-worn E-textile antennas: The good, the lowmass,the conformal,*IEEE Trans. Antennas Propag.,* vol. 57, no. 4,pp. 910-918, Apr. 2009.

[33] P. Salonen, Y. Rahmat-Samii, M. Schaffrath, and M. Kivikoski, Effect of textile materials on wearable antenna performance: A case study of GPS antennas,in *Proc. IEEE Int. Symp. Antennas Propag.* Soc., 2004, vol. 1, pp. 459-462.

[34] D. Psychoudakis, G. Y. Lee, C.-C. Chen, and J. L. Volakis, Estimating diversity for body-worn antennas, presented at the *3rd Eur. Conf. Antennas and Propagation (EuCAP),* Berlin, Germany, Mar. 23-27, 2009.

[35] P. J. Callus, Conformal load-bearing antenna structure for australian defense force aircraft, in *DSTO Platforms Sciences Laboratory,* Victoria, Australia, 2007.

[36] Dan Sun, Rong Shen, and Xuequan Yan,A Broadband Conformal Phased Array Antenna on Spherical Surface,*International Journal of Antennas and Propagation,* vol. 2014, Article ID 206736, 5 pages, 2014.

[37] Dong, Jiazhi; Wang, Yuwen; Meng, Fanji; Feng, Wei, "A Research on Airborne Conformal Array with High Gain and Low SLL," *Computational Intelligence and Communication Networks (CICN), 2014 International Conference on,* vol., no., pp.334,338, 14-16 Nov. 2014.

[38] Braaten, B.D.; Roy, S.; Irfanullah; Nariyal, S.; Anagnostou, D.E., "An autonomous self-adapting conformal array for cylindrical surfaces with a changing radius," *Antennas and Propagation Society International Symposium (APSURSI), 2014 IEEE,* vol., no., pp.1784,1785, 6-11 July 2014.

[39] Roy, S.; Ijaz, B.; Braaten, B.D., "Using Bezier curves to design self-adapting conformal phased-array antennas," *Antennas and Propagation Society International Symposium (APSURSI), 2014 IEEE,* vol., no., pp.1786,1787, 6-11 July 2014.

[40] M. and Gmez-Daz, J. S. and Mosig, J. R. and Perruisseau-Carrier, J., "Reconfigurable terahertz plasmonic antenna concept using a graphene stack Tamagnone," *Applied Physics Letters,* 101, 214102 (2012).

[41] Dragoman, M. and Muller, A. A. and Dragoman, D. and Coccetti, F. and Plana, R., "Terahertz antenna based on graphene," *Journal of Applied Physics,* 107, 104313 (2010).

[42] Carrasco, E.; Perruisseau-Carrier, J., "Reflectarray Antenna at Terahertz Using Graphene," *Antennas and Wireless Propagation Letters, IEEE ,* vol.12, no., pp.253,256, 2013.

[43] Ignacio Llatser, Christian Kremers, Albert Cabellos-Aparicio, Josep Miquel Jornet, Eduard Alarcn, Dmitry N. Chigrin, "Graphene-based nano-patch antenna for terahertz radiation, Photonics and Nanostructures", *Fundamentals and Applications,* Volume 10, Issue 4, October 2012, Pages 353-358, ISSN 1569-4410.

[44] Graphene Laboratories Inc., [online], Available: www.graphene-supermarket.com, Last accessed: March 19th, 2017.

[45] Sulky, Inc., [online], Available: www.sulky.com, Last accessed: March 19th, 2017.

[46] Boise Paper, [online], Available: www.boisepaper.com, Last accessed: March 19th, 2017.

[47] Cricut, Inc., [online], Available: www.cricut.com, Last accessed: March 19th, 2017.

[48] Ander Products, [online], Available: www.anderproducts.com, Last accessed: March 19th, 2017.

[49] D. M. Pozar, *Microwave Engineering,* 3rd Ed., 2005, John Wiley and Sons, Inc., Hoboken, NJ, pp. 145.

[50] Advanced Design System (ads), *Agilent technologies,* Version:2013.06. Available: www.keysight.com, Last accessed: March 19th, 2017.

[51] J.R. James, P.S. Hall and C. Wood, *Microstrip Antenna Theory and Design,* 1981.

[52] K. L. Wu, M. Spenuk, J. Litva and D,-G, Fang, "Theoretical and experimental study of feed network effects on the radiation pattern of series-fed microstrip antenna arrays", *IEEE Proceedings,* Vol. 138, No. 3, June 1991.

[53] S. Z. Sajal, B. D. Braaten and V. R. Marinov, "A microstrip patch antenna manufactured with flexible graphene-based conducting material," *2015 IEEE International Symposium on Antennas and Propagation and USNC/URSI National Radio Science Meeting,* Vancouver, BC, 2015, pp. 2415-2416.

[54] D. A. Hill, Kenneth H. Cavcey and Robert T. Johnk, "Crosstalk between microstrip transmission lines," *IEEE Trans. on Electromagnetic Compatibility,* Vol.36, No.4, November 1994, pp. 314-321.

[55] S. Asif, A. Iftikhar, B. Braaten and M. S. Khan, "Mutual coupling between conventional right-handed transmission line and carbon microfiber transmission lines," Presented at *IEEE International Symposium on Antennas and Propagation,* Jul. 2015.

[56] S. M. Asif, A. Iftikhar, B. D. Braaten and M. S. Khan, "Wave propagation and coupling of graphene-based conductor transmission lines on a conformal surface — An experimental study," *2016 IEEE International Symposium on Antennas and Propagation (APSURSI),* Fajardo, 2016, pp. 1925-1926.

[57] LPKF, Inc., [online], Available: www.lpkfusa.com, Last accessed: March 19th, 2017.

[58] B. Braaten et al., "An initial investigation on the use of carbon microfibers for conformal transmission lines," *IEEE International Conference on Electro-Information Technology,* EIT 2013, Rapid City, SD, 2013, pp. 1-5.

[59] K. Wincza and S. Gruszczynski, "Influence of curvature radius on radiation patterns in multibeam conformal antennas," in *Proc. 36th Eur. Microw. Conf.,* Sep. 10–15, 2006, pp. 1410–1413.

[60] M. A. Aziz, S. Roy, L. A. Berge, I. Ullah and B. D. Braaten, "A Conformal CPW Folded Slot Antenna Array Printed on a Kapton Substrate," *Proceedings of the 2012 European Conference*

on Antennas and Propagation (EUCAP), Prague, Czech. Republic, March 26 - 30, 2012, pp. 159-162.

[61] J.-L. Guo and J.-Y. Li, "Pattern synthesis of conformal array antenna in the presence of platform using differential evolution algorithm," *IEEE Trans. Antennas Propag.,* vol. 57, no. 9, pp. 2615–2621, Sep. 2009.

[62] S. Nikolaou, G. E. Ponchak, J. Papapolymerou, and M. M. Tentzeris, "Conformal double exponentially tapered slot antenna (DETSA) on LCP or UWB applications," *IEEE Trans. Antennas Propag.,* vol. 54, no. 6, pp. 1663–1669, Jun. 2006.

[63] D. J. Chung, S. K. Bhattacharya, G. E. Ponchak and J. Papapolymerou, "An 8×8 lightweight flexible multilayer antenna array," *2009 IEEE Antennas and Propagation Society International Symposium,* Charleston, SC, 2009, pp. 1-4.

[64] P. L. O'Donovan and A. W. Rudge, "Adaptive control of a flexible linear array," *Electron. Lett.,* vol. 9, no. 6, pp. 121–122, Mar. 22, 1973.

[65] S. Zhu and R. Langley, "Dual-band wearable textile antenna on an EBG substrate," *IEEE Trans. Antennas Propag.,* vol. 57, no. 4, pp. 926–935, Apr. 2009.

[66] T. F. Kennedy, P. W. Fink, A. W. Chu, N. J. Champagne, G. Y. Lin, M. A. Khayat, and M. A. , "Body-worn e-textile antennas: The good, the low-mass, and the conformal," *IEEE Trans. Antennas Propag.,* vol. 57, no. 4, pp. 910–918, Apr. 2009.

[67] E. Patrick, M. Ordonez, N. Alba, J. C. Sanchez and T. Nishida, "Design and Fabrication of a Flexible Substrate Microelectrode Array for Brain Machine Interfaces," *2006 International Conference of the IEEE Engineering in Medicine and Biology Society,* New York, NY, 2006, pp. 2966-2969.

[68] F. Wang and T. Arslan, "Inkjet-printed antenna on flexible substrate for wearable microwave imaging applications," *2016 Loughborough Antennas and Propagation Conference (LAPC),* Loughborough, 2016, pp. 1-4.

[69] Rogers Corporation [online] Available: www.rogerscorp.com, Last accessed: Jan. 26th, 2017.

[70] M. Klemm and G. Troester, "Textile UWB antennas for wirelessbody area networks," *IEEE Trans. Antennas Propag.,* vol. 54, pp. 3192-3197, 2006.

[71] K. S. Novoselov, A. K. Gleim, S. V. Morozov, D. Jiang, Y. Zhang, S. V. Dubonos, I. V. Grigorieva and A. A. Firsov, "Electric field effect in atomically thin carbon films," *Science,* 306, Oct. 22, 2004, pp. 666 – 669.

[72] S. Z. Sajal, B. D. Braaten, T. Tolstedt and M. J. Schroeder, Design of a CPW-Fed Graphene-Based Conformal Monopole on a Paper Substrate,*2016 IEEE International Symposium on Antennas and Propagation,* Jun. 26 - Jul. 1, 2016, Fajardo, Puerto Rico.

[73] S. Asif, A. Iftikhar, S. Z. Sajal, B. D. Braaten and M. S. Khan, On Using Graphene-Based Conductors as Transmission Lines for Feed Networks in Printed Antenna Arrays,*2015 IEEE International Conference on Electro/Information Technology,* May 21 - 23, 2015, Northern Illinois University, DeKalb IL, USA, pp.681-683.

[74] S. Z. Sajal, A. Iftikhar and B. D. Braaten, Analysis of an Array with Graphene-Based Conductors,*2016 IEEE International Conference on Wireless Information Technology and Systems and Applied Computational Electromagnetics,* Mar. 13-17, 2016, Honolulu Hawaii USA.

[75] S. Sajal, B. D. Braaten, T. Tolstedt, S. Asif and M. J. Schroeder, "Design of a Conformal Monopole Antenna on a Paper Substrate using the Properties of Graphene-Based Conductors," *Microwave and Optical Technology Letters,* vol. 59, no. 6, Jun. 2017, pp. 1279-1283.

[76] S. Sajal and B. D. Braaten, "A Conformal Antenna on a Passive UHF RFID tag using 97% Carbon Content Graphene-Based Conductors and Paper Substrates," accepted for presentation at the *2017 IEEE International Symposium on Antennas and Propagation,* Jul. 9 - 14, 2017, San Diego, CA USA.

[77] S. Sajal, B. D. Braaten, V. Marinov, Y. Atanasov and O. Swenson, "A Low-Cost Antenna Design on a Paper Substrate for Near-Field Passive UHF RFID Tags," *Microwave and Optical Technology Letters,* vol. 59, no. 5, May 2017, pp. 1052-1056.

[78] K. Finkenzeller, *RFID Handbook:Fundamentals and Applications in Contactless Smart Cards and Identification,* John Wiley and Sons,West Sussex, England, 2003.

[79] G. Marrocco, "Gain-optimized self-resonant meander line antennas for RFID applications," *IEEE Antennas Wireless Propag. Lett.,* vol. 2, pp. 302-305, 2003.

[80] D. E. Anagnostou and A. A. Gheethan, "A Low-Cost WLAN Green PIFA Antenna on Eco-Friendly Paper Substrate", *2009 IEEE Int. Symp. on Ant. and Propag.,* Charleston, SC, USA, June 01-05, 2009.

[81] W. Thomas, R. C. Hall and D. I. Wu, "Effects of curvature on the fabrication of wraparound antennas," *1997 IEEE Int. Symp. on Ant. and Propag.,* Jul. 13-18, 1997, pp. 1512-1515.

[82] Ansys Inc., HFSS, Version 13.0.1, [Online]. Available: www.ansoft.com, Last accessed: Jan. 26th, 2017.

[83] S.Sajal, Y. Atanasov, B. D. Braaten, V. Marinov and O. Swenson, "A Low Cost Flexible Passive UHF RFID Tag for Sensing Moisture Based on Antenna Polarization," *IEEE Int. Conf. on Electro/Info. Tech.,* Jun. 5 - 7, 2014, Milwaukee, WI, USA, pp. 542-545.

[84] Alien Technologies, [Online]. Available: www.alientechnologies.com, Last accessed: January 26th, 2017.

[85] J.-Y. Kim, J. Lee, W. H. Lee, I. N. Kholmanov, J. W. Suk, T. Y. Kim, Y. Hao, H. Chou, D. Akinwande and R. S. Ruoff, "Flexible and Transparent Dielectric Film with a High Dielectric Constant Using Chemical Vapor Deposition-Grown Graphene Interlayer", *ACS Nano,* Dec. 2013, pp. 269-274.

[86] Agilent, Inc., [online], Available: www.agilent.com, Last accessed: March 19th, 2017.

[87] S. M. Asif, A. Iftikhar, B. D. Braaten and M. S. Khan, "Design of an ultra-wideband antenna using flexible graphene-based conductor sheets," *2016 IEEE International Symposium on Antennas and Propagation (APSURSI),* Fajardo, 2016, pp. 1863-1864.

[88] M. S. Khan, A. D. Capobianco, S. M. Asif, A. Iftikhar, B. D. Braaten and R. M. Shubair, "A properties comparison between copper and graphene-based UWB MIMO planar antennas," *2016 IEEE International Symposium on Antennas and Propagation (APSURSI), Fajardo, 2016,* pp. 1767-1768.

[89] R. Barco, P. Lazaro and P. Munoz, "A unified framework for redundancy in wireless networks," *IEEE Communications Magazine,* vol. 50, no. 12, pp. 134-142, December 2012.

[90] Yongyi Yang and H. Stark, "Design of self-healing arrays using vector-space projections," *IEEE Transactions on Antennas and Propagation,* vol. 49, no. 4, pp. 526-534, Apr 2001.

[91] Asrani, Vijay L., Krishna Katragadda, and Peruvemba Ranganathan Sai Ananthanarayanan. "Self-healing antenna system." *U.S. Patent No. 9,241,050. 19 Jan. 2016.*

[92] K. Jayaraman, Q. Khan, B. Chi, W. Beattie, Z. Wang and P. Chiang, "A self-healing 2.4GHz LNA with on-chip S11/S21 measurement/calibration for in-situ PVT compensation," *2010 IEEE Radio Frequency Integrated Circuits Symposium,* Anaheim, CA, 2010, pp. 311-314.

APPENDIX. MATLAB CODE

The following Matlab codes were used on the previous chapters of this dissertation.

Ch3SparaSimMeaCu.m: The code was used to find out the simulated and measured S-parameters (S_{11}, S_{21}) results of copper microstrip TLs. [Figures 2.6 - 2.9].

```
clear all
close all
figure
importdata CuS11.xlsx
fr1=ans.data(:,1)./10^9;
r3=ans.data(:,2);
plot(fr1,r3,' ks','LineWidth',4);
set(gca,'fontsize',40,'fontweight','normal')
grid on;
hold on;

importdata CuS11.xlsx
fr1=ans.data(:,1)./10^9;
r3=ans.data(:,3);
plot(fr1,r3,'--k','LineWidth',4);
set(gca,'fontsize',40,'fontweight','normal')
grid on;
hold on;

xlabel('f (GHz)')
ylabel('|S_{11}| (dB)')
grid on;
hold on;
h= legend ('Copper (sim)','Copper (meas)',2)

ylim([-50 0])
xlim([0 4])
```

```
figure
importdata CuS21.xlsx
fr1=ans.data(:,1)./10^9;
r3=ans.data(:,2);
plot(fr1,r3,' ks','LineWidth',4);
set(gca,'fontsize',40,'fontweight','normal')
grid on;
hold on;

importdata CuS21.xlsx
fr1=ans.data(:,1)./10^9;
r3=ans.data(:,3);
plot(fr1,r3,'--k','LineWidth',4);
set(gca,'fontsize',40,'fontweight','normal')
grid on;
hold on;

xlabel('f (GHz)')
ylabel('|S_{21}| (dB)')
grid on;
hold on;
h= legend ('Copper (sim)','Copper (meas)',2)

ylim([-10 0])
xlim([0 4])

figure
importdata GrS11.xlsx
fr1=ans.data(:,1)./10^9;
r3=ans.data(:,2);
plot(fr1,r3,' ks','LineWidth',4);
set(gca,'fontsize',40,'fontweight','normal')
grid on;
hold on;

importdata GrS11.xlsx
```

```
fr1=ans.data(:,1)./10^9;
r3=ans.data(:,3);
plot(fr1,r3,'--k','LineWidth',4);
set(gca,'fontsize',40,'fontweight','normal')
grid on;
hold on;

xlabel('f (GHz)')
ylabel('|S_{11}| (dB)')
grid on;
hold on;
h= legend ('Graphene-based (sim)','Graphene-based (meas)',2)

ylim([-50 0])
xlim([0 4])

figure
importdata GrS21.xlsx
fr1=ans.data(:,1)./10^9;
r3=ans.data(:,2);
plot(fr1,r3,' ks','LineWidth',4);
set(gca,'fontsize',40,'fontweight','normal')
grid on;
hold on;

importdata GrS21.xlsx
fr1=ans.data(:,1)./10^9;
r3=ans.data(:,3);
plot(fr1,r3,'--k','LineWidth',4);
set(gca,'fontsize',40,'fontweight','normal')
grid on;
hold on;

xlabel('f (GHz)')
ylabel('|S_{21}| (dB)')
grid on;
```

```
hold on;
h= legend ('Graphene-based (sim)','Graphene-based (meas)',2)

ylim([-10 0])
xlim([0 4])
```

Ch3SparaSimMeaGr.m: The code was used to find out S_{11} of copper and graphene-based antennas. [Figures 3.10 - 3.11].

```
clear all
close all
figure
importdata CuAntennaS11.xlsx
fr1=ans.data(:,1)./10^9;
r3=ans.data(:,2);
plot(fr1,r3,' ks','LineWidth',4);
set(gca,'fontsize',40,'fontweight','normal')
grid on;
hold on;

importdata CuAntennaS11.xlsx
fr1=ans.data(:,1)./10^9;
r3=ans.data(:,3);
plot(fr1,r3,'--k','LineWidth',4);
set(gca,'fontsize',40,'fontweight','normal')
grid on;
hold on;

xlabel('f (GHz)')
ylabel('|S_{11}| (dB)')
grid on;
hold on;
h= legend ('Copper (sim)','Copper (meas)',2)

ylim([-20 0])
xlim([0 3.5])
```

```
figure
importdata GrAntennaS11.xlsx
fr1=ans.data(:,1)./10^9;
r3=ans.data(:,2);
plot(fr1,r3,' ks','LineWidth',4);
set(gca,'fontsize',40,'fontweight','normal')
grid on;
hold on;

importdata GrAntennaS11.xlsx
fr1=ans.data(:,1)./10^9;
r3=ans.data(:,3);
plot(fr1,r3,'--k','LineWidth',4);
set(gca,'fontsize',40,'fontweight','normal')
grid on;
hold on;

xlabel('f (GHz)')
ylabel('|S_{11}| (dB)')
grid on;
hold on;
h= legend ('Graphene-based (sim)','Graphene-based (meas)',2)

ylim([-20 0])
xlim([0 3.5])
```

Ch3S11AntennaManuGr.m: The code was used to find out S_{11} results of graphene-based microstrip antenna. [Figure 3.13].

```
clear all
close all
figure
importdata GrAntennaManuS11.xlsx
fr1=ans.data(:,1)./10^9;
r3=ans.data(:,2);
```

```
plot(fr1,r3,' --k','LineWidth',4);
set(gca,'fontsize',40,'fontweight','normal')
grid on;
hold on;

importdata GrAntennaManuS11.xlsx
fr1=ans.data(:,1)./10^9;
r3=ans.data(:,3);
plot(fr1,r3,'k','LineWidth',4);
set(gca,'fontsize',40,'fontweight','normal')
grid on;
hold on;

xlabel('f (GHz)')
ylabel('|S_{11}| (dB)')
grid on;
hold on;
h= legend ('Simulated','Measured',2)

ylim([-20 0])
xlim([0 3.5])
```

Ch4SparaFlatTL.m: The code was used to find out S-parameters (S_{11}, S_{21}, S_{31} and S_{41}) results of flat Copper-Copper TLs and Copper-GBC TLs [Figures 4.3 - 4.6].

```
clear all
close all
figure
importdata FS11.xlsx
fr1=ans.data(:,1)./10^9;
r3=ans.data(:,2);
plot(fr1,r3,'k','LineWidth',4);
set(gca,'fontsize',40,'fontweight','normal')
grid on;
hold on;
```

```
importdata FS11.xlsx
fr1=ans.data(:,1)./10^9;
r3=ans.data(:,3);
plot(fr1,r3,'--k','LineWidth',4);
set(gca,'fontsize',40,'fontweight','normal')
grid on;
hold on;

importdata FS11.xlsx
fr1=ans.data(:,1)./10^9;
r3=ans.data(:,4);
plot(fr1,r3,':k','LineWidth',4);
set(gca,'fontsize',40,'fontweight','normal')
grid on;
hold on;

xlabel('f (GHz)')
ylabel('|S_{11}| (dB)')
grid on;
hold on;
h= legend ('Simulated Copper TL','Measured Copper TL','Measured Graphene TL',2)

ylim([-90 0])
xlim([0.1 8.5])

figure
importdata FS21.xlsx
fr1=ans.data(:,1)./10^9;
r3=ans.data(:,2);
plot(fr1,r3,'k','LineWidth',4);
set(gca,'fontsize',40,'fontweight','normal')
grid on;
hold on;

importdata FS21.xlsx
fr1=ans.data(:,1)./10^9;
```

```
r3=ans.data(:,3);
plot(fr1,r3,'--k','LineWidth',4);
set(gca,'fontsize',40,'fontweight','normal')
grid on;
hold on;

importdata FS21.xlsx
fr1=ans.data(:,1)./10^9;
r3=ans.data(:,4);
plot(fr1,r3,':k','LineWidth',4);
set(gca,'fontsize',40,'fontweight','normal')
grid on;
hold on;

xlabel('f (GHz)')
ylabel('|S_{21}| (dB)')
grid on;
hold on;
h= legend ('Simulated Copper TL','Measured Copper TL','Measured Graphene TL',2)

ylim([-6.5 0])
xlim([0.1 8.5])

figure
importdata FS31.xlsx
fr1=ans.data(:,1)./10^9;
r3=ans.data(:,2);
plot(fr1,r3,'k','LineWidth',4);
set(gca,'fontsize',40,'fontweight','normal')
grid on;
hold on;

importdata FS31.xlsx
fr1=ans.data(:,1)./10^9;
r3=ans.data(:,3);
plot(fr1,r3,'--k','LineWidth',4);
```

```
set(gca,'fontsize',40,'fontweight','normal')
grid on;
hold on;

importdata FS31.xlsx
fr1=ans.data(:,1)./10^9;
r3=ans.data(:,4);
plot(fr1,r3,':k','LineWidth',4);
set(gca,'fontsize',40,'fontweight','normal')
grid on;
hold on;

xlabel('f (GHz)')
ylabel('|S_{31}| (dB)')
grid on;
hold on;
h= legend ('Simulated Copper TL','Measured Copper TL','Measured Graphene TL',2)

ylim([-90 0])
xlim([0.1 8.5])

figure
importdata FS41.xlsx
fr1=ans.data(:,1)./10^9;
r3=ans.data(:,2);
plot(fr1,r3,'k','LineWidth',4);
set(gca,'fontsize',40,'fontweight','normal')
grid on;
hold on;

importdata FS41.xlsx
fr1=ans.data(:,1)./10^9;
r3=ans.data(:,3);
plot(fr1,r3,'--k','LineWidth',4);
set(gca,'fontsize',40,'fontweight','normal')
grid on;
```

```
hold on;

importdata FS41.xlsx
fr1=ans.data(:,1)./10^9;
r3=ans.data(:,4);
plot(fr1,r3,':k','LineWidth',4);
set(gca,'fontsize',40,'fontweight','normal')
grid on;
hold on;

xlabel('f (GHz)')
ylabel('|S_{41}| (dB)')
grid on;
hold on;
h= legend ('Simulated Copper TL','Measured Copper TL','Measured Graphene TL',2)

ylim([-90 0])
xlim([0.1 8.5])
```

Ch4SparaConformalTL.m: The code was used to find out S-parameters (S_{11}, S_{21}, S_{31} and S_{41}) results of conformal Copper-Copper TLs and Copper-GBC TLs [Figures 4.8 - 4.11].

```
clear all
close all
figure
importdata CS11.xlsx
fr1=ans.data(:,1)./10^9;
r3=ans.data(:,2);
plot(fr1,r3,'k','LineWidth',4);
set(gca,'fontsize',40,'fontweight','normal')
grid on;
hold on;

importdata CS11.xlsx
fr1=ans.data(:,1)./10^9;
r3=ans.data(:,3);
```

```
plot(fr1,r3,'b','LineWidth',4);
set(gca,'fontsize',40,'fontweight','normal')
grid on;
hold on;

xlabel('f (GHz)')
ylabel('|S_{11}| (dB)')
grid on;
hold on;
h= legend ('Two Copper TL','A copper TL and a GBC TL',2)

ylim([-50 0])
xlim([0.1 4.0])

figure
importdata CS21.xlsx
fr1=ans.data(:,1)./10^9;
r3=ans.data(:,2);
plot(fr1,r3,'k','LineWidth',4);
set(gca,'fontsize',40,'fontweight','normal')
grid on;
hold on;

importdata CS21.xlsx
fr1=ans.data(:,1)./10^9;
r3=ans.data(:,3);
plot(fr1,r3,'b','LineWidth',4);
set(gca,'fontsize',40,'fontweight','normal')
grid on;
hold on;

xlabel('f (GHz)')
ylabel('|S_{21}| (dB)')
grid on;
hold on;
h= legend ('Two Copper TL','A copper TL and a GBC TL',2)
```

```
ylim([−10 0])
xlim([0.1 4.0])

figure
importdata CS31.xlsx
fr1=ans.data(:,1)./10^9;
r3=ans.data(:,2);
plot(fr1,r3,'k','LineWidth',4);
set(gca,'fontsize',40,'fontweight','normal')
grid on;
hold on;

importdata CS31.xlsx
fr1=ans.data(:,1)./10^9;
r3=ans.data(:,3);
plot(fr1,r3,'b','LineWidth',4);
set(gca,'fontsize',40,'fontweight','normal')
grid on;
hold on;

xlabel('f (GHz)')
ylabel('|S_{31}| (dB)')
grid on;
hold on;
h= legend ('Two Copper TL','A copper TL and a GBC TL',2)

ylim([−70 0])
xlim([0.1 4.0])

figure
importdata CS41.xlsx
fr1=ans.data(:,1)./10^9;
r3=ans.data(:,2);
plot(fr1,r3,'k','LineWidth',4);
set(gca,'fontsize',40,'fontweight','normal')
```

```
grid on;
hold on;

importdata CS41.xlsx
fr1=ans.data(:,1)./10^9;
r3=ans.data(:,3);
plot(fr1,r3,'b','LineWidth',4);
set(gca,'fontsize',40,'fontweight','normal')
grid on;
hold on;

xlabel('f (GHz)')
ylabel('|S_{41}| (dB)')
grid on;
hold on;
h= legend ('Two Copper TL','A copper TL and a GBC TL',2)

ylim([-70 0])
xlim([0.1 4.0])
```

Ch5SparaMecha.m: The code was used to find out S-parameters (S_{11}, S_{12}, S_{21} and S_{22}) results of transmission lines of three different conductive materials (alliminium, copper and graphene-based) [Figures 5.2 - 5.5].

```
clear all
close all
figure
importdata MeS11.xlsx
fr1=ans.data(:,1)./10^9;
r3=ans.data(:,2);
plot(fr1,r3,'black:','LineWidth',2.5);
set(gca,'fontsize',40,'fontweight','bold')
grid on;
hold on;
```

```
importdata MeS11.xlsx
fr1=ans.data(:,1)./10^9;
r3=ans.data(:,3);
plot(fr1,r3,'blue','LineWidth',2.5);
set(gca,'fontsize',40,'fontweight','normal')
grid on;
hold on;

importdata MeS11.xlsx
fr1=ans.data(:,1)./10^9;
r3=ans.data(:,4);
plot(fr1,r3,'red','LineWidth',2.5);
set(gca,'fontsize',40,'fontweight','normal')
grid on;
hold on;

xlabel('f (GHz)')
ylabel('|S_{11}| (dB)')
grid on;
hold on;
h= legend ('Aluminum','Copper','Graphene-based',2)

ylim([-80 -20])
xlim([0.5 4.5])

figure
importdata MeS12.xlsx
fr1=ans.data(:,1)./10^9;
r3=ans.data(:,2);
plot(fr1,r3,'black:','LineWidth',2.5);
set(gca,'fontsize',40,'fontweight','bold')
grid on;
hold on;

importdata MeS12.xlsx
fr1=ans.data(:,1)./10^9;
```

```
r3=ans.data(:,3);
plot(fr1,r3,'blue','LineWidth',2.5);
set(gca,'fontsize',40,'fontweight','normal')
grid on;
hold on;

importdata MeS12.xlsx
fr1=ans.data(:,1)./10^9;
r3=ans.data(:,4);
plot(fr1,r3,'red','LineWidth',2.5);
set(gca,'fontsize',40,'fontweight','normal')
grid on;
hold on;

xlabel('f (GHz)')
ylabel('|S_{12}| (dB)')
grid on;
hold on;
h= legend ('Aluminum','Copper','Graphene-based',2)

ylim([-1 0])
xlim([0.5 4.5])

figure
importdata MeS21.xlsx
fr1=ans.data(:,1)./10^9;
r3=ans.data(:,2);
plot(fr1,r3,'black:','LineWidth',2.5);
set(gca,'fontsize',40,'fontweight','bold')
grid on;
hold on;

importdata MeS21.xlsx
fr1=ans.data(:,1)./10^9;
r3=ans.data(:,3);
plot(fr1,r3,'blue','LineWidth',2.5);
```

```
set(gca,'fontsize',40,'fontweight','normal')
grid on;
hold on;

importdata MeS21.xlsx
fr1=ans.data(:,1)./10^9;
r3=ans.data(:,4);
plot(fr1,r3,'red','LineWidth',2.5);
set(gca,'fontsize',40,'fontweight','normal')
grid on;
hold on;

xlabel('f (GHz)')
ylabel('|S_{21}| (dB)')
grid on;
hold on;
h= legend ('Aluminum','Copper','Graphene-based',2)

ylim([-1 0])
xlim([0.5 4.5])

figure
importdata MeS22.xlsx
fr1=ans.data(:,1)./10^9;
r3=ans.data(:,2);
plot(fr1,r3,'black:','LineWidth',2.5);
set(gca,'fontsize',40,'fontweight','bold')
grid on;
hold on;

importdata MeS22.xlsx
fr1=ans.data(:,1)./10^9;
r3=ans.data(:,3);
plot(fr1,r3,'blue','LineWidth',2.5);
set(gca,'fontsize',40,'fontweight','normal')
grid on;
```

```
hold on;

importdata MeS22.xlsx
fr1=ans.data(:,1)./10^9;
r3=ans.data(:,4);
plot(fr1,r3,'red','LineWidth',2.5);
set(gca,'fontsize',40,'fontweight','normal')
grid on;
hold on;

xlabel('f (GHz)')
ylabel('|S_{22}| (dB)')
grid on;
hold on;
h= legend ('Aluminum','Copper','Graphene-based',2)

ylim([-80 -20])
xlim([0.5 4.5])
```

Ch6S11CMono.m: The code was used to find out S_{11} of conformal graphene-based monopole antenna [Figure 6.4].

```
clear all
close all
figure
importdata CMonoS11.xlsx
fr1=ans.data(:,1)./10^9;
r3=ans.data(:,2);
plot(fr1,r3,' ks','LineWidth',4);
set(gca,'fontsize',40,'fontweight','normal')
grid on;
hold on;

importdata CMonoS11.xlsx
fr1=ans.data(:,1)./10^9;
r3=ans.data(:,3);
```

```
plot(fr1,r3,'--k','LineWidth',4);
set(gca,'fontsize',40,'fontweight','normal')
grid on;
hold on;

xlabel('f (GHz)')
ylabel('|S_{11}| (dB)')
grid on;
hold on;
h= legend ('Simulated','Measured',2)

ylim([-20 0])
xlim([0 4])
```

Ch6ImpedanceReIm.m: The code was used to find out the real and imaginary part of the antenna impedance [Figure 6.8].

```
clear all
close all
figure
importdata ReIm.csv
fr1=ans.data(:,1)*1000;
r2=ans.data(:,2);
plot(fr1,r2,'black:','LineWidth',2.5);
set(gca,'fontsize',18,'fontweight','normal')
grid on;
hold on;

fr1=ans.data(:,1)*1000;
r3=ans.data(:,3);
plot(fr1,r3,'blue:','LineWidth',2.5);
set(gca,'fontsize',40,'fontweight','normal')
grid on;
hold on;

xlabel('f (MHz)')
```

```
ylabel('Z_{11}')
grid on;
hold on;
h= legend ('Real part','Imaginary Part',2)
ylim([0 175])
xlim([866 956])
```

Ch6Higgs2.m: The code was used to find out the input impedance of the Higgs2 IC at particular frequency.

```
clear all;
r=1500;
c=1.2e-12;
f=860e6:1e6:960e6;
f1=915e6
Xc=1./(2.*j.*pi.*f.*c)
Z=(Xc.*r)./(r+Xc)
Imag=abs(imag(Z))
Real=real(Z)
figure;
[hAx,hLine1,hLine2]=plotyy(f/1e6,Real,f/1e6,Imag)
R=r/(1+4*pi*pi*f1*f1*c*c*r*r)
I=2*pi*f1*c*R*r
title('Frequency vs. IC Impedance')
xlabel('Frequency (MHz)')
ylabel(hAx(1),'Real | Z | ')
ylabel(hAx(2),'Imag | Z | ')
```

Ch6CPW.m: The code was used to find out S_{11} of CPW graphene-based monopole antenna [Figure 6.11].

```
clear all
close all
figure
importdata S11_Sim.csv;
```

```
fr1=ans.data(:,1);
r3=ans.data(:,2);
plot(fr1,r3,'k','LineWidth',2.5);
set(gca,'fontsize',40,'fontweight','normal')
grid on;
hold on;

importdata S11_Measure.csv;
fr1=ans.data(:,1)./10^9;
r3=ans.data(:,2);
plot(fr1,r3,'b','LineWidth',2.5);
set(gca,'fontsize',40,'fontweight','normal')
grid on;
hold on;

xlabel('f (GHz)')
ylabel('|S_{11}| (dB)')
grid on;
hold on;
h= legend ('Simulated','Measured',2)

ylim([-30 0])
xlim([2.5 4.5])
```

Ch7S11Array.m: The code was used to find out the simulated and measured S_{11} of copper and graphene-based antenna array [Figure 7.4].

```
clear all
close all
figure
importdata CU_SIM.csv
fr1=ans.data(:,1);
r3=ans.data(:,2);
plot(fr1,r3,'b*-','LineWidth',2.5);
set(gca,'fontsize',40,'fontweight','normal')
grid on;
```

```
hold on;

importdata GR_SIM.csv
fr1=ans.data(:,1);
r3=ans.data(:,2);
plot(fr1,r3,'go-','LineWidth',2.5);
set(gca,'fontsize',40,'fontweight','normal')
grid on;
hold on;

importdata CU.csv
fr1=ans.data(:,1)./10^9;
r3=ans.data(:,2);
plot(fr1,r3,'rv-','LineWidth',2.5);
set(gca,'fontsize',40,'fontweight','normal')
grid on;
hold on;

importdata GR.csv
fr1=ans.data(:,1)./10^9;
r3=ans.data(:,2);
plot(fr1,r3,'k^-','LineWidth',2.5);
set(gca,'fontsize',40,'fontweight','normal')
grid on;
hold on;

xlabel('Frequency (GHz)')
ylabel('|S_{11}| (dB)')
grid on;
hold on;
h= legend ('Simulated Cu Array','Simulated GBC Array','Measured Cu ...
    Array','Measured GBC Array',4)

ylim([-37 0])
xlim([1.5 2.5])
```

Ch8S11SimMeas.m: The code was used to find out the simulated and measured S_{11} of

different combination of copper and graphene-based Tls [Figure 8.7].

```
clear all
close all
figure
importdata S11.xlsx
fr1=ans.data(:,1)./10^9;
r3=ans.data(:,3);
plot(fr1,r3,'b*','LineWidth',2.5);
set(gca,'fontsize',40,'fontweight','normal')
grid on;
hold on;

importdata S11.xlsx
fr1=ans.data(:,1)./10^9;
r3=ans.data(:,2);
plot(fr1,r3,'--k*','LineWidth',2.5);
set(gca,'fontsize',40,'fontweight','normal', 'Xlim',[0.5 4.5])
grid on;
hold on;

importdata S11HFSS.xlsx
fr1=ans.data(:,1);
r3=ans.data(:,2);
plot(fr1,r3,'--go','LineWidth',2.5);
set(gca,'fontsize',40,'fontweight','normal', 'Xlim',[0.5 4.5])
grid on;
hold on;

importdata S11.xlsx
fr1=ans.data(:,1)./10^9;
r3=ans.data(:,4);
plot(fr1,r3,':r','LineWidth',2.5);
set(gca,'fontsize',40,'fontweight','normal', 'Xlim',[0.5 4.5])
grid on;
```

```
hold on;

importdata S11HFSS.xlsx
fr1=ans.data(:,1);
r3=ans.data(:,3);
plot(fr1,r3,':m','LineWidth',2.5);
set(gca,'fontsize',40,'fontweight','normal', 'Xlim',[0.5 4.5])
grid on;
hold on;

xlabel('f (GHz)')
ylabel('|S_{11}| (dB)')
grid on;
hold on;
h= legend ('Cu TL + break (measured)', 'Only Cu TL (measured)', 'Only Cu TL ...
    (HFSS)','Cu TL + break + GBC TL (measured)', 'Cu TL + break + GBC TL (HFSS)',2)
```

Ch8S21MeasGain.m: The code was used to find out the measured S_{21} of different combination of copper and graphene-based Tls [Figure 8.8].

```
clear all
close all
figure
importdata Gain.xlsx
fr1=ans.data(:,1)./10^9;
r3=ans.data(:,2);
plot(fr1,r3,'black:','LineWidth',2.5);
set(gca,'fontsize',40,'fontweight','normal', 'XLim', [1 4])
grid on;
hold on;

importdata Gain.xlsx
fr1=ans.data(:,1)./10^9;
r3=ans.data(:,3);
plot(fr1,r3,'blue','LineWidth',2.5);
set(gca,'fontsize',40,'fontweight','normal','XLim', [1 4])
```

```
grid on;
hold on;

xlabel('f (GHz)')
ylabel('|S_{21}| Gain(dB)')
grid on;
hold on;
h= legend ('Copper TL','Copper TL + break + GBC TL',2);
```

Ch9S11SimMeasurement.m: The code was used to find out S_{11} (both simulation and measurement) of 2×1 anetnna array [Figure 9.4].

```
clear all
close all
figure
importdata S11Mea.xlsx
fr1=ans.data(:,2);
r3=ans.data(:,3);
plot(fr1,r3,'k:','LineWidth',2.5)
set(gca,'fontsize',40,'fontweight','normal','xlim',[0.5 4.5])
grid on;
hold on;

importdata S11Sim.xlsx
fr1=ans.data(:,1);
r3=ans.data(:,2);
plot(fr1,r3,'b-','LineWidth',2.5)
set(gca,'fontsize',40,'fontweight','normal','xlim',[0.5 4.5])
grid on;
hold on;

xlabel('f (GHz)')
ylabel('|S_{11}| (dB)')
grid on;
hold on;
h= legend ('Measurement','ADS Simulation',2)
```

Ch9S11BendingIterations.m: The code was used to find out S_{11} of 2×1 anetnna array on the event of 8 different bending iterations [Figure 9.10].

```
clear all
close all
figure
importdata S11.xlsx
fr1=ans.data(:,2);
r3=ans.data(:,4);
plot(fr1,r3,'-k*');
set(gca,'fontsize',40,'fontweight','normal','Xlim',[1 4.5], 'Ylim', [-20,0])
grid on;
hold on;

importdata S11.xlsx
fr1=ans.data(:,2);
r3=ans.data(:,3);
plot(fr1,r3,'-g*');
set(gca,'fontsize',40,'fontweight','normal','Xlim',[1 4.5], 'Ylim', [-20,0])
grid on;
hold on;

importdata S11.xlsx
fr1=ans.data(:,2);
r3=ans.data(:,5);
plot(fr1,r3,'-b*');
set(gca,'fontsize',40,'fontweight','normal','Xlim',[1 4.5], 'Ylim', [-20,0])
grid on;
grid on;
hold on;

importdata S11.xlsx
fr1=ans.data(:,2);
r3=ans.data(:,6);
plot(fr1,r3,'-kd');
```

```
set(gca,'fontsize',40,'fontweight','normal','Xlim',[1 4.5], 'Ylim', [−20,0])
grid on;
grid on;
hold on;

importdata S11.xlsx
fr1=ans.data(:,2);
r3=ans.data(:,7);
plot(fr1,r3,'−gd');
set(gca,'fontsize',40,'fontweight','normal','Xlim',[1 4.5], 'Ylim', [−20,0])
grid on;
grid on;
hold on;

importdata S11.xlsx
fr1=ans.data(:,2);
r3=ans.data(:,8);
plot(fr1,r3,'−bd');
set(gca,'fontsize',40,'fontweight','normal','Xlim',[1 4.5], 'Ylim', [−20,0])
grid on;
grid on;
hold on;

importdata S11.xlsx
fr1=ans.data(:,2);
r3=ans.data(:,9);
plot(fr1,r3,'−k*');
set(gca,'fontsize',40,'fontweight','normal','Xlim',[1 4.5], 'Ylim', [−20,0])
grid on;
grid on;
hold on;

importdata S11.xlsx
fr1=ans.data(:,2);
r3=ans.data(:,10);
plot(fr1,r3,'−b*');
```

```
set(gca,'fontsize',40,'fontweight','normal','Xlim',[1 4.5], 'Ylim', [-20,0])
grid on;
grid on;
hold on;

xlabel('f (GHz)')
ylabel('|S_{11}| (dB)')
grid on;
hold on;
h= legend ('scenario a','scenario b','scenario c','scenario d','scenario ...
    e','scenario f','scenario g','scenario h',2)
```

Ch10S11FlatAntenna.m: The code was used to find out S_{11} value of 4 different scenarios of the flat antenna [Figure 10.6].

```
clear all
close all
figure
importdata S11.xlsx
fr1=ans.data(:,2);
r3=ans.data(:,3);
plot(fr1,r3,'-k*','LineWidth',2.5);
set(gca,'fontsize',40,'fontweight','normal','Xlim',[0 4.5], 'Ylim', [-15,0])
grid on;
grid on;
hold on;

importdata S11.xlsx
fr1=ans.data(:,2);
r3=ans.data(:,4);
plot(fr1,r3,'-bd','LineWidth',2.5);
set(gca,'fontsize',40,'fontweight','normal','Xlim',[0 4.5], 'Ylim', [-15,0])
grid on;
hold on;
```

```
importdata S11.xlsx
fr1=ans.data(:,2);
r3=ans.data(:,5);
plot(fr1,r3,'-go','LineWidth',2.5);
set(gca,'fontsize',40,'fontweight','normal','Xlim',[0 4.5], 'Ylim', [-15,0])
grid on;
hold on;

importdata S11.xlsx
fr1=ans.data(:,2);
r3=ans.data(:,6);
plot(fr1,r3,'-rx','LineWidth',2.5);
set(gca,'fontsize',40,'fontweight','normal','Xlim',[0 4.5], 'Ylim', [-15,0])
grid on;
hold on;

xlabel('f (GHz)')
ylabel('|S_{11}| (dB)')
grid on;
hold on;
h= legend ('Only Cu layer','Cu layer + a break','Cu layer + GBC layer','Cu + GBC + ...
    a break',2)
```

Ch10GainFlatAntenna.m: The code was used to find out the S_{21} value of 4 different scenarios of the flat antenna [Figure 10.8].

```
clear all
close all
figure
importdata Gain.xlsx
fr1=ans.data(:,1)./10^9;
r3=ans.data(:,2);
plot(fr1,r3,'-k*','LineWidth',2.5);
set(gca,'fontsize',40,'fontweight','normal','Xlim',[0.5 4], 'Ylim', [-60,0])
grid on;
hold on;
```

```
importdata Gain.xlsx
fr1=ans.data(:,1)./10^9;
r3=ans.data(:,3);
plot(fr1,r3,'-bd','LineWidth',2.5);
set(gca,'fontsize',40,'fontweight','normal','Xlim',[0.5 4], 'Ylim', [-60,0])
grid on;
hold on;

importdata Gain.xlsx
fr1=ans.data(:,1)./10^9;
r3=ans.data(:,4);
plot(fr1,r3,'-go','LineWidth',2.5);
set(gca,'fontsize',40,'fontweight','normal','Xlim',[0.5 4], 'Ylim', [-60,0])
grid on;
hold on;

importdata Gain.xlsx
fr1=ans.data(:,1)./10^9;
r3=ans.data(:,5);
plot(fr1,r3,'-rx','LineWidth',2.5);
set(gca,'fontsize',40,'fontweight','normal','Xlim',[0.5 4], 'Ylim', [-60,0])
grid on;
hold on;

xlabel('f (GHz)')
ylabel('|S_{21}|(dB)')
grid on;
hold on;
h= legend ('Only Cu layer','Cu layer + a break','Cu layer + GBC layer','Cu + GBC + ...
    a break',2)
```

Ch10S11ConformAntenna.m: The code was used to find out S_{11} value of 4 different scenarios of the conformal antenna [Figure 10.13].

```
clear all
```

```
close all
figure
importdata S11.xlsx
fr1=ans.data(:,1)./10^9;
r3=ans.data(:,2);
plot(fr1,r3,'-k*','LineWidth',2.5);
set(gca,'fontsize',40,'fontweight','normal','Xlim',[0 4.5])
grid on;
hold on;

importdata S11.xlsx
fr1=ans.data(:,1)./10^9;
r3=ans.data(:,3);
plot(fr1,r3,'-bd','LineWidth',2.5);
set(gca,'fontsize',40,'fontweight','normal','Xlim',[0 4.5])
grid on;
hold on;

xlabel('f (GHz)')
ylabel('|S_{11}| (dB)')
grid on;
hold on;
h= legend ('Both layers (Cu and GBC )','Both layers (Cu and GBC) + a break',2)
```

Ch10GainConformAntenna.m: The code was used to find out S_{21} value of 4 different scenarios of the conformal antenna [Figure 10.15].

```
clear all
close all
figure
importdata Gain.xlsx
fr1=ans.data(:,1)./10^9;
r3=ans.data(:,2);
plot(fr1,r3,'-k*','LineWidth',2.5);
set(gca,'fontsize',40,'fontweight','normal','Xlim',[0.5 4],'Ylim',[-100 0])
grid on;
```

```
hold on;

importdata Gain.xlsx
fr1=ans.data(:,1)./10^9;
r3=ans.data(:,3);
plot(fr1,r3,'—bd','LineWidth',2.5);
set(gca,'fontsize',40,'fontweight','normal','Xlim',[0.5 4],'Ylim',[—100 0])
grid on;
hold on;

xlabel('f (GHz)')
ylabel('|S_{21}| (dB)')
grid on;
hold on;
h= legend ('Both layers (Cu and GBC )','Both layers (Cu and GBC) + a break',2)
```